



Universidad de Concepción  
Dirección de Postgrado  
Facultad de Ciencias Físicas y Matemáticas  
Programa de Doctorado en Ciencias de Ingeniería con mención en Ingeniería Matemática

**MÉTODOS DE ELEMENTOS FINITOS ADAPTATIVOS  
PARA PROBLEMAS DE LA GEOCIENCIA**

**ADAPTIVE FINITE ELEMENT METHODS FOR  
PROBLEMS OF GEOSCIENCE**

*Tesis para optar al grado de  
Doctor en Ciencias Aplicadas con mención en Ingeniería Matemática*

**Ramiro James Rebolledo Cormack**

CONCEPCIÓN–CHILE, 19 JUNE 2019

## **Adaptive Finite Element Methods for Problems of Geoscience**

**Ramiro James Rebolledo Cormack**

**Supervisors:** Prof. Rodolfo Araya, Universidad de Concepción, Chile.

Prof. Frédéric Valentin, Laboratório Nacional de Computação Científica, Brazil.

**Director of the Program:** Prof. Rodolfo Rodríguez, Universidad de Concepción, Chile.

### **REVIEW PANEL**

Prof. Roland Becker, LMAP, Université de Pau, France.

Prof. Gabriel R. Barrenechea, University of Strathclyde, Scotland.

Prof. Miguel A. Fernández, INRIA, France.

Prof. Sônia M. Gomez, University of Campinas, Brazil.

Prof. Alessandro Russo, University of Milano-Bicocca, Italy.

### **EVALUATION PANEL**

Signature: \_\_\_\_\_

Prof. Rodolfo Araya, Universidad de Concepción, Chile.

Signature: \_\_\_\_\_

Prof. Diego Paredes, Universidad de Concepción, Chile.

Signature: \_\_\_\_\_

Prof. Manuel Solano, Universidad de Concepción, Chile.

Signature: \_\_\_\_\_

Prof. Abner Poza, Universidad Católica de la Santísima Concepción, Chile.

**Score:** \_\_\_\_\_

*Concepción, 19 June 2019*

## **ACKNOWLEDGEMENT**

This thesis was supported by the *Comisión Nacional de Investigación Científica y Tecnológica CONICYT* through the scholarship program to pursue national doctorates, *Red Doctoral Ciencia, Tecnología y Medio Ambiente REDOC.CTA*, and the *Programa BASAL PFB003* and *Programa PIA AFB170001* guaranteed by *Centro de Modelamiento Matemático (CMM)* of the *Universidad de Chile* and *Centro de Investigación en Ingeniería Matemática (CI<sup>2</sup>MA)* of the *Universidad de Concepción*.

## RESUMEN

En esta tesis estudiamos aspectos matemáticos y numéricos de métodos de elementos finitos adaptativos con aplicaciones a la geociencia.

Primero desarrollamos un estimador a posteriori del tipo jerárquico para un esquema de elementos finitos LPS (Local Projection Stabilized) aplicado a las ecuaciones de Navier–Stokes incompresibles. La técnica utiliza la solución de problemas locales puestos en espacios de dimensión finita del tipo funciones burbujas para aproximar el error.

A continuación proponemos y analizamos un estimador a posteriori del tipo residual para el método de elementos finitos Mixtos Hibridizados Multiescala (MHM por sus nombre en inglés) para las ecuaciones de Stokes y Brinkman. El estimador de error se basa en la estructura multiescala del método MHM y considera la aproximación del segundo nivel del método. Como resultado, el estimador del error está compuesto por un estimador para primer nivel global sobre el esqueleto de la partición y un estimador que considera las contribuciones del segundo nivel. Además, esta nueva estrategia adaptativa sobre el esqueleto de la malla evita cambiar la topología de la malla global. Especialmente diseñado para funcionar en problemas multiescala, el estimador puede ser calculado en forma paralela debido a que los estimadores locales son independientes uno del otro.

Por último, consideramos un problema de Stokes no lineal que modela el comportamiento de un glaciar. La no linealidad del problema es debido a la relación entre la viscosidad del fluido y su velocidad, y que en este contexto viene dada por la ley de Glen. Proponemos un método numérico MHM para resolver el problema que está inspirado en el caso lineal previamente estudiado.

Para todas las situaciones descritas, se reportan múltiples resultados numéricos que ilustran y confirman los resultados teóricos obtenidos.

## ABSTRACT

In this thesis we study mathematical and numerical aspects of adaptive finite element methods with applications to geosciences.

First we develop an a posteriori error estimator of hierarchical type for the Local Projection Stabilized (LPS) finite element method, applied to the incompressible Navier–Stokes equations. To approach the error, the technique uses the solution of local problems posed on appropriate finite dimensional spaces of bubble-like functions.

Next we propose and analyze a residual a posteriori error estimator for the Multiscale Hybrid-Mixed (MHM) method for the Stokes and Brinkman equations. The error estimator relies on the multi-level structure of the MHM method and considers the two levels of approximation of the method. As a result, the error estimator accounts for a first-level global estimator defined on the skeleton of the partition and second-level contributions from element-wise approximations. The analysis establishes local efficiency and reliability of the complete multiscale estimator. Also, it yields a new face-adaptive strategy on the mesh’s skeleton which avoids changing the topology of the global mesh. Specially designed to work on multiscale problems, the present estimator can leverage parallel computers since local error estimators are independent of each other.

Finally, we consider a non-linear Stokes problem that models the behavior of a glacier. The nonlinearity of the problem is due to the relationship between the viscosity of the fluid and its velocity, which in this context is given by Glen’s law. We propose a MHM scheme to solve the non-linear problem inspired on the MHM scheme for the linear Stokes problem previously studied.

For the situations described above, we report several numerical results which assess the performance of the method and confirm theoretical results.

# Contents

|  |      |
|--|------|
| <b>Acknowledgement</b>   | ii   |
| <b>Resumen</b>   | iii  |
| <b>Abstract</b>  | iv   |
| <b>Contents</b>  | v    |
| <b>List of Tables</b>  | viii |
| <b>List of Figures</b>   | ix   |
| <b>Introducción</b>  | 1    |
| <b>Introduction</b>  | 10   |
| <b>Notation</b>  | 20   |
| <b>1 An a posteriori error estimator for a LPS method for Navier-Stokes equations.</b> | 24   |
| 1.1 Introduction . . . . .   | 24   |
| 1.2 Model problem and preliminary results . . . . .                                    | 24   |
| 1.3 The local projection stabilized method . . . . .                                   | 27   |
| 1.4 A Hierarchical Error Estimator . . . . .   | 29   |
| 1.4.1 The Auxiliary Problem . . . . .  | 29   |
| 1.4.2 Hierarchical Error Estimator . . . . .   | 32   |
| 1.5 Numerical validation . . . . .   | 37   |
| 1.5.1 Two-dimensional analytic solution . . . . .                                      | 38   |
| 1.5.2 Three-dimensional analytic solution . . . . .                                    | 40   |
| 1.5.3 Two-dimensional lid-driven cavity problem . . . . .                              | 42   |

|          |   |           |
|----------|---|-----------|
| 1.5.4    | Flow around of a circular cylinder . . . . .  | 43        |
| 1.6      | Conclusions . . . . .   | 46        |
| <b>2</b> | <b>On a Multiscale a Posteriori Error Estimator for the Stokes and Brinkman Equations</b> | <b>47</b> |
| 2.1      | Introduction . . . . .  | 47        |
| 2.2      | Model problem and Preliminaries . . . . .   | 48        |
| 2.2.1    | Notations . . . . .   | 48        |
| 2.2.2    | Preliminar results . . . . .  | 50        |
| 2.3      | The MHM method . . . . .  | 54        |
| 2.3.1    | Characterizing the exact solution . . . . .   | 54        |
| 2.3.2    | The one-level MHM method . . . . .  | 56        |
| 2.3.3    | The two-level MHM method . . . . .  | 57        |
| 2.4      | A posteriori error analysis . . . . .   | 60        |
| 2.4.1    | The multiscale a posteriori error estimator . . . . .                                     | 60        |
| 2.4.2    | Efficiency and reliability . . . . .  | 61        |
| 2.5      | Numerical results . . . . .   | 70        |
| 2.5.1    | First strategy: Adaptivity by elements . . . . .  | 70        |
| 2.5.2    | Second strategy: Adaptivity by faces . . . . .  | 70        |
| 2.5.3    | An example with analytical solution . . . . .   | 71        |
| 2.5.4    | The 2D lid-driven cavity problem . . . . .  | 73        |
| 2.5.5    | A highly heterogeneous case . . . . .   | 75        |
| 2.6      | Appendix: Some technical lemmas . . . . .   | 78        |
| 2.7      | Conclusion . . . . .  | 83        |
| <b>3</b> | <b>A Multiscale Hybrid-Mixed Method for a nonlinear-Stokes problem in glaciology</b>      | <b>84</b> |
| 3.1      | Model problem and preliminaries . . . . .   | 85        |
| 3.1.1    | Picard iteration for the solution of the nonlinear system . . . . .                       | 86        |
| 3.2      | The one-level MHM method . . . . .  | 89        |
| 3.3      | The two-level MHM method . . . . .  | 90        |
| 3.3.1    | The two-level MHM method for a problem with only Dirichlet boundary conditions . . . . .  | 91        |
| 3.3.2    | The two-level MHM method for a problema with mixed boundary conditions . . . . .          | 92        |

|   |            |
|---|------------|
| 3.4 Numerical algorithm for the MHM method for a problem with mixed boundary conditions . . . . . | 93         |
| 3.5 Numerical experiments . . . . .   | 96         |
| 3.5.1 First example . . . . .   | 96         |
| 3.5.2 Second example . . . . .  | 99         |
| 3.6 Conclusion . . . . .  | 102        |
| <b>Concluding remarks and future work</b>   | <b>107</b> |
| <b>Bibliography</b>   | <b>107</b> |

# List of Tables

|     |  |    |
|-----|--|----|
| 1.1 | Exact error, a posteriori error estimator and effectivity index for the 2D example with analytical solution with $\nu = 1$ . . . . .   | 38 |
| 1.2 | Exact error, a posteriori error estimator and effectivity index for the 2D example with analytical solution with $\nu = 10^{-2}$ . . . . .   | 39 |
| 1.3 | Exact error, a posteriori error estimator and effectivity index for the 3D example with analytical solution with $\nu = 1$ . . . . .   | 40 |
| 1.4 | Exact error, a posteriori error estimator and effectivity index for the 3D example with analytical solution with $\nu = 10^{-2}$ . . . . .   | 41 |
| 1.5 | Position of the center of the primary vortex. The LPS results were obtained with the adaptive mesh of Figure 1.6. . . . .  | 43 |
| 1.6 | The benchmark coefficients $C_{\text{drag}}$ , $C_{\text{lift}}$ and $\Delta p$ . . . . .  | 44 |
| 2.1 | History of convergence for the Stokes problem with $\nu = 1$ , $\mathbf{u}_{H,h} \in \mathbb{P}^3(\mathcal{T}_H)^2$ , $p_h \in \mathbb{P}^3(\mathcal{T}_H)$ and $\boldsymbol{\lambda}_{H,h} \in \boldsymbol{\Lambda}_l^1$ . . . . .                        | 72 |
| 2.2 | History convergence for the Stokes problem with $\nu = 1$ , $\mathbf{u}_{H,h} \in \mathbb{P}^3(\mathcal{T}_H)^2$ , $p_h \in \mathbb{P}^3(\mathcal{T}_H)$ and $\boldsymbol{\lambda}_{H,h} \in \boldsymbol{\Lambda}_l^1$ . Here $h = H^2$ . . . . .          | 72 |
| 2.3 | History of convergence for the Stokes problem with $\nu = 10^{-2}$ , $\mathbf{u}_{H,h} \in \mathbb{P}^3(\mathcal{T}_H)^2$ , $p_h \in \mathbb{P}^3(\mathcal{T}_H)$ and $\boldsymbol{\lambda}_{H,h} \in \boldsymbol{\Lambda}_l^1$ . . . . .                  | 73 |
| 2.4 | History of convergence for the Stokes problem with $\nu = 10^{-2}$ , $\mathbf{u}_{H,h} \in \mathbb{P}^3(\mathcal{T}_H)^2$ , $p_h \in \mathbb{P}^3(\mathcal{T}_H)$ and $\boldsymbol{\lambda}_{H,h} \in \boldsymbol{\Lambda}_l^1$ . Here $h = H^2$ . . . . . | 73 |
| 3.1 | Physical parameters for the glaciär model. . . . .   | 96 |

# List of Figures

|     |  |    |
|-----|--|----|
| 0.1 | Descripción esquemática de varias escalas en un medio poroso (Figura tomada desde [44]). . . . .   | 5  |
| 0.2 | Permeabilidad de un problema 3D sobre una malla regular. El gráfico de la izquierda representa la permeabilidad 3D con un corte 2D a través del dominio, donde se realiza la simulación. El gráfico de la derecha muestra el corte 2D de la permeabilidad graficado en escala logarítmica. . . . . | 6  |
| 0.3 | Glaciar Balmaceda <sup>1</sup> , parque nacional Bernardo O'Higgins, Magallanes, Chile, septiembre 2018. . . . .   | 8  |
| 0.4 | Schematic description of various scales in porous media (figure from [44]). . .  | 15 |
| 0.5 | Permeability for a 3D model given on a regular grid. The left plot shows the 3D permeability with a 2D cut through the domain, where we do the simulation. Here, red color denotes the void spaces (vugs). The right plot shows a 2D cut with permeability plotted on a logarithmic scale. . . . . | 16 |
| 0.6 | Balmaceda glacier <sup>2</sup> , Bernardo O'Higgins national park, Magallanes, Chile, September 2018. . . . .  | 18 |
| 1.1 | Convergence history for the 2D example with analytical solution, case $\nu = 1$ (left) and the behavior of $T$ when $H$ goes to 0 (right). . . . .   | 39 |
| 1.2 | Convergence history for the 2D example with analytical solution, case $\nu = 10^{-2}$ (left) and the behavior of $T$ when $H$ goes to 0 (right). . . . .   | 39 |
| 1.3 | Convergence history for the 3D example with analytical solution, case $\nu = 1$ (left) and the behavior of $T$ when $H$ goes to 0 (right). . . . .   | 41 |
| 1.4 | Convergence history for the 3D example with analytical solution, case $\nu = 10^{-2}$ (left) and the behavior of $T$ when $H$ goes to 0 (right). . . . .   | 41 |
| 1.5 | Domain and boundary conditions for the driven cavity problem. . . . .  | 42 |
| 1.6 | Lid-driven cavity problem for $Re = 5,000$ . Adaptive mesh and streamlines. The mesh has 345,947 elements. . . . .   | 43 |

---

|  |    |
|--|----|
| 1.7 Configuration of the cylinder benchmark problem. . . . .   | 44 |
| 1.8 Initial mesh (left), final adapted mesh with 1,080,148 elements (center) and<br>a cut through the plane $z = 0.205$ (right). . . . .   | 45 |
| 1.9 Streamtracers (left) and velocity vector field (right). . . . .  | 45 |
| 1.10 Isovalues of the magnitude of the velocity field (left) and of the pressure (right). .  | 46 |
| 2.1 Two examples of $\Lambda_H$ restricted to an element $K \in \mathcal{T}_H$ . . . . .   | 56 |
| 2.2 Lid-driven cavity problem for the Stokes equation with $\mathbf{u}_h \in \mathbb{P}^2(K)^2, p_h \in \mathbb{P}^2(K), \boldsymbol{\lambda}_{H,h} \in \boldsymbol{\Lambda}_0$ and $\nu = 1$ . Second and third rows correspond, respectively, to the final step of the adaptive procedure by elements (6,216 dof) and adaptive procedure by faces (912 dof), and the first row shows the start step in both adaptive procedures. Second and third columns represent the magnitude of the velocity and pressure, respectively. . . . .                              | 74 |
| 2.3 Lid-driven cavity problem for the Brinkman equation with $\mathbf{u}_h \in \mathbb{P}^2(K)^2, p_h \in \mathbb{P}^2(K), \boldsymbol{\lambda}_{H,h} \in \boldsymbol{\Lambda}_0, \nu = 1$ and $\gamma = 10^4 \mathbf{I}$ . Second and third rows correspond, respectively, to the final step of the adaptive procedure by elements (32,337 dof) and adaptive procedure by faces (786 dof), and the first row shows the start step in both adaptive procedures. Second and third columns represent the magnitude of the velocity and pressure, respectively. . . . . | 75 |
| 2.4 Boundary conditions (left) and the permeability $\kappa$ (right) in logarithmic scale. .   | 76 |
| 2.5 Initial mesh (left) with 1,652 dof, an intermediate adapted mesh (center) with<br>3,352 dof and the final adapted mesh (right) with 7,800 dof. . . . .   | 76 |
| 2.6 Isolines of the pressure corresponding (from left to right) to the solution using<br>the initial mesh (1,652 dofs), the adaptive one (7,800 dofs), and the reference<br>solution (1,625,283 dofs), respectively. . . . .   | 77 |
| 2.7 Magnitude of velocity corresponding (from left to right) to the solution using<br>the initial mesh (1,652 dofs), the adaptive one (7,800 dofs), and the reference<br>solution (1,625,283 dofs), respectively. . . . .  | 77 |
| 3.1 Solution of Example 3.5.2 with the MHM method with $\mathbf{u}_h \in \mathbb{P}^3(K)^2, p_h \in \mathbb{P}^3(K)$ and $\boldsymbol{\lambda}_{H,h} \in \boldsymbol{\Lambda}_1^1$ , using a first-level mesh with 3077 elements, considering<br>the physical parameters given in Table 3.1 and an incline of $\alpha = 0.1^\circ$ . . . . .   | 98 |
| 3.2 Solution of Example 3.5.2 using a $P^2/P^1$ scheme considering a mesh with<br>9232 elements, considering the physical parameters given in Table 3.1 and an<br>incline of $\alpha = 0.1^\circ$ . . . . .  | 99 |



# Introducción

Las ecuaciones diferenciales parciales tienen un rol importante en muchas disciplinas, desde la aeronáutica (flujo de aire alrededor de las alas), ingeniería civil (estabilidad de puentes), geociencia (deformación de placas y procesos de subducción, flujo en hielo y casquetes glaciares), ingeniería biomédica (flujo de sangre en vasos sanguíneos, flujo de aire en cuerdas vocales), sólo por nombrar algunos. Los métodos analíticos permiten calcular soluciones sólo de problemas que no son muy complicados. Para obtener soluciones a problemas realistas es necesario disponer de métodos numéricos que permitan hallar soluciones aproximadas de los modelos. El desarrollo numérico y matemático es también motivado por la creciente necesidad de que los procedimientos para resolver los problemas sean más simples, más precisos y más eficientes. En particular, el Método de Elementos Finitos es útil cuando la geometría de los problemas es compleja, pero las soluciones que entrega se ven deterioradas por la presencia de singularidades provenientes de, por ejemplo, esquinas reentrantas, capas límite, ondas de choque o fenómenos de turbulencia. Otra familia de problemas que es difícil de simular es donde los datos del problema contienen muchas escalas espaciales, los denominados problemas multiescala. Una alternativa obvia para obtener buenas soluciones es refinar la malla completa lo suficiente pero con esto, en problemas realistas, pueden obtenerse problemas imposibles de resolver incluso en supercomputadores debido a la tremenda cantidad de memoria CPU y tiempo de procesamiento requeridos, que puede fácilmente exceder las capacidades de cómputo actuales.

El *análisis de error a posteriori* permite detectar las regiones donde la solución es menos regular lo que permite generar mallas con un buen balance entre las regiones refinadas y no refinadas tales que la precisión global es óptima. En general, para una ecuación diferencial definida en un dominio  $\Omega$  con incógnitas  $(\mathbf{u}, p)$ , las estimaciones de error a posteriori consisten en construir para cada elemento  $K$  de la malla un término calculable  $\eta_K$  llamado *estimador de error local* dependiente sólo de del tamaño de la malla  $H$ , la solución discreta calculada por el método de elementos finitos  $(\mathbf{u}_H, p_H)$  y los datos y parámetros físicos del problema, con el objetivo de poder predecir el comportamiento del error en el elemento  $K$ ,

para así construir una malla nueva la cual esté más de acuerdo con el problema físico y por ende permita obtener una mejor solución aproximada asociada a esta nueva malla. A partir de  $\eta_K$  se define un *estimador de error global*

$$\eta = \left\{ \sum_K \eta_K^2 \right\}^{1/2}.$$

El objetivo es probar que este estimador es *eficiente* y *confiable*, esto es, se busca probar que existen constantes  $C_1, C_2 > 0$ , independientes de  $H$ , tales que

$$\|(\mathbf{u} - \mathbf{u}_H, p - p_H)\| \leq C_1 \eta \quad (\dagger)$$

y

$$C_2 \eta_K \leq \|(\mathbf{u} - \mathbf{u}_H, p - p_H)|_K\|,$$

con lo que se prueba que el estimador de error es equivalente al error del método de elementos finitos. Además, la última desigualdad nos permite detectar en qué elementos se están cometiendo los errores más grandes, lo cual es fundamental para proponer una estrategia adaptativa. El procedimiento adaptativo estándar es el siguiente: Dado  $\theta \in (0, 1)$ :

1. Resolver el esquema de elementos finitos y calcular los  $\eta_K$  correspondientes a cada elemento  $K$  de la malla  $\mathcal{T}_H$ .
2. Marcar los elementos  $K$  tales que  $\eta_K \geq \theta \max_{K \in \mathcal{T}_H} \eta_K$ .
3. Calcular una nueva malla  $\mathcal{T}_H$  que refina los  $K$  marcados y repetir el proceso hasta alcanzar una tolerancia preestablecida.

En ciertos problemas, como los estudiados en esta tesis, se obtienen estimaciones para la eficiencia ( $\dagger$ ) de la forma

$$\|(\mathbf{u} - \mathbf{u}_H, p - p_H)\| \leq C_1 \eta + E(\mathbf{u}_H, p_H),$$

donde el término extra  $E(\mathbf{u}_H, p_H)$  tiene mayor orden que  $\eta$ , por lo que a partir de cierto  $H$  será despreciable al compararlo con  $\eta$  por lo que puede omitirse en la práctica. Una bibliografía parcial sobre análisis de error a posteriori puede hallarse en [6, 22, 62, 95].

Una medida de calidad del estimador  $\eta$  está dada por el *índice de efectividad global* definido por

$$E_i = \frac{\eta}{\|(\mathbf{u} - \mathbf{u}_H, p - p_H)\|}.$$

El caso óptimo es cuando el índice de efectividad es cercano a 1, es decir, cuando

$$\lim_{H \rightarrow 0} \frac{\eta}{\|(\mathbf{u} - \mathbf{u}_H, p - p_H)\|} = 1,$$

pero en la práctica, un índice global acotado es aceptable.

El primer problema que consideramos en esta tesis es el de Navier–Stokes. Estas ecuaciones, nombradas en honor a Claude–Louis Navier (1785–1836) y George Gabriel Stokes (1819–1903), describen el movimiento de fluidos viscosos y surgen de la aplicación de la segunda ley de Newton aplicada a movimientos de fluidos junto con suponer que la tensión del fluido es la suma de términos difusivos viscosos (proporcionales al gradiente de velocidad) y un término dependiente de la presión. Este problema es uno de los más desafiantes en diferentes áreas de las matemáticas y, particularmente, la comunidad de análisis numérico ha trabajado por décadas ideando métodos numéricos más eficientes y precisos para aproximar su solución. Pros y contras de estos métodos se encuentran en [49, 90, 91].

Debido a la complejidad de las ecuaciones de Navier–Stokes, es usual y necesario estudiar modelos simplificados dependiendo del fenómeno que interesa modelar. En particular, en el Capítulo 1 estudiamos la versión estacionaria de las ecuaciones de Navier–Stokes con viscosidad constante, más precisamente, el problema: Hallar una velocidad  $\mathbf{u} : \Omega \rightarrow \mathbb{R}^d$  y una presión  $p : \Omega \rightarrow \mathbb{R}$  tales que:

$$\left\{ \begin{array}{ll} -\nu \Delta \mathbf{u} + (\nabla \mathbf{u}) \mathbf{u} + \nabla p = \mathbf{f} & \text{en } \Omega, \\ \nabla \cdot \mathbf{u} = 0 & \text{en } \Omega, \\ (\text{más condiciones de borde}), \end{array} \right. \quad (0.1)$$

donde la viscosidad del fluido, el término fuente  $\mathbf{f} \in L^2(\Omega)^d$  y las condiciones de borde son dados. De ahora en adelante  $\Omega$  representa un subconjunto (dominio) de  $\mathbb{R}^d$ , con  $d = 2, 3$ . Nuestro primer objetivo es desarrollar un análisis a posteriori al esquema LPS (Local Projection Stabilized) introducido en [15] para las ecuaciones de Navier–Stokes (0.1) tanto para 2D como para 3D. Los esquemas estabilizados para ecuaciones de fluidos tiene una larga historia desde que fueron introducidos por primera vez en el trabajo de Hughes y Brooks [33, 47, 60]. La idea principal detrás de estos métodos es añadir “estabilidad” a la solución numérica del problema. Por otra parte, los métodos estabilizados también ayudan a disminuir inestabilidades no físicas provenientes de la presencia de capas límites, por ejemplo, cuando la advección es dominante con respecto a la viscosidad.

Desafortunadamente, el método LPS no es fuertemente consistente para espacios finitos de bajo orden, lo que no permite usar técnicas estándar como las descritas en [93] para

desarrollar un estimador de error a posteriori basado en el cálculo de normas de términos residuales, debido a la dificultad de obtener términos volumétricos y superficiales al demostrar la confiabilidad del estimador. Por esta razón, en el Capítulo 1 consideramos otro tipo de estimación del error, llamado *estimación jerárquica*, el cual en la práctica es más cara de calcular que la residual, pero con la ventaja de que normalmente produce una mejor aproximación del error real, y presenta un mejor índice de efectividad. Esta estrategia de análisis a posteriori fue introducida por primera vez por Bank y otros colaboradores en [23, 24]. La idea es enriquecer los espacios de elementos finitos con funciones de tipo “burbuja” para mejorar la calidad del estimador de error. Esta estimación jerárquica fue extendida en [13] para las ecuación de advección-difusión-reacción, en [9] al problema de Stokes generalizado y en [14] para ecuaciones de Navier-Stokes estacionarias en 2D usando un esquema SUPG. Nuestro enfoque jerárquico permite superar la falta de consistencia del método LPS, con el precio de añadir un término de alto orden al estimador de confiabilidad.

Los contenidos del Capítulo 1 dieron origen a la siguiente publicación:

- [16] Rodolfo Araya and Ramiro Rebollo. An a posteriori error estimator for a LPS method for Navier-Stokes equations. *Appl. Numer. Math.*, 127:179–195, 2018.

En el Capítulo 2 consideramos las ecuaciones de Stokes y Brinkman, que consisten en: Hallar una velocidad  $\mathbf{u} : \Omega \rightarrow \mathbb{R}^d$  y una presión  $p : \Omega \rightarrow \mathbb{R}$  tales que

$$\begin{aligned} -\nu \Delta \mathbf{u} + \boldsymbol{\gamma} \mathbf{u} + \nabla p &= \mathbf{f} \quad \text{en } \Omega, \\ \nabla \cdot \mathbf{u} &= 0 \quad \text{en } \Omega, \end{aligned} \tag{0.2}$$

(más condiciones de borde).

Aquí  $\nu \in \mathbb{R}^+$  es el término difusivo,  $\boldsymbol{\gamma} \in L^\infty(\Omega)^{d \times d}$  es un tensor que puede contener características multiescala del medio, y  $\mathbf{f} \in L^2(\Omega)^d$  es un término fuente.

En muchos problemas científicos y de ingeniería es fundamental considerar las distintas escalas presentes, como por ejemplo, en ingeniería de materiales [87, 88, 98], ingeniería biométrica [97], física aplicada [3], geofísica espacial [99], geociencia [66, 69], meteorología [34], neurociencia [72], procesamiento de señales [2] y química aplicada [20], sólo por nombrar algunos. Específicamente, las ecuaciones de Stokes y Brinkman son ampliamente aceptadas como modelo matemático de fluidos en ambientes heterogéneos, por ejemplo, reservorios y filtración en medios porosos [52, 67]. La figura 0.1 ilustra la naturaleza multiescala de la conductividad en un modelo de subsuelo típico. Aquí se ilustra que la información en la escala a nivel poro es fundamental para comprender la conductividad en el modelo. Sin

embargo, para obtener un modelo que describa la filtración de un fluido en un medio poroso es igualmente importante entender las características en escalas más grandes.

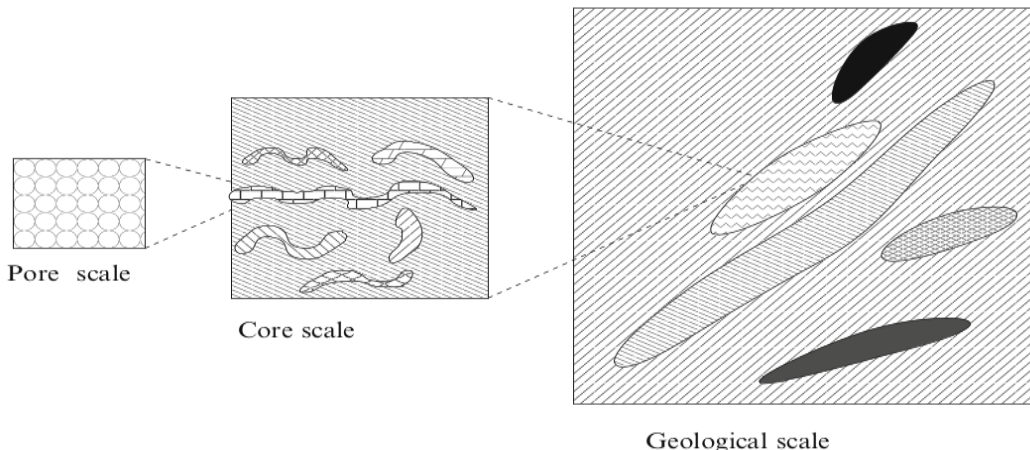


Figure 0.1: Descripción esquemática de varias escalas en un medio poroso (Figura tomada desde [44]).

Cuando se trabaja con procesos multiescala, es frecuente el caso cuando los datos de entrada de las propiedades de los materiales no está disponible en todos los puntos de la malla. Por ejemplo, cuando se necesita estudiar el flujo de fluidos en el subsuelo, las propiedades del subsuelo en la escala de los poros no está disponible en todos los puntos del reservorio. En este caso, una alternativa es usar un *elemento de volumen representativo* que contenga la información escencial sobre la heterogeneidad. La figura 0.2, correspondiente al Ejemplo 2.5.5, representa un prototipo de reservorio realista. Este dato es parte de el proyecto SPE10 [38]. Este modelo tiene una geometría sencilla, sin estructuras en la superficie ni fracturas. La escala más fina es descrita por una malla cartesiana regular. El modelo tiene dimensiones 1200x2200x170 (ft). El tamaño de las escalas más pequeñas corresponden a celdas de dimensión is 20x10x2 (ft). Para resolver el problema mediante métodos numéricos clásicos, se requiere disponer de mallas lo suficientemente finas como para capturar las escalas pequeñas.

En problemas multiescala, la presión y velocidad exactas puede presentar variaciones altas tanto debido a altas heterogeneidades o singularidades de los coeficientes físicos, o cuando el medio presenta cavidades o fracturas, las cuales pueden provocar grandes alteraciones en el campo de flujo. Técnicas estándar de elementos finitos deben utilizar mallas muy finas para poder capturar el comportamiento multiescala de la velocidad y presión, significa trabajar con grandes sistemas lineales. Este hecho hace simulaciones realistas tridi-

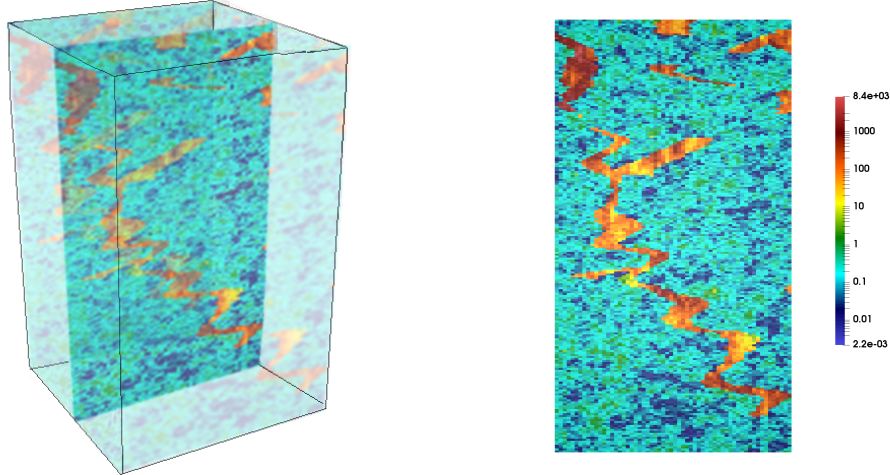


Figure 0.2: Permeabilidad de un problema 3D sobre una malla regular. El gráfico de la izquierda representa la permeabilidad 3D con un corte 2D a través del dominio, donde se realiza la simulación. El gráfico de la derecha muestra el corte 2D de la permeabilidad graficado en escala logarítmica.

mensionales puedan ser prohibitivas incluso en computadores paralelos modernos.

Los métodos de elementos finitos multiescala se han convertido en una alternativa atractiva para simular fenómenos complejos en mallas gruesas. Detrás de estos métodos está la idea fundamental de usar funciones base que capturan el comportamiento multiescala de las estructuras. Tales bases son solución de problemas locales que son similares a la original, y de este modo incorpora los coeficientes reales y elementos de la geometría en su diseño. Esta estrategia fue primero propuesta y analizada en [19] para el problema de Poisson unidimensional y luego extendida a mayores dimensiones en [58]. A partir de ahí se han propuesto otras variantes para problemas de flujos de fluidos como el Método Multiescala Heterogéneo (HMM, por su nombre en inglés) [96], Método Multiescala Variacional (VMS, por su nombre en inglés) [59], el Método de Elementos Finitos Generalizado Multiescala [43], y el Método de Descomposición Ortogonal Localizada (LOD, por sus nombre en inglés) [73], por mencionar algunos. Para algunos de estos métodos se ha desarrollado un análisis a posteriori, ver, por ejemplo, [1, 21, 36, 57, 61, 78, 80, 89] y sus referencias.

El Método Híbrido-Mixto Multiescala (MHM, por su nombre en inglés) pertenece a la familia de métodos multiescala. Inicialmente propuesto para el modelo de Darcy en [55], el método MHM produce soluciones superconvergentes y provee estimaciones de error a posteriori basado en lo que ocurre en el esqueleto de la malla (c.f. [11]). El método MHM parte aplicando una hibridización [81] a la formulación débil original. La estrategia consiste en caracterizar la solución exacta de la formulación híbrida como solución de un problema

equivalente que consiste en problemas locales y un problema global definido sobre el esqueleto de una malla gruesa. Luego, la discretización desacopla los problemas locales y el global utilizando los problemas locales, que son independientes unos de otros, para construir las funciones base con la información multiescala. Además, el método MHM ha sido utilizado para aproximar la solución del problema reacción-advección-difusión singularmente perturbado [56], elasticidad lineal [54] y ecuaciones de Maxwell [68]. Es importante mencionar que la estrategia de hibridización es utilizada también en el problema discreto para desarrollar el método de descomposición de dominios [5, 31, 32].

Proponemos un nuevo estimador a posteriori del tipo residual para el método MHM aplicado al problema de Stokes/Brinkman, considerando el esquema introducido en [12]. El estimador de error considera ambos niveles del método:  $\eta_1$  relativo al salto sobre las caras del esqueleto de la velocidad discreta, similar al que aparece en trabajos previos [11, 54], y  $\eta_2$  proveniente del error cometido al aproximar la solución de los problemas locales. Las demostraciones de eficiencia y confiabilidad de  $\eta_1$  son muy similares a las desarrolladas en [11, 54] para las ecuaciones de transporte y elasticidad, respectivamente. En esta tesis extendemos el análisis para los problemas Stokes/Brinkman. La demostración de la eficiencia de  $\eta_2$  depende de la elección del método en el segundo nivel. Aquí elegimos el método de elementos finitos estabilizado USFEM [25], el cual permite igual orden de interpolación para la velocidad y presión, por lo cual podemos seguir las demostraciones clásicas en el contexto de a posteriori para métodos estabilizados, por ejemplo el trabajo [94]. Esto nos permite demostrar que el estimador que proponemos es localmente eficiente y confiable. Además, usamos la información del segundo nivel del estimador para dirigir el refinamiento sobre el esqueleto de la malla y para seleccionar las mallas del segundo nivel en cada paso del algoritmo adaptativo. Lo anterior es fundamental para asegurar la superconvergencia. El estimador a posteriori propuesto es, hasta donde sabemos, el primero para el método MHM que considera la influencia del error de aproximación proveniente de las soluciones de los problemas locales.

Los convenidos del Capítulo 2 dieron origen a la siguiente publicación (enviada):

- [17] R. Araya, R. Rebollo, and F. Valentin. A posteriori analysis of the Multiscale Hybrid-Mixed method for Brinkman problem. *IMA J. Numer. Anal.*, (submitted).

Finalmente, en el Capítulo 3 estudiamos un modelo que describe el flujo de glaciares. El término glaciar se refiere a todos los cuerpos de hielo creados por la acumulación de nieve, por ejemplo, glaciares de montaña, casquetes glaciares, hielo continental y plataformas de hielo.



Figure 0.3: Glaciar Balmaceda<sup>4</sup>, parque nacional Bernardo O'Higgins, Magallanes, Chile, septiembre 2018.

El hielo en los glaciares es un fluido en movimiento por lo que su movimiento es descrito mediante un campo de velocidades  $\mathbf{u}$  (m/s). Luego, podemos modelarlo utilizando las ecuaciones de the Navier–Stokes

$$\left\{ \begin{array}{ll} \rho_{\text{ice}}(\mathbf{u}_t + (\nabla \mathbf{u}) \mathbf{u}) = -\nabla p + \nabla \cdot (\nu \nabla \mathbf{u}) + \mathbf{f}, & \text{(balance de tensiones)} \\ \nabla \cdot \mathbf{u} = 0, & \text{(incompresibilidad)} \\ \text{(más condiciones de borde)}, & \end{array} \right.$$

donde  $\nu > 0$  es la viscosidad del fluido (Pa s),  $p$  es la presión del fluido (Pa), y la función  $\mathbf{f}$  es un dato dato que en este contexto usualmente es  $\mathbf{f} = \rho_{\text{ice}} g \hat{\mathbf{k}}$ , donde  $\rho_{\text{ice}}$  es la densidad del hielo ( $\text{kg/m}^3$ ),  $g$  es la constante gravitacional ( $\text{m/s}^2$ ) y  $\hat{\mathbf{k}}$  es un vector unitario que apunta al centro de la tierra.

Note que  $\mathbf{u}_t + (\nabla \mathbf{u}) \mathbf{u}$ , el término en el lado izquierdo de la ecuación de balance de tensiones, es una aceleración y el término del lado derecho es la tensión total, por lo que esta ecuación corresponde a la segunda ley de Newton. Dado que el hielo es un fluido “lento”, se tiene que  $\mathbf{u}_t + (\nabla \mathbf{u}) \mathbf{u} \approx 0$ , lo que implica que las fuerzas (tensiones) de incercia son despreciables, obteniéndose las ecuaciones de Stokes clásicas

$$\left\{ \begin{array}{l} -\nabla \cdot (\nu \nabla \mathbf{u}) + \nabla p = \mathbf{f}, \\ \nabla \cdot \mathbf{u} = 0, \\ \text{(más condiciones de borde)}. \end{array} \right.$$

---

<sup>4</sup>Agradecimientos a Daniel Rebolledo Cormack por la fantástica foto.

Sin embargo, el hielo también presenta un adelgazamiento por cizalladura donde tensiones grandes implican viscosidades pequeñas. Luego, la viscosidad  $\nu$  no es constante. La ecuación más utilizada para representar la viscosidad en el contexto de glaciología es la denominada ley de Glen [70, 77]

$$\nu(|\nabla \mathbf{u}|) = \frac{\alpha}{2} |\nabla \mathbf{u}|^{\beta-2}, \quad (0.3)$$

donde  $\beta \in (1, 2]$  y la función  $\alpha(\mathbf{x}) \in L^\infty(\Omega)$  son dadas, con  $0 < \alpha_0 \leq \alpha(\mathbf{x})$  para algún  $\alpha_0$ . Note que la ley de Glen es una función lineal cuando  $\beta = 2$ , el cual es precisamente el problema de Stokes lineal estudiado en el Capítulo 2.

Desde el punto de vista físico, el problema de Stokes considerando el tensor de deformación  $\varepsilon(\mathbf{v}) := \frac{1}{2}(\nabla \mathbf{v} + \nabla \mathbf{v}^T)$  en vez de  $\nabla \mathbf{u}$  es también importante. Luego, el problema modelo que consideramos en el Capítulo 3 es el siguiente: *Hallar una velocidad  $\mathbf{u} : \Omega \rightarrow \mathbb{R}^d$  y una presión  $p : \Omega \rightarrow \mathbb{R}$  tales que*

$$\left\{ \begin{array}{l} \nabla \cdot (-\nu(|\mathbf{D}(\mathbf{u})|) \mathbf{D}(\mathbf{u}) + p \mathbf{I}) = \mathbf{f} \quad \text{en } \Omega, \\ \nabla \cdot \mathbf{u} = 0 \quad \text{en } \Omega, \\ (\text{más condiciones de borde}), \end{array} \right. \quad (0.4)$$

donde  $\mathbf{I}$  denota la matriz identidad de dimensión  $d$  y el operador  $\mathbf{D}$  representa el gradiente

$$\mathbf{D}(\mathbf{v}) := \nabla \mathbf{v}$$

o el tensor de deformación

$$\mathbf{D}(\mathbf{v}) := \varepsilon(\mathbf{v}).$$

Los datos del problema son la viscosidad  $\nu : \mathbb{R}^+ \rightarrow \mathbb{R}$  dada por la ley de Glen (0.3) y la fuerza de cuerpo  $\mathbf{f} = \rho_{\text{ice}} g \hat{\mathbf{k}}$ .

El problema (0.4) es el típico modelo de un glaciar, habiendo muchos resultados teóricos y análisis numéricos disponibles en la literatura (vea, por ejemplo, [37, 65, 76]) motivados por la creciente necesidad de procedimientos más simples, más precisos y más eficientes. Los problemas geológicos, como los modelos de glaciares, usualmente presentan dominios con fracturas y zonas de permeabilidad, en las cuales se puede presentar un comportamiento multiescala tanto de los datos como de la solución, por lo que el método MHM es una técnica prometedora en este contexto. Para una discusión más profunda sobre el modelamiento de glaciares y distintas variantes puede revisar [41, 74].

Hasta donde sabemos, éste es el primer trabajo donde se presenta un algoritmo basado en el método MHM aplicado a problemas no lineales. La implementación numérica de los

métodos presentados en esta tesis fueron completamente desarrollados en Fortran 90/95, y para resolver los sistemas lineales utilizamos los solvers MKL PARDISO [84] y MUMPS [7, 8]. Las mallas adaptadas 2D y 3D fueron generadas con Triangle [85] y Tetgen [86], respectivamente. Los gráficos de las soluciones fueron generados con Paraview [18].

# Introduction

Partial differential equations have an important role in many fields, from airplane industry (air flows around a wing), civil engineering (stability of bridges), geoscience (plate deformation and subduction processes, flow of ice in glaciers and ice sheets, petroleum reservoir), biomedical engineering (blood flow in vessels, air flow in vocal cords), just to name a few. Analytical methods are able to compute solutions only for simple problems. In order to obtain solutions to realistic problems, it is mandatory to provide of numerical methods that allow obtaining approximate solutions of the models. Developing theoretical and numerical analyses are also motivated by the increasing need for simpler, more accurate, and more efficient procedures to solve problems. In particular, the Finite Elements Method is useful when the geometry of the problem is complex, but the numerical solution is deteriorated by the presence of singularities arising from, for example, re-entrant corners, interior or boundary layers, sharp shock-like fronts or turbulence phenomena. Another family of problems that is difficult to simulate is when the solution or data of the problem contains many spatial scales, called *multiscale problems*. An obvious alternative to obtain good solutions is to refine the mesh, however, in realistic problems, it may be impossible to solve such problems even in supercomputers due to the tremendous amount of computer memory and CPU time required, that can easily exceed the limit of today's computing resource.

The *a posteriori error analysis* allows detecting the regions where the solution is less regular, and then to generate meshes with good balance between the refined and unrefined regions such that the global precision is optimal. In general, for a differential equation defined in a domain  $\Omega$  with unknown  $(\mathbf{u}, p)$ , the a posteriori error analysis consists of computing, for each element  $K$  of the mesh  $\mathcal{T}_H$ , a calculable term  $\eta_K$  called *local error estimator* it depends only on the mesh size  $H$ , the discrete solution calculated by the finite element method  $(\mathbf{u}_H, p_H)$  and the data and physical parameters of the problem. The aim is to predict the behavior of the error in each element  $K$ , and to calculate a better approximate solution by adapting the mesh.

From  $\eta_K$  we define the *global error estimator* as follow

$$\eta = \left\{ \sum_K \eta_K^2 \right\}^{1/2}.$$

The goal is to prove that this estimator is *reliable* and *efficient*, that is, there exist constants  $C_1, C_2 > 0$ , independent of  $H$ , such that

$$\|(\mathbf{u} - \mathbf{u}_H, p - p_H)\| \leq C_1 \eta \quad (\dagger)$$

y

$$C_2 \eta_K \leq \|(\mathbf{u} - \mathbf{u}_H, p - p_H)|_K\|.$$

Note that this proves that the error estimator is equivalent to the error of the finite element method. Furthermore, last inequality allows us to detect the elements where the error is important, which is fundamental to propose an adaptive strategy. The standard adaptive procedure is the following: Given  $\theta \in (0, 1)$ :

1. Solve the finite element scheme and calculate, for each element  $K$  of the mesh  $\mathcal{T}_H$ , the term  $\eta_K$ .
2. Mark the elements  $K$  such that  $\eta_K \geq \theta \max_{K \in \mathcal{T}_H} \eta_K$ .
3. Calculate a new mesh  $\mathcal{T}_H$  that refines the marked  $K$  and repeat the procedure until reaching a pre-established tolerance.

In some problems, like the ones considered in this thesis, the efficiency estimation  $(\dagger)$  has the form

$$\|(\mathbf{u} - \mathbf{u}_H, p - p_H)\| \leq C_1 \eta + E(\mathbf{u}_H, p_H)$$

where the extra term  $E(\mathbf{u}_H, p_H)$  is of higher order than  $\eta$ . As such from some  $H$  the term  $E(\mathbf{u}_H, p_H)$  is negligible compared with  $\eta$ , so it can be omitted in practice. Bibliography on the posterior error analysis can be found, for instance, in: [6, 22, 62, 95].

A measure of the quality of the estimator  $\eta$  is given by the *global effectivity index*, defined as follows

$$E_i = \frac{\eta}{\|(\mathbf{u} - \mathbf{u}_H, p - p_H)\|},$$

which is searched such that it is as close to as possible to one, e.g.

$$\lim_{H \rightarrow 0} \frac{\eta}{\|(\mathbf{u} - \mathbf{u}_H, p - p_H)\|} = 1.$$

Nevertheless, in the practice, a bounded index, constant and not equal to one, is acceptable.

The first problem that we consider in this thesis is the Navier–Stokes problem. These equations, named after Claude–Louis Navier (1785–1836) and George Gabriel Stokes (1819–1903), describe the motion of viscous fluid substances and arise from applying Newton’s second law to fluid motion together with the assumption that the stress in the fluid is the sum of a diffusing viscous term (proportional to the gradient of velocity) and a pressure term—hence describing viscous flows. This problem is one of the most challenging problems in different areas of mathematics and, particularly, the numerical analysis community has been working for decades in developing accurate and efficient numerical methods to approximate its solution. See pros and cons in ([49, 90, 91].

The importance of studying these equations are its several applications, for example, models of weather, ocean currents, water flow in a pipe and how air flows around a wing, and this way, help with the design of aircraft and cars, the study of blood flow, the design of power stations, the analysis of pollution, and many other things.

Due to the complexity of the Navier–Stokes equations, it is usual and necessary to study simplified models depending on the phenomenon modeled. In particular, in Chapter 1 we study the stationary version of Navier–Stokes equations with constant viscosity, namely, the problem: Find a velocity  $\mathbf{u} : \Omega \rightarrow \mathbb{R}^d$  and a pressure  $p : \Omega \rightarrow \mathbb{R}$  such as

$$\left\{ \begin{array}{ll} -\nu \Delta \mathbf{u} + (\nabla \mathbf{u}) \mathbf{u} + \nabla p = \mathbf{f} & \text{in } \Omega, \\ \nabla \cdot \mathbf{u} = 0 & \text{in } \Omega, \\ \text{(plus boundary conditions),} \end{array} \right. \quad (0.5)$$

where the fluid viscosity  $\nu > 0$ , the force field  $\mathbf{f} \in L^2(\Omega)^d$  and the boundary conditions are given. Hereafter,  $\Omega$  represents a subset (domain) of  $\mathbb{R}^d$ , with  $d = 2, 3$ . Our first goal is to develop an a posteriori analysis for a Local Projection Stabilized (LPS) scheme introduced in [15] for the Navier–Stokes equations (0.5) both in 2D as in 3D. Stabilized schemes for fluid equations have a long history since the first works of Hughes and Brooks [33, 47, 60]. The main idea behind these methods is to add “stability” to the numerical solution of the problems preserving consistency allowing the use of equal order of polynomials both for velocity and pressure, which is a very appreciated property at the moment of the numerical implementation. On the other hand, stabilized methods also help to diminish non-physical instabilities coming from inner or boundary layers present, for example, when the advection is dominant with respect to viscosity.

Unfortunately, the LPS method is not strongly consistent for low-order finite spaces, not allowing us to use the standard techniques, as those described in [93], to develop an

a posteriori error estimate based in the computations of the norm of the residual terms, due to the difficulty to obtain volumetric and edge residuals in the reliability proof. For this reason in Chapter 1 we consider another type of error estimator, called *hierarchical estimator*, which in practice is more expensive to compute than the residual, but with the advantage that usually yields an approximation of the true approximation error, with a better effectivity index. This kind of a posteriori error estimator was first introduced by Bank and collaborators in [23, 24]. The idea is to enrich the standard finite element subspace with some “bubble” like functions to improve the quality of the error estimator. This hierarchical approach was extended in [13] to the advection-diffusion-reaction equation, in [9] to the generalized Stokes equations and later to the 2D steady incompressible Navier–Stokes equations, using a SUPG scheme, in [14]. With our hierarchical approach, we were able to overcome the lack of consistency of the LPS method, at the price of adding a higher order term to the reliability estimate.

The contents of Chapter 1 gave rise to the following paper:

- [16] Rodolfo Araya and Ramiro Rebolledo. An a posteriori error estimator for a LPS method for Navier-Stokes equations. *Appl. Numer. Math.*, 127:179?195, 2018.

In Chapter 2 we consider the Stokes and Brinkman equations, that consists of: Finding a velocity  $\mathbf{u} : \Omega \rightarrow \mathbb{R}^d$  and a pressure  $p : \Omega \rightarrow \mathbb{R}$  such that

$$\begin{aligned} -\nu \Delta \mathbf{u} + \boldsymbol{\gamma} \mathbf{u} + \nabla p &= \mathbf{f} \quad \text{in } \Omega, \\ \nabla \cdot \mathbf{u} &= 0 \quad \text{in } \Omega, \end{aligned} \tag{0.6}$$

(plus boundary conditions).

Here  $\nu \in \mathbb{R}^+$  is the diffusion coefficient,  $\boldsymbol{\gamma} \in L^\infty(\Omega)^{d \times d}$  is a tensor which may contains multiscale features of the media, and  $\mathbf{f} \in L^2(\Omega)^d$  is a body force and the function.

A broad range of scientific and engineering problems involve multiple scales like, for example, material science [87, 88, 98], computational hemodynamics [97], applied physics [3], spatial geophysics [99], geoscience [66, 69], meteorology [34], neuroscience [72], signal processing [2], and applied chemistry [20], just to name a few. Specifically, the Stokes and Brinkman equations are widely accepted in the mathematical modeling of flows in heterogeneous fields, e.g., vuggy carbonate reservoirs and low porosity filtration devices [52, 67]. The figure 0.4 illustrates the multiscale nature of the conductivity in typical subsurface problems. Here, we illustrate that pore scale information is needed for understanding the conductivity of the core sample, however, it is also essential to understand the large-scale

features of the media in order to build a comprehensive model of porous media. More complicated situations in geomodeling can occur. When dealing with multiscale processes,

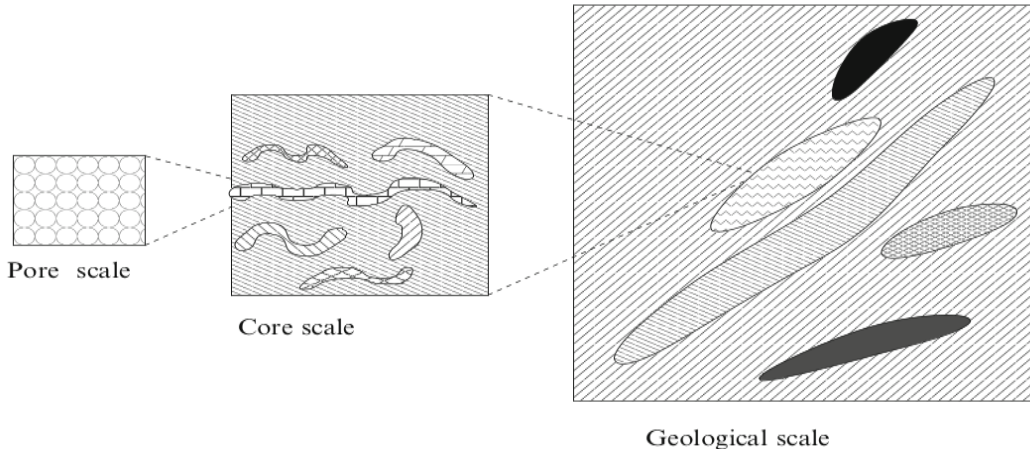


Figure 0.4: Schematic description of various scales in porous media (figure from [44]).

it is often the case that input information about processes or material properties is not available everywhere. For example, if one would like to study the fluid flows in a subsurface, then the subsurface properties at the pore scale are not available everywhere in the reservoir. In this case, one can use *representative volume element* which contains essential information about the heterogeneities. Figure 0.5, corresponding to the Example 2.5.5, represents a quite realistic prototype of a reservoir. This data is part of the Comparative Solution Project SPE10 [38].

The model has a simple geometry, with no top structure or faults. At the fine geological model scale, the model is described on a regular cartesian grid. The model dimensions are 1200x2200x170 (ft). The fine-scale cell size is 20x10x2 (ft). To solve this problem through classical numerical methods, we require to refine the mesh enough to capture the small scales.

In multiscale problems, exact pressure and velocity may show highly changing behaviors either due to highly heterogeneous or singularly perturbed physical coefficients, or when the media presents cavities and fractures as those structures can dramatically change the flow field. Standard finite element methods must rely on very fine meshes to capture such multiscale features of the velocity and pressure solutions, which yields to costly linear systems. This fact makes realistic three-dimensional simulations prohibitive even on modern parallel computers.

Multiscale finite element methods became an attractive alternative to simulate complex

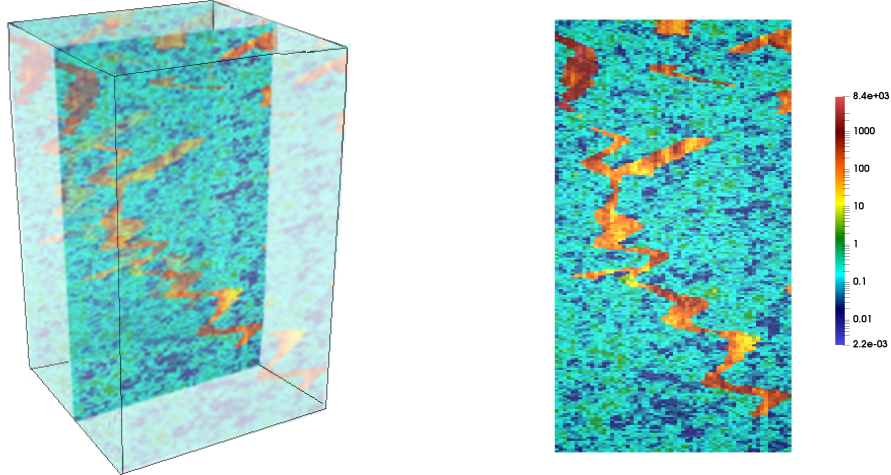


Figure 0.5: Permeability for a 3D model given on a regular grid. The left plot shows the 3D permeability with a 2D cut through the domain, where we do the simulation. Here, red color denotes the void spaces (vugs). The right plot shows a 2D cut with permeability plotted on a logarithmic scale.

phenomena on coarse meshes. Behind the multiscale methods is the fundamental idea that base functions can upscale unresolved multiscale structures. Such a basis satisfies local problems that resemble the original one, and then, they incorporate real coefficients and element's geometry in their design. This strategy was first proposed and analyzed in [19] for a one-dimensional Poisson problem and further extended to higher dimensions in [58]. Since, several variants of it have been proposed for fluid flow problems as the Heterogeneous Multiscale method (HMM) [96], the Variational Multiscale method (VMS) [59], the Generalized Multiscale finite element method [43], and the Localized Orthogonal Decomposition method (LOD) [73], to mention a few. For some of those methods a posteriori error analysis is provided, see for instance [1, 21, 36, 57, 61, 78, 80, 89] and the references therein.

The Multiscale Hybrid-Mixed (MHM) method is a member of the family of multiscale methods. Initially proposed for the Darcy model in [55], the MHM method yields superconvergent solutions and provides a face-based a posteriori error estimates which drive the adaptivity process (c.f. [11]). The MHM method is a byproduct of the primal hybridization of the original weak formulation analyzed in [81]. The strategy consists of characterizing, first, the exact solution of the hybrid formulation as the solution of an equivalent local-global problem. Then, discretization uncouples local and global problems making the (independent) local problems responsible for the computation of the multiscale base functions. The global problem, defined on the skeleton of the coarse partition, responds for the computa-

tions of degrees of freedom. Also, the MHM method can be used to approximate the solution of singularly perturbed reactive-advection-diffusive problems [56], linear elasticity [54] and Maxwell equations [68]. It is important to mention that the hybridization strategy has also been used at the discrete level to develop domain decomposition methods (c.f. [5, 31, 32]).

We propose a new residual a posteriori error estimator for the MHM method applied to the Stokes/Brinkman problem. It accounts for the multi-level numerical approximation of the method presented in [12]. Indeed, the error indicator has two-levels of contributions:  $\eta_1$  related to the jump of the discrete velocity on the skeleton of the first-level mesh, similar to those that appear in previous works (see [11, 54], for instance), and  $\eta_2$  coming from the approximation error of the solutions at the local problems. The proofs of efficiency and reliability of  $\eta_1$  follow closely the strategy presented in [11, 54] for the transport and elasticity equations, respectively. Here, we extend it to cope with mixed Stokes/Brinkman problems. The proof of the efficiency of  $\eta_2$  depends on the choice of the second-level solver. Here, we chose the stabilized finite element method USFEM [25], which allow equal-order interpolations for the pressure and velocity, and then, we revisit the proof of efficiency proposed in the classic work [94] in the context of the MHM methodology. As a result, we prove that the new multiscale a posteriori error estimator is locally efficient and reliable. Also, we use the two-level information of the error estimator to drive skeleton mesh refinement and to select appropriate independent second-level meshes. The latter is fundamental to secure MHM's super-convergence. The proposed a posteriori error estimator is, up to our knowledge, the first for the MHM method to leverage the approximation error coming from the second-level solutions.

The contents of Chapter 2 gave rise to the following (submitted) paper:

- [17] R. Araya, R. Rebollo, and F. Valentin. A posteriori analysis of the Multiscale Hybrid-Mixed method for Brinkman problem. *IMA J. Numer. Anal.*, (submitted).

Finally, in Chapter 3 we apply the MHM to a model describing the flow of ice in glaciers and ice sheets.

The term glacier refers to all bodies of ice created by the accumulation of snowfall, e.g., mountain glaciers, ice caps, continental ice sheets, and ice shelves.



Figure 0.6: Balmaceda glacier<sup>6</sup>, Bernardo O’Higgins national park, Magallanes, Chile, September 2018.

Ice in glaciers is a moving fluid, so we describe its motion by a velocity field  $\mathbf{u}$  (m/s). We adopt the Navier–Stokes equations as the model:

$$\left\{ \begin{array}{ll} \rho_{\text{ice}}(\mathbf{u}_t + (\nabla \mathbf{u}) \mathbf{u}) = -\nabla p + \nabla \cdot (\nu \nabla \mathbf{u}) + \mathbf{f}, & \text{(stress balance)} \\ \nabla \cdot \mathbf{u} = 0, & \text{(incompressibility)} \\ \text{(plus boundary conditions),} & \end{array} \right.$$

where  $\nu > 0$  is the viscosity of the fluid (Pa s),  $p$  is the pressure of the fluid (Pa), and the function  $\mathbf{f}$  is a given data that in this context usually is  $\mathbf{f} = \rho_{\text{ice}} g \hat{\mathbf{k}}$ , where  $\rho_{\text{ice}}$  is the density of the ice ( $\text{kg/m}^3$ ),  $g$  is the gravity constant ( $\text{m/s}^2$ ) and  $\hat{\mathbf{k}}$  the unit vector pointing to the center of the earth.

Note that  $\mathbf{u}_t + (\nabla \mathbf{u}) \mathbf{u}$ , the left-hand term in the stress balance equation, is an acceleration and the right-hand term is the total stress, and so this equation represents the Newton’s second law. Since ice is a “slow” fluid, which means that  $\mathbf{u}_t + (\nabla \mathbf{u}) \mathbf{u} \approx 0$ , then it implies that the forces (stresses) of inertia are negligible, obtaining the classical Stokes equations

$$\left\{ \begin{array}{l} -\nabla \cdot (\nu \nabla \mathbf{u}) + \nabla p = \mathbf{f}, \\ \nabla \cdot \mathbf{u} = 0, \\ \text{(plus boundary conditions).} \end{array} \right.$$

However, ice is also a shear-thinning fluid with a specific kind of nonlinearly-viscous (“non-Newtonian”) behavior in which larger strain rates imply smaller viscosity. The viscosity  $\nu$

---

<sup>6</sup>Thanks to Daniel Rebolledo Cormack for the beautiful photo.

is therefore not constant. The most widely used flow relation for glacier ice is given by the Glen's law [70, 77]

$$\nu(|\nabla \mathbf{u}|) = \frac{\alpha}{2} |\nabla \mathbf{u}|^{\beta-2} \quad (0.7)$$

where  $\beta \in (1, 2]$  and the function  $\alpha(\mathbf{x}) \in L^\infty(\Omega)$  are given, with  $0 < \alpha_0 \leq \alpha(\mathbf{x})$  for some  $\alpha_0$ . Note that Glen's law becomes linear when  $\beta = 2$ , which is precisely the linear Stokes problem studied in Chapter 2.

From a physical point of view, the Stokes model considering the strain tensor  $\varepsilon(\mathbf{v}) := \frac{1}{2}(\nabla \mathbf{v} + \nabla \mathbf{v}^T)$  instead of  $\nabla \mathbf{u}$  is also important. Then, the model problem that we consider in this chapter is the following: *Find a velocity  $\mathbf{u} : \Omega \rightarrow \mathbb{R}^d$  and a pressure  $p : \Omega \rightarrow \mathbb{R}$  such that*

$$\left\{ \begin{array}{l} \nabla \cdot (-\nu(|\mathbf{D}(\mathbf{u})|) \mathbf{D}(\mathbf{u}) + p \mathbf{I}) = \mathbf{f} \quad \text{in } \Omega \\ \nabla \cdot \mathbf{u} = 0 \quad \text{in } \Omega \\ \text{(plus boundary conditions)} \end{array} \right. \quad (0.8)$$

where  $\mathbf{I}$  denotes the identity matrix of size  $d$  and the operator  $\mathbf{D}$  represents the gradient

$$\mathbf{D}(\mathbf{v}) := \nabla \mathbf{v}$$

or the strain tensor

$$\mathbf{D}(\mathbf{v}) := \varepsilon(\mathbf{v}).$$

The known data are  $\mathbf{g} \in H^{-1/2}(\Omega)$ , the viscosity  $\nu : \mathbb{R}^+ \rightarrow \mathbb{R}$  given by the Glen's law (0.7) and the body force  $\mathbf{f} = \rho_{\text{ice}} g \hat{\mathbf{k}}$ .

Problem (0.8) is the typical glacier model, and several theoretical and numerical analyses are available in the literature (see, e.g., [37, 65, 76]) motivated by increasing need for simpler, more accurate, and more efficient procedures to solve it. Geological problems, such as glacier models, usually present fractures and permeability zones, which can have a multiscale behavior of the data or solution or boundary layers, and then the MHM method is a promising technique in this context. We refer to [41, 74] for a more in-depth physical discussion of this model and its variants, as well as specific applications including geophysical contexts.

The numerical method in Chapter 3 is motivated by the linear method used in Chapter 2, and then we also chose the stabilized finite element method USFEM [25] to solve the local problems.

As far as we know, this is the first work where the MHM method is applied to a non-linear problem. The numerical implementations of the methods presented in this thesis were

completely developed in Fortran 90/95, and the solvers used to solve the linear systems were MKL PARDISO [84] and MUMPS [7, 8]. The 2D and 3D adaptive meshes were generated by Triangle [85] and Tetgen [86], respectively. Paraview [18] was employed for visualization.

# Notation

The laplacian and gradient operators of a scalar function  $v$  and divergence of a vectorial function  $\mathbf{w} := (w_i)_{i=1,\dots,d}$  are defined, respectively, by

$$\Delta v = \sum_{i=1}^d \frac{\partial^2 v}{\partial x_i^2}, \quad \nabla v := \left( \frac{\partial v}{\partial x_i} \right)_{i=1,\dots,d} \quad \text{and} \quad \nabla \cdot \mathbf{w} := \sum_{i=1}^d \frac{\partial w_i}{\partial x_i},$$

with  $d = 2, 3$ . The gradient (laplacian) of a vector  $\mathbf{w}$  is a tensor (vector) which rows correspond to the gradient (laplacian) of the components of  $\mathbf{w}$ , and the divergence applied to a tensor is the divergence operator acting along its rows.

Let  $D$  be a bounded set of  $\mathbb{R}^d$ . The set  $L^2(D)$  denotes the space of square-integrable functions over  $D$ . We also consider the following spaces

$$L_0^2(D) := \{v \in L^2(D) : \int_D v = 0\},$$

$$H^1(D) := \{v \in L^2(D) : \nabla v \in L^2(D)^d\},$$

$$H_0^1(D) := \{v \in H^1(D) : v = 0 \text{ on } \partial D\}$$

and

$$H(\text{div}; D) := \{\mathbf{v} \in L^2(D)^{d \times d} : \nabla \cdot \mathbf{v} \in L^2(D)\}.$$

We denote by  $(\cdot, \cdot)_D$  and  $\|\cdot\|_{0,D}$  the usual inner product and norm, respectively, of square-integrable functions for scalar, vector or tensor valued functions, as appropriate. Also, for all  $v \in H^1(D)$  (or in  $H^1(D)^d$ ) we denote its norm and seminorm as

$$\|v\|_{1,D} := \sqrt{\|v\|_{0,D}^2 + |v|_{1,D}^2} \quad \text{where} \quad |\mathbf{v}|_{1,D} := \|\nabla \mathbf{v}\|_{0,D},$$

respectively. We denote by  $|\cdot|$  the euclidean norm of a scalar, vector or tensor, as appropriate.

Let  $\mathcal{O}$  be an open and bounded set of  $\mathbb{R}^d$ . We denote by  $H^{-1}(\mathcal{O})$  and  $H^{-1/2}(\partial \mathcal{O})$  the

dual spaces of the Sobolev spaces  $H_0^1(\mathcal{O})$  y  $H^{1/2}(\partial\mathcal{O})$ , equipped with the norms  $\|\cdot\|_{-1,\mathcal{O}}$  and  $\|\cdot\|_{-1/2,\partial\mathcal{O}}$ , where  $\partial\mathcal{O}$  denotes the boundary of  $\mathcal{O}$ . The duality pairing between the spaces  $H^{-1/2}(\partial\mathcal{O})$  and  $H^{1/2}(\partial\mathcal{O})$  is denoted by  $\langle \cdot, \cdot \rangle_{\partial\mathcal{O}}$ .

In this thesis,  $\Omega$  is an open bounded polytopal set of  $\mathbb{R}^d$  (the domain of each model problem considered) with boundary  $\partial\Omega$  and diameter  $d_\Omega$ .

Let  $\{\mathcal{T}_H\}_{H>0}$  be a family of shape-regular meshes of  $\bar{\Omega}$ , composed by simplex  $K$  of diameter  $H_K$  and  $H := \max\{H_K : K \in \mathcal{T}_H\}$ , that is, exists  $\sigma_0$  such that

$$\forall h, \forall K \in \mathcal{T}_H, \quad \frac{H_K}{\rho_K} \leq \sigma_0,$$

where  $\rho_K$  is the diameter of the ball inscribed in  $K$ . In the document, we use terminology usually employed for three-dimensional domains, with the restriction to two-dimensional problems being straightforward. As such, each element  $K$  has a boundary  $\partial K$  consisting of faces  $F$ , with diameter  $H_F$ . The collection of all faces  $F$ , in a triangulation  $\mathcal{T}_H$ , is denoted by  $\mathcal{E}_H$ , which is decomposed into the set of internal faces  $\mathcal{E}_0$  and the set of faces on the Dirichlet boundary  $\mathcal{E}_D$ . Also, we fix a unit normal vector  $\mathbf{n}_F$  on each  $F \in \mathcal{E}_H$ , taking care points out on  $\partial\Omega$ . For each  $K \in \mathcal{T}_H$ , we denote by  $\mathbf{n}^K$  the outward normal on  $\partial K$ , and let  $\mathbf{n}_F^K := \mathbf{n}^K|_F$  for each  $F \subset \partial K$ .

For  $F \in \mathcal{E}_0$ , we define the jump of  $v$  (a scalar or vectorial function) across  $F$  by

$$[v]_F(\mathbf{x}) := \lim_{\delta \rightarrow 0^+} v(\mathbf{x} + \delta \mathbf{n}_F) - \lim_{\delta \rightarrow 0^+} v(\mathbf{x} - \delta \mathbf{n}_F), \quad \text{for all } \mathbf{x} \in F.$$

When there is no ambiguity, we omit the subindex in the jump notation.

Given  $K \in \mathcal{T}_H$  and  $F \in \mathcal{E}_H$  we define the following patch:

$$\begin{aligned} \omega_K &:= \bigcup_{\mathcal{E}(K) \cap \mathcal{E}(K') \neq \emptyset} K', & \tilde{\omega}_K &:= \bigcup_{\mathcal{N}(K) \cap \mathcal{N}(K') \neq \emptyset} K', \\ \omega_F &:= \bigcup_{F \in \mathcal{E}(K')} K', & \tilde{\omega}_F &:= \bigcup_{\mathcal{N}(F) \cap \mathcal{N}(K') \neq \emptyset} K', \end{aligned}$$

where  $\mathcal{E}(K)$  is the set of all faces of  $K$ ,  $\mathcal{N}(K)$  is the set of nodes of  $K$  and  $\mathcal{N}(F)$  the set of nodes of  $F$ .

In chapters 2 and 3 we need, besides the mesh  $\mathcal{T}_H$  for the domain  $\Omega$  (called *first-level mesh*), meshes on each element of it (called *second-level meshes*). To this end, for each  $K \in \mathcal{T}_H$  we denote by  $\{\mathcal{T}_h^K\}_{h>0}$  a regular family of meshes of  $K$ , where  $h$  is the characteristic length of  $\mathcal{T}_h^K$ . We notice that the family  $\{\mathcal{T}_h^K\}_{h>0}$  may differ in each  $K \in \mathcal{T}_H$ . Also, we denote by  $\mathcal{E}_h^K$  the set of faces on  $\mathcal{T}_h^K$ , and by  $\mathcal{E}_0^K$  the set of internal faces. To each

$\zeta \in \mathcal{E}_h^K$  we associate a normal vector  $\mathbf{n}_\zeta^\tau$ , taking care to ensure this is facing outward on  $\partial K$ . Furthermore, we denote by  $\mathcal{T}_{\tilde{H}}(F)$  a triangulation of  $F \in \mathcal{E}_H$ , where  $\tilde{H}$  is the maximum size of all  $\tilde{F}$  belonging to  $\mathcal{T}_{\tilde{H}}(F)$ .

In the document, we adopt the following notation

$$\begin{aligned} a \preceq b &\iff a \leq C b, \\ a \simeq b &\iff a \preceq b \text{ and } b \preceq a, \end{aligned}$$

where the positive constant  $C$  is independent of  $H$  and  $h$ .

Finally, if  $\mathcal{O}$  is a subset of  $\mathbb{R}^d$  or  $\mathbb{R}^{d-1}$ ,  $\mathbb{P}_l(\mathcal{O})$  stands for the space of polynomials on  $\mathcal{O}$  of total degree at most  $l \geq 0$ , and

$$\mathbb{P}_l(P(\mathcal{O})) := \{v \in L^2(\mathcal{O}) : v|_D \in \mathbb{P}_l(D), \forall D \in P(D)\}$$

is the broken polynomial set, where  $P(\mathcal{O})$  is a partition of  $\mathcal{O}$ .

# Chapter 1

## An a posteriori error estimator for a LPS method for Navier-Stokes equations.

### 1.1 Introduction

In this chapter we develop an a posteriori error estimator, of the hierarchical type, for the Local Projection Stabilized (LPS) finite element method introduced in [15], applied to the incompressible Navier–Stokes equations. The technique use the solution of locals problems posed on appropriate finite dimensional spaces of bubble-like functions, to approach the error. Several numerical tests confirm the theoretical properties of the estimator and its performance.

The outline of this chapter is as follows: in Section 1.2 we introduce our model problem and some useful preliminary results. In Section 1.3 we present the LPS method and its main approximation results. In Section 1.4 we define our a posteriori error estimator, of hierarchical type, and prove the equivalence of this error estimator with the approximation error, using an intermediate auxiliary problem. Finally, in Section 1.5, we present some numerical tests which allows us to assess the convergence property of the LPS method and the quality of our a posteriori error estimator.

### 1.2 Model problem and preliminary results

Let  $\Omega \subset \mathbb{R}^d$  ( $d = 2$  or  $d = 3$ ) be a bounded polygonal open domain. The steady incompressible Navier–Stokes problem consists in finding a velocity vector field  $\mathbf{u}$  and a pressure

scalar field  $p$  such as

$$\begin{cases} -\nu \Delta \mathbf{u} + (\nabla \mathbf{u}) \mathbf{u} + \nabla p = \mathbf{f} & \text{in } \Omega, \\ \nabla \cdot \mathbf{u} = 0 & \text{in } \Omega, \\ \mathbf{u} = \mathbf{0} & \text{on } \partial\Omega, \end{cases} \quad (1.1)$$

where the fluid viscosity  $\nu > 0$  and the force field  $\mathbf{f} \in L^2(\Omega)^d$  are given.

We define the spaces

$$\mathbf{V} := H_0^1(\Omega)^d \quad \text{and} \quad Q := L_0^2(\Omega),$$

equipped with the norms  $|\cdot|_{1,\Omega}$  and  $\|\cdot\|_{0,\Omega}$ , respectively, recalling that, thanks to Poincaré's inequality, the seminorm  $|\cdot|_{1,\Omega}$  is indeed a norm on  $\mathbf{V}$ .

The standard weak formulation for the problem (1.1) is the following: *Find  $(\mathbf{u}, p) \in \mathbf{V} \times Q$  such that*

$$a(\mathbf{u}, \mathbf{v}) - b(\mathbf{u}, q) + b(\mathbf{v}, p) + c(\mathbf{u}; \mathbf{u}, \mathbf{v}) = (\mathbf{f}, \mathbf{v})_\Omega \quad (1.2)$$

for all  $(\mathbf{v}, q) \in \mathbf{V} \times Q$ , where the bilinear forms  $a(\cdot, \cdot)$  and  $b(\cdot, \cdot)$ , and the trilinear form  $c(\cdot; \cdot, \cdot)$  are given by

$$a(\mathbf{u}, \mathbf{v}) := \nu (\nabla \mathbf{u}, \nabla \mathbf{v})_\Omega \quad \forall \mathbf{u}, \mathbf{v} \in \mathbf{V}, \quad (1.3)$$

$$b(\mathbf{v}, q) := -(q, \nabla \cdot \mathbf{v})_\Omega \quad \forall q \in Q, \forall \mathbf{v} \in \mathbf{V}, \quad (1.4)$$

$$c(\mathbf{u}; \mathbf{v}, \mathbf{w}) := ((\nabla \mathbf{v}) \mathbf{u}, \mathbf{w})_\Omega \quad \forall \mathbf{u}, \mathbf{v}, \mathbf{w} \in \mathbf{V}. \quad (1.5)$$

In addition, we introduce the symmetric bilinear form  $d : Q \times Q \rightarrow \mathbb{R}$  given by

$$d(p, q) := \frac{1}{\nu} (p, q)_\Omega.$$

The bilinear forms  $a(\cdot, \cdot)$  and  $d(\cdot, \cdot)$  induce the norms

$$\begin{aligned} \|\mathbf{v}\|_a &:= a(\mathbf{v}, \mathbf{v})^{1/2} \quad \forall \mathbf{v} \in \mathbf{V}, \\ \|q\|_d &:= d(q, q)^{1/2} \quad \forall q \in Q. \end{aligned}$$

Also, we denote by  $\|\cdot\|_{a,\mathcal{O}}$  the norm induced by  $a(\cdot, \cdot)$  on the set  $\mathcal{O} \subset \Omega$ . We equip the space  $\mathbf{V} \times Q$  with the product norm given by

$$\|(\mathbf{v}, q)\| := \left\{ \|\mathbf{v}\|_a^2 + \|q\|_d^2 \right\}^{1/2} \quad \forall (\mathbf{v}, q) \in \mathbf{V} \times Q.$$

The next result states some important inequalities related to the forms  $a$ ,  $b$  and  $c$ .

**Lemma 1.1** *Let  $a(\cdot, \cdot)$  and  $b(\cdot, \cdot)$  be the bilinear forms given by (1.3) and (1.4), respectively, and let  $c(\cdot, \cdot, \cdot)$  be the trilinear form given by (1.5). Then*

$$\begin{aligned} |a(\mathbf{v}, \mathbf{w})| &\leq \|\mathbf{v}\|_a \|\mathbf{w}\|_a \quad \forall \mathbf{v}, \mathbf{w} \in \mathbf{V}, \\ |b(\mathbf{v}, q)| &\leq \sqrt{d} \|\mathbf{v}\|_a \|q\|_d \quad \forall (\mathbf{v}, q) \in \mathbf{V} \times Q, \\ \sup_{\substack{\mathbf{v} \in \mathbf{V} \\ \mathbf{v} \neq 0}} \frac{b(\mathbf{v}, q)}{\|\mathbf{v}\|_a} &\geq \alpha_b \|q\|_d \quad \forall q \in Q, \\ c(\mathbf{w}; \mathbf{u}, \mathbf{v}) &\leq \beta |\mathbf{w}|_{1,\Omega} |\mathbf{u}|_{1,\Omega} |\mathbf{v}|_{1,\Omega} \quad \forall \mathbf{u}, \mathbf{v}, \mathbf{w} \in \mathbf{V}, \end{aligned}$$

where  $\alpha_b$  and  $\beta$  are positive constants depending only on  $\Omega$ . Moreover, for all  $\mathbf{u}, \mathbf{v}, \mathbf{w} \in H^1(\Omega)^d$  such that  $\nabla \cdot \mathbf{w} = 0$  and  $\mathbf{w} \cdot \mathbf{n} = 0$ , it holds

$$\begin{aligned} c(\mathbf{w}; \mathbf{u}, \mathbf{v}) &= -c(\mathbf{w}; \mathbf{v}, \mathbf{u}), \\ c(\mathbf{w}; \mathbf{v}, \mathbf{v}) &= 0. \end{aligned}$$

*Proof.* The first two statements are straightforward and the others are classical results (see, for instance, [49]). ■

The well-posedness of the variational problem (1.2) is ensured by the following result

**Theorem 1.1** *Assume that  $\nu$  and  $\mathbf{f} \in L^2(\Omega)^d$  satisfy the following condition:*

$$|(\mathbf{f}, \mathbf{v})_\Omega| \leq \gamma \frac{\nu^2}{\beta} |\mathbf{v}|_{1,\Omega} \quad \forall \mathbf{v} \in \mathbf{V} \tag{1.6}$$

for some fixed number  $\gamma \in [0, 1[$ . Then, there exists a unique solution  $(\mathbf{u}, p) \in \mathbf{V} \times Q$  of (1.2) and it holds

$$|\mathbf{u}|_{1,\Omega} \leq \gamma \frac{\nu}{\beta}.$$

*Proof.* See Theorem 2.4, Chapter IV in [49]. ■

The finite element subspaces to be used in this work are defined as follows

$$\mathbf{V}_H := \{\mathbf{v} \in \mathcal{C}^0(\bar{\Omega})^d : \mathbf{v}|_K \in \mathbb{P}_1(K)^d, \forall K \in \mathcal{T}_H\} \cap \mathbf{V},$$

and

$$Q_H := \{q \in L^2(\Omega) : q|_K \in \mathbb{P}_0(K), \forall K \in \mathcal{T}_H\} \cap Q,$$

Let  $\mathcal{I}_h : \mathbf{V} \rightarrow \mathbf{V}_H$  be the Clément interpolation operator introduced in [39]. It can be easily shown (see [39, 45] for details) that the Clément interpolation operator satisfies the

following estimates

$$\|\mathbf{v} - \mathcal{I}_h \mathbf{v}\|_{0,K} \leq C \nu^{-1/2} H_K \|\mathbf{v}\|_{a,\tilde{\omega}_K}, \quad (1.7)$$

$$\|\mathbf{v} - \mathcal{I}_h \mathbf{v}\|_{0,F} \leq C \nu^{-1/2} H_F^{1/2} \|\mathbf{v}\|_{a,\tilde{\omega}_F}, \quad (1.8)$$

$$\|\mathcal{I}_h \mathbf{v}\|_{a,K} \leq C \|\mathbf{v}\|_{a,\tilde{\omega}_K}, \quad (1.9)$$

for all  $\mathbf{v} \in H^1(\Omega)^d$ .

Finally, for each  $K \in \mathcal{T}_H$ , we denote by  $\Pi_K q$  the average of a function  $q \in L^2(K)$ , i.e.,

$$\Pi_K q := \frac{1}{|K|} \int_K q \, dx.$$

### Lemma 1.2

$$\|v - \Pi_K v\|_{0,K} \leq \frac{H_K}{\pi} |v|_{1,K} \quad \forall v \in H^1(K), \quad (1.10)$$

$$\|\Pi_K v\|_{0,K} \leq \|v\|_{0,K} \quad \forall v \in L^2(K). \quad (1.11)$$

*Proof.* See Proposition 1.134 and Lemma 1.131 in [45].  $\blacksquare$

Hereafter, we will use intensively the *fluctuation* operator  $\chi_h$  defined by  $\chi_h := \mathbf{I} - \Pi_K$ , where  $\mathbf{I}$  is the identity operator. Observe that, from Lemma 1.2, it holds

$$\|\chi_h(\mathbf{x} \cdot \Pi_K \mathbf{v})\|_{0,K} \leq \frac{H_K}{\pi} \|\mathbf{v}\|_{0,K} \quad \forall \mathbf{v} \in L^2(K)^d. \quad (1.12)$$

## 1.3 The local projection stabilized method

The Local Projection Stabilized (LPS) method for the Navier–Stokes equations, introduced and analyzed in [15], has the following form: *Find  $(\mathbf{u}_H, p_H) \in \mathbf{V}_H \times Q_H$  such that*

$$(LPS) \left\{ \begin{array}{l} \nu (\nabla \mathbf{u}_H, \nabla \mathbf{v}_H)_\Omega + ((\nabla \mathbf{u}_H) \mathbf{u}_H, \mathbf{v}_H)_\Omega - (p_H, \nabla \cdot \mathbf{v}_H)_\Omega + (q_H, \nabla \cdot \mathbf{u}_H)_\Omega \\ \quad + \sum_{K \in \mathcal{T}_H} \frac{\alpha_K}{\nu} (\chi_h(\mathbf{x} \cdot \Pi_K[(\nabla \mathbf{u}_H) \mathbf{u}_H]), \chi_h(\mathbf{x} \cdot \Pi_K[(\nabla \mathbf{v}_H) \mathbf{u}_H]))_K \\ \quad + \sum_{K \in \mathcal{T}_H} \frac{\gamma_K}{\nu} (\chi_h(\mathbf{x} \nabla \cdot \mathbf{u}_H), \chi_h(\mathbf{x} \nabla \cdot \mathbf{v}_H))_K + \sum_{F \in \mathcal{E}_H} \tau_F([\![p_H]\!], [\![q_H]\!])_F = (\mathbf{f}, \mathbf{v}_H)_\Omega, \end{array} \right.$$

where the stabilization parameters are given by

$$\alpha_K := \frac{1}{\max\{1, Pe_K\}} \quad \text{and} \quad \gamma_K := \frac{1}{\max\left\{1, \frac{Pe_K}{24}\right\}},$$

with

$$Pe_K := \frac{|\mathbf{u}_H|_K H_K}{18\nu} \quad \text{and} \quad |\mathbf{u}_H|_K := \frac{\|\mathbf{u}_H\|_{0,K}}{|K|^{\frac{1}{2}}},$$

and

$$\tau_F := \begin{cases} \frac{H_F}{12\nu}, & \text{if } |\mathbf{u}_H|_F = 0, \\ \frac{1}{2|\mathbf{u}_H|_F} - \frac{1}{|\mathbf{u}_H|_F(1 - \exp(Pe_F))} \left(1 + \frac{1}{Pe_F}(1 - \exp(Pe_F))\right), & \text{otherwise.} \end{cases}$$

Here

$$Pe_F := \frac{|\mathbf{u}_H|_F H_F}{\nu} \quad \text{with} \quad |\mathbf{u}_H|_F := \frac{\|\mathbf{u}_H\|_{0,F}}{H_F^{1/2}}.$$

We recall, from Lemma 2 in [26], that  $\tau_F$  satisfies

$$\tau_F \leq C \frac{H_F}{\nu}$$

for all  $F \in \mathcal{E}_H$ .

**Remark 1.1** Note that the method LPS has the disadvantage of being non consistent, which complicate the a priori and a posteriori analysis. On the other hand, LPS is easier to implement than the traditional residual projection methods (RELP). Finally, note that in the presence of Neumann boundary conditions, we only need to change the jump term accordingly.

The well-posedness and error estimates for the LPS method were studied in [15], for completeness we present some of the main results concerning existence and uniqueness of the discrete solution, as well as error bounds.

**Theorem 1.2** There is a positive constant  $C$ , independent of  $h$  and  $\nu$ , such that if

$$\frac{H^{1/2}}{\nu^2} \|\mathbf{f}\|_{-1,\Omega} \leq C,$$

then LPS problem admits at least one solution.

*Proof.* See Theorem 3.4 in [15]. ■

**Theorem 1.3** *There exists a positive constant  $C$ , independent of  $h$  and  $\nu$ , such that if*

$$\frac{1}{\nu} \left\{ 1 + \frac{1}{\nu^{3/2}} \right\} (1+H)^2 < C,$$

*then the solution of the LPS problem is unique.*

*Proof.* See Theorem 3.5 in [15]. ■

The next theorem establishes an optimal convergence result of the LPS method in the natural norm.

**Theorem 1.4** *Assume that  $(\mathbf{u}, p)$  belongs to the space  $H^2(\Omega)^d \times H^1(\Omega)$ . Then there exists a positive constant  $H_0$ , such that for all  $H$  with  $0 < H \leq H_0$ , the following estimate holds*

$$\{|\mathbf{u} - \mathbf{u}_H|_{1,\Omega}^2 + \|p - p_H\|_{0,\Omega}^2\}^{1/2} \leq CH,$$

*where  $C > 0$  does not depend on  $h$  but can depend on  $\nu$ .*

*Proof.* See Theorem 4.4 in [15]. ■

## 1.4 A Hierarchical Error Estimator

In this section we propose and analyze a hierarchical estimator for the LPS method adapting the ideas of [14] to our problem.

### 1.4.1 The Auxiliary Problem

In what follows, the functions  $\mathbf{e}$  and  $E$  stand for the velocity and pressure approximation errors, i.e.,

$$\mathbf{e} := \mathbf{u} - \mathbf{u}_H,$$

$$E := p - p_H.$$

In the sequel we will need the following linear auxiliary problem: *Find  $(\phi, \psi) \in \mathbf{V} \times Q$  such that*

$$a(\phi, \mathbf{v}) + d(\psi, q) = a(\mathbf{e}, \mathbf{v}) - b(\mathbf{e}, q) + b(\mathbf{v}, E) + l(\mathbf{u}; \mathbf{u}_H, \mathbf{v}) \quad \forall (\mathbf{v}, q) \in \mathbf{V} \times Q, \quad (1.13)$$

where

$$l(\mathbf{u}; \mathbf{u}_H, \mathbf{v}) := c(\mathbf{u}; \mathbf{u}, \mathbf{v}) - c(\mathbf{u}_H; \mathbf{u}_H, \mathbf{v}).$$

Clearly, the well-posedness of the above system arises from the ellipticity of  $a(\cdot, \cdot)$  and  $d(\cdot, \cdot)$  on  $\mathbf{V}$  and  $Q$ , respectively.

Next, we establish an equivalence between the norms of  $(\mathbf{e}, E) \in \mathbf{V} \times Q$  and the norms of the solution  $(\phi, \psi) \in \mathbf{V} \times Q$  of (1.13), thus opening the door to design an error estimate based on the functions  $(\phi, \psi)$  only.

**Theorem 1.5** *Assume that (1.6) holds and  $|\mathbf{e}|_{1,\Omega}$  is sufficiently small in the sense that there exists  $\varepsilon > 0$  such that*

$$\gamma + \frac{\varepsilon^2}{2} + \frac{\beta}{\nu} |\mathbf{e}|_{1,\Omega} < 1.$$

*Then, there exists positive constants  $C_1$  and  $C_2$ , independent of  $h$ , such that*

$$C_1 \{ \|\phi\|_a^2 + \|\psi\|_d^2 \} \leq \|\mathbf{e}\|_a^2 + \|E\|_d^2 \leq C_2 \{ \|\phi\|_a^2 + \|\psi\|_d^2 \}.$$

*Proof.* See Theorem 4.1 in [14]. ■

From the definition of  $\mathbf{e}$  and  $E$ , the auxiliary problem (1.13) is equivalent to

$$a(\phi, \mathbf{v}) + d(\psi, q) = (\mathbf{f}, \mathbf{v})_\Omega - a(\mathbf{u}_H, \mathbf{v}) + b(\mathbf{u}_H, q) - b(\mathbf{v}, p_H) - c(\mathbf{u}_H; \mathbf{u}_H, \mathbf{v}) \quad (1.14)$$

for all  $(\mathbf{v}, q) \in \mathbf{V} \times Q$ . The above equation can be rewritten in a more compact form as

$$a(\phi, \mathbf{v}) + d(\psi, q) = \mathcal{R}_H(\mathbf{v}, q) \quad \forall (\mathbf{v}, q) \in \mathbf{V} \times Q,$$

where  $\mathcal{R}_H \in (\mathbf{V} \times Q)'$  stands for the residual functional given by

$$\mathcal{R}_H(\mathbf{v}, q) := (\mathbf{f}, \mathbf{v})_\Omega - a(\mathbf{u}_H, \mathbf{v}) + b(\mathbf{u}_H, q) - b(\mathbf{v}, p_H) - c(\mathbf{u}_H; \mathbf{u}_H, \mathbf{v}) \quad \forall (\mathbf{v}, q) \in \mathbf{V} \times Q.$$

**Remark 1.2** Note that the auxiliary problem (1.13), or equivalently (1.14), can be decoupled in two different problems. First, taking  $\mathbf{v} = \mathbf{0}$  in (1.14) we obtain

$$d(\psi, q) = b(\mathbf{u}_H, q) \quad \forall q \in Q,$$

now, using that  $\nabla \cdot \mathbf{u}_H \in Q$ , we get that

$$\psi = -\nu \nabla \cdot \mathbf{u}_H. \quad (1.15)$$

Second, taking  $q = 0$  in (1.14), we arrive at

$$a(\phi, \mathbf{v}) = \mathcal{R}_H^1(\mathbf{v}) \quad \forall \mathbf{v} \in \mathbf{V}, \quad (1.16)$$

where  $\mathcal{R}_H^1 \in \mathbf{V}'$  is given by the expression

$$\mathcal{R}_H^1(\mathbf{v}) := (\mathbf{f}, \mathbf{v})_\Omega - a(\mathbf{u}_H, \mathbf{v}) - b(\mathbf{v}, p_H) - c(\mathbf{u}_H; \mathbf{u}_H, \mathbf{v}) \quad \forall \mathbf{v} \in \mathbf{V}.$$

An equivalent and useful expression for  $\mathcal{R}_H^1$  is obtained using integration by parts, which leads to

$$\mathcal{R}_H^1(\mathbf{v}) = \sum_{K \in \mathcal{T}_H} (\mathbf{R}_K, \mathbf{v})_K + \sum_{F \in \mathcal{E}_H} (\mathbf{R}_F, \mathbf{v})_F,$$

where  $\mathbf{R}_K$  and  $\mathbf{R}_F$  are the local residuals defined by

$$\mathbf{R}_K := (\mathbf{f} + \nu \Delta \mathbf{u}_H - (\nabla \mathbf{u}_H) \mathbf{u}_H - \nabla p_H)|_K \quad \text{and} \quad \mathbf{R}_F := [-\nu \partial_{\mathbf{n}} \mathbf{u}_H + p_H \mathbf{n}]_F.$$

The following technical result will be useful in the sequel.

**Lemma 1.3** *For all  $\mathbf{v}_H \in \mathbf{V}_H$  it holds*

$$\mathcal{R}_H^1(\mathbf{v}_H) \leq C \left[ \sum_{K \in \mathcal{T}_H} \frac{H_K^4}{\nu^3} \left\{ (\|\mathbf{R}_K\|_{0,K} + \|\mathbf{f}\|_{0,K}) \|\mathbf{u}_H\|_{\infty,K} + \|\nabla \cdot \mathbf{u}_H\|_{0,K} \right\}^2 \right]^{1/2} \|\mathbf{v}_H\|_a.$$

*Proof.* From the definition of  $\mathcal{R}_H^1$ , using LPS scheme with  $q_H = 0$  and recalling that  $\mathbf{u}_H|_K$  and  $p_H|_K$  are a linear and constant polynomial in each  $K \in \mathcal{T}_H$ , respectively, it holds

$$\begin{aligned} \mathcal{R}_H^1(\mathbf{v}_H) &= (\mathbf{f}, \mathbf{v}_H)_\Omega - a(\mathbf{u}_H, \mathbf{v}_H) - b(\mathbf{v}_H, p_H) - c(\mathbf{u}_H; \mathbf{u}_H, \mathbf{v}_H) \\ &= \sum_{K \in \mathcal{T}_H} \left\{ \frac{\alpha_K}{\nu} (\chi_H(\mathbf{x} \cdot \Pi_K[(\nabla \mathbf{u}_H) \mathbf{u}_H]), \chi_H(\mathbf{x} \cdot \Pi_K[(\nabla \mathbf{v}_H) \mathbf{u}_H]))_K + \frac{\gamma_K}{\nu} (\chi_H(\mathbf{x} \nabla \cdot \mathbf{u}_H), \chi_H(\mathbf{x} \nabla \cdot \mathbf{v}_H))_K \right\} \\ &= \sum_{K \in \mathcal{T}_H} \left\{ \frac{\alpha_K}{\nu} \left[ -(\chi_H(\mathbf{x} \cdot \Pi_K[\mathbf{R}_K]), \chi_H(\mathbf{x} \cdot \Pi_K[(\nabla \mathbf{v}_H) \mathbf{u}_H]))_K + (\chi_H(\mathbf{x} \cdot \Pi_K[\mathbf{f}]), \chi_H(\mathbf{x} \cdot \Pi_K[(\nabla \mathbf{v}_H) \mathbf{u}_H]))_K \right] \right. \\ &\quad \left. + \frac{\gamma_K}{\nu} (\chi_H(\mathbf{x} \nabla \cdot \mathbf{u}_H), \chi_H(\mathbf{x} \nabla \cdot \mathbf{v}_H))_K \right\}. \end{aligned} \quad (1.17)$$

Thus, using Hölder's inequality, (1.12), (1.17), Cauchy–Schwarz's inequality, and recalling

that  $\alpha_K, \gamma_K \leq 1$ , we obtain

$$\begin{aligned} \mathcal{R}_H^1(\mathbf{v}_H) &\leq C \sum_{K \in \mathcal{T}_H} \frac{H_K^2}{\nu} \left\{ (\|\mathbf{R}_K\|_{0,K} + \|\mathbf{f}\|_{0,K}) \|\mathbf{u}_H\|_{\infty,K} \|\nabla \mathbf{v}_H\|_{0,K} + \|\nabla \cdot \mathbf{u}_H\|_{0,K} \|\nabla \cdot \mathbf{v}_H\|_{0,K} \right\} \\ &\leq C \sum_{K \in \mathcal{T}_H} \frac{H_K^2}{\nu} \left\{ (\|\mathbf{R}_K\|_{0,K} + \|\mathbf{f}\|_{0,K}) \|\mathbf{u}_H\|_{\infty,K} + \|\nabla \cdot \mathbf{u}_H\|_{0,K} \right\} \|\nabla \mathbf{v}_H\|_{0,K} \\ &\leq C \left[ \sum_{K \in \mathcal{T}_H} \frac{H_K^4}{\nu^3} \left\{ (\|\mathbf{R}_K\|_{0,K} + \|\mathbf{f}\|_{0,K}) \|\mathbf{u}_H\|_{\infty,K} + \|\nabla \cdot \mathbf{u}_H\|_{0,K} \right\}^2 \right]^{1/2} \|\mathbf{v}_H\|_a. \end{aligned}$$

■

**Remark 1.3** The equivalence result in Theorem 1.5 can be rewritten using the characterization of  $\psi$ , given in (1.15), as follows

$$C_1 \{ \|\phi\|_a^2 + \nu \|\nabla \cdot \mathbf{u}_H\|_{0,\Omega}^2 \} \leq \|e\|_a^2 + \|E\|_d^2 \leq C_2 \{ \|\phi\|_a^2 + \nu \|\nabla \cdot \mathbf{u}_H\|_{0,\Omega}^2 \}. \quad (1.18)$$

Therefore, we only need to estimate  $\|\phi\|_a$  using an a posteriori error estimator. This idea is pursued in the next section.

#### 1.4.2 Hierarchical Error Estimator

Following closely the ideas of [9, 14], let  $\mathbf{W}_H$  be a finite element subspace such that  $\mathbf{V}_H \subseteq \mathbf{W}_H \subseteq \mathbf{V}$ . Let us suppose that  $\mathbf{W}_H$  can be decomposed in the following way

$$\mathbf{W}_H = \mathbf{V}_H + \sum_{K \in \mathcal{T}_H} \mathbf{V}_K^b + \sum_{F \in \mathcal{E}_H} \mathbf{V}_F^b,$$

where the finite dimensional subspaces  $\mathbf{V}_K^b$  and  $\mathbf{V}_F^b$  satisfy

$$\mathbf{V}_K^b \subset H_0^1(K)^d \quad \text{and} \quad \mathbf{V}_F^b \subset H_0^1(\omega_F)^d.$$

Associated to each subspace  $\mathbf{V}_S^b$ , with  $S = K$  or  $F$ , there is a projection operator  $P_S : \mathbf{V} \rightarrow \mathbf{V}_S^b$  defined as the solution of the local problem

$$a(P_S \mathbf{v}, \mathbf{v}_S) = a(\mathbf{v}, \mathbf{v}_S) \quad \forall \mathbf{v}_S \in \mathbf{V}_S^b. \quad (1.19)$$

Thus we define our *a posteriori* error estimator  $\eta$  by

$$\eta := \left\{ \sum_{K \in \mathcal{T}_H} a(P_K \phi, P_K \phi) + \sum_{F \in \mathcal{E}_H} a(P_F \phi, P_F \phi) \right\}^{1/2}. \quad (1.20)$$

Using the definition of  $\phi$  we obtain that  $P_S \phi$ , with  $S = K$  or  $F$ , is the solution of the local problem

$$a(P_S \phi, \mathbf{v}_S) = \mathcal{R}_H^1(\mathbf{v}_S) \quad \forall \mathbf{v}_S \in \mathbf{V}_S^b. \quad (1.21)$$

**Remark 1.4** Notice that the solution  $\phi$  of (1.16), used throughout previous estimates, does not need to be computed but only its projection  $P_S \phi$  onto finite dimensional subspaces  $\mathbf{V}_S^b$ .

**Remark 1.5** The linear local problem (1.21) incorporates the Navier–Stokes non-linearity through its right hand side. This way of accounting for non-linearities in the *a posteriori* estimator represents a compromise between low computational cost and accuracy in the context of high speed flow.

We also require that the local subspaces  $\mathbf{V}_K^b$  and  $\mathbf{V}_F^b$ , hereafter called *bubble* subspaces, be piecewise affine-equivalent to a finite-dimensional space on a reference configuration, so that the following estimate holds:

$$\|\mathbf{b}_S\|_{0,K}^2 \leq CH_K^2 |\mathbf{b}_S|_{1,K}^2 \quad \forall \mathbf{b}_S \in \mathbf{V}_S^b, S = K \text{ or } F,$$

for all  $K \in \mathcal{T}_H$ .

Second, the bubble spaces must fulfil the following inf-sup conditions: there exists  $\beta^* > 0$ , independent of  $H$  and  $\nu$ , such that

$$\sup_{\substack{\mathbf{b}_K \in \mathbf{V}_K^b \\ \mathbf{b}_K \neq \mathbf{0}}} \frac{(\mathbf{b}_K, \mathbf{R}_K)_K}{\|\mathbf{b}_K\|_{a,K}} \geq \beta^* \nu^{-1/2} H_K \|\mathbf{R}_K\|_{0,K} \quad \forall K \in \mathcal{T}_H, \quad (1.22)$$

$$\sup_{\substack{\mathbf{b}_F \in \mathbf{V}_F^b \\ \mathbf{b}_F \neq \mathbf{0}}} \frac{(\mathbf{b}_F, \mathbf{R}_F)_F}{\|\mathbf{b}_F\|_{a,\omega_F}} \geq \beta^* \nu^{-1/2} H_F^{1/2} \|\mathbf{R}_F\|_{0,F} \quad \forall F \in \mathcal{E}_H. \quad (1.23)$$

In [9, Appendix B] was proved that the following pair of bubble subspaces satisfy conditions (1.22) and (1.23)

$$\begin{aligned} \mathbf{V}_K^b &= \langle \{b_K \mathbf{R}_K\} \rangle & \forall K \in \mathcal{T}_H, \\ \mathbf{V}_F^b &= \langle \{b_F \mathbf{R}_F\} \rangle & \forall F \in \mathcal{E}_H, \end{aligned}$$

where  $b_K$  and  $b_F$  are the standard polynomial bubble functions defined with respect to

the barycentric coordinates. We recall that  $\mathbf{V}_F^b$  is well defined because in our case  $\mathbf{R}_F$  is constant on each  $F \in \mathcal{E}_H$ .

The next result is recalled as it is needed for the proof of the reliability of our estimator.

**Lemma 1.4** *Suppose that (1.22) and (1.23) hold. Then,*

$$\begin{aligned} \mathcal{R}_H^1(\mathbf{v}) &\leq C\nu^{1/2} \left\{ \sum_{K \in \mathcal{T}_H} H_K^{-1} a(P_K \phi, P_K \phi)^{1/2} \|\mathbf{v}\|_{0,K} \right. \\ &\quad \left. + \sum_{F \in \mathcal{E}_H} H_F^{-1/2} \left[ a(P_F \phi, P_F \phi)^{1/2} + \sum_{K' \subset \omega_F} a(P_{K'} \phi, P_{K'} \phi)^{1/2} \right] \|\mathbf{v}\|_{0,F} \right\} \end{aligned}$$

for all  $\mathbf{v}$  in  $\mathbf{V}$ .

*Proof.* See Lemma 12 in [9]. ■

Now we are ready to prove the reliability of the error estimator.

**Lemma 1.5** *Let  $\phi$  be the solution of (1.16). If (1.22) and (1.23) hold, then*

$$\|\phi\|_a \leq C \left\{ \eta + \left[ \sum_{K \in \mathcal{T}_H} \frac{H_K^4}{\nu^3} \left\{ (\|\mathbf{R}_K\|_{0,K} + \|\mathbf{f}\|_{0,K}) \|\mathbf{u}_H\|_{\infty,K} + \|\nabla \cdot \mathbf{u}_H\|_{0,K} \right\}^2 \right]^{1/2} \right\}.$$

*Proof.* Using, Lemma 1.4 with  $\mathbf{v} = \phi - \mathcal{I}_h \phi$ , the mesh regularity, Cauchy–Schwarz inequality, (1.7) and (1.8), it holds

$$\begin{aligned} \mathcal{R}_H^1(\phi - \mathcal{I}_h \phi) &\leq C\nu^{1/2} \sum_{K \in \mathcal{T}_H} H_K^{-1} a(P_K \phi, P_K \phi)^{1/2} \|\phi - \mathcal{I}_h \phi\|_{0,K} \\ &\quad + C\nu^{1/2} \sum_{F \in \mathcal{E}_H} H_F^{-1/2} \left[ a(P_F \phi, P_F \phi)^{1/2} + \sum_{K' \subset \omega_F} a(P_{K'} \phi, P_{K'} \phi)^{1/2} \right] \|\phi - \mathcal{I}_h \phi\|_{0,F} \\ &\leq C \left\{ \sum_{K \in \mathcal{T}_H} a(P_K \phi, P_K \phi) + \sum_{F \in \mathcal{E}_H} a(P_F \phi, P_F \phi) \right\}^{1/2} \\ &\quad \times \left\{ \sum_{K \in \mathcal{T}_H} \nu H_K^{-2} \|\phi - \mathcal{I}_h \phi\|_{0,K}^2 + \sum_{F \in \mathcal{E}_H} \nu H_F^{-1} \|\phi - \mathcal{I}_h \phi\|_{0,F}^2 \right\}^{1/2} \\ &\leq C \eta \left\{ \sum_{K \in \mathcal{T}_H} \|\phi\|_{a,\tilde{\omega}_K}^2 + \sum_{F \in \mathcal{E}_H} \|\phi\|_{a,\tilde{\omega}_F}^2 \right\}^{1/2} \leq C \eta \|\phi\|_a. \end{aligned} \tag{1.24}$$

Now, from (1.16), Lemma 1.3, estimates (1.24) and (1.9), Cauchy–Schwarz inequality and

mesh regularity, it holds

$$\begin{aligned} \|\phi\|_a^2 &= a(\phi, \phi) = \mathcal{R}_H^1(\phi) = \mathcal{R}_H^1(\phi - \mathcal{I}_h \phi) + \mathcal{R}_H^1(\mathcal{I}_h \phi) \\ &\leq C \eta \|\phi\|_a + C \nu^{-3/2} \sum_{K \in \mathcal{T}_H} H_K^2 \left\{ (\|\mathbf{R}_K\|_{0,K} + \|\mathbf{f}\|_{0,K}) \|\mathbf{u}_H\|_{\infty,K} + \|\nabla \cdot \mathbf{u}_H\|_{0,K} \right\} \|\mathcal{I}_h \phi\|_a \\ &\leq C \left\{ \eta^2 + \sum_{K \in \mathcal{T}_H} \frac{H_K^4}{\nu^3} \left[ (\|\mathbf{R}_K\|_{0,K} + \|\mathbf{f}\|_{0,K}) \|\mathbf{u}_H\|_{\infty,K} + \|\nabla \cdot \mathbf{u}_H\|_{0,K} \right]^2 \right\}^{1/2} \|\phi\|_a, \end{aligned}$$

and the result follows.  $\blacksquare$

From the previous results, we can state the following auxiliary equivalence theorem.

**Theorem 1.6** *Let  $\phi$  be the solution of (1.16), and assume that (1.22) and (1.23) hold. Then, there exist  $C_1, C_2 > 0$ , independents of  $H$  and  $\nu$ , such that*

$$C_1 \eta \leq \|\phi\|_a \leq C_2 \left\{ \eta + \left[ \sum_{K \in \mathcal{T}_H} \frac{H_K^4}{\nu^3} \left\{ (\|\mathbf{R}_K\|_{0,K} + \|\mathbf{f}\|_{0,K}) \|\mathbf{u}_H\|_{\infty,K} + \|\nabla \cdot \mathbf{u}_H\|_{0,K} \right\}^2 \right]^{1/2} \right\},$$

where  $\eta$  is given by (1.20).

*Proof.* The upper bound has been stated in Lemma 1.5. To proof the lower bound we first write the subspace  $\mathbf{W}_H$  in the following way

$$\mathbf{W}_H = \mathbf{V}_H + \sum_{K \in \mathcal{T}_H} \mathbf{V}_K^b + \sum_{F \in \mathcal{E}_H} \mathbf{V}_F^b =: \mathbf{V}_H + \sum_{i \in \mathcal{T}_H \cup \mathcal{E}_H} \mathbf{V}_i^b.$$

From the definition of  $P_i \phi$  in (1.21), and by Cauchy–Schwarz’s inequality we have

$$\begin{aligned} \left[ \sum_{i \in \mathcal{T}_H \cup \mathcal{E}_H} a(P_i \phi, P_i \phi) \right]^2 &= \left[ \sum_{i \in \mathcal{T}_H \cup \mathcal{E}_H} a(\phi, P_i \phi) \right]^2 = \left[ a \left( \phi, \sum_{i \in \mathcal{T}_H \cup \mathcal{E}_H} P_i \phi \right) \right]^2 \\ &\leq a(\phi, \phi) a \left( \sum_{i \in \mathcal{T}_H \cup \mathcal{E}_H} P_i \phi, \sum_{i \in \mathcal{T}_H \cup \mathcal{E}_H} P_i \phi \right) = a(\phi, \phi) \sum_{i \in \mathcal{T}_H \cup \mathcal{E}_H} \sum_{j \in I_i} a(P_i \phi, P_j \phi) \\ &\leq a(\phi, \phi) \sum_{i \in \mathcal{T}_H \cup \mathcal{E}_H} \sum_{j \in I_i} \left\{ \frac{1}{2} a(P_i \phi, P_i \phi) + \frac{1}{2} a(P_j \phi, P_j \phi) \right\} \leq K_{\max} a(\phi, \phi) \sum_{i \in \mathcal{T}_H \cup \mathcal{E}_H} a(P_i \phi, P_i \phi), \end{aligned} \tag{1.25}$$

here  $I_i$  denotes the set of spaces  $\mathbf{V}_j^b$  which are neighbors of  $\mathbf{V}_i^b$ , i.e.,

$$I_i := \{j : \exists \mathbf{v}_j \in \mathbf{V}_j^b \text{ and } \mathbf{v}_i \in \mathbf{V}_i^b \text{ such that } a(\mathbf{v}_i, \mathbf{v}_j) \neq 0\}$$

and  $K_{\max}$  is the maximum number of neighbors, i.e.,

$$K_{\max} := \max\{\text{card}(I_l) : l \in \mathcal{T}_H \cup \mathcal{E}_H\},$$

which is uniformly bounded due to the mesh regularity. Then, the result follows from (1.25), the definition of the norm  $\|\cdot\|_a$  and noticing that

$$\eta^2 = \sum_{K \in \mathcal{T}_H} a(P_K \phi, P_K \phi) + \sum_{F \in \mathcal{E}_H} a(P_F \phi, P_F \phi) = \sum_{i \in \mathcal{T}_H \cup \mathcal{E}_H} a(P_i \phi, P_i \phi).$$

■

Finally, we establish the main result of this work. From (1.18), (1.20) and Theorem 1.6 the approximation error can be estimated as follows.

**Theorem 1.7** *Let  $(\mathbf{u}, p)$  and  $(\mathbf{u}_H, p_H)$  be the solution of (1.2) and LPS, respectively, and suppose that (1.22) and (1.23) hold. Then*

$$C_1 \tilde{\eta} \leq \|(\mathbf{u} - \mathbf{u}_H, p - p_H)\| \leq C_2 \left( \tilde{\eta} + \left[ \sum_{K \in \mathcal{T}_H} \frac{H_K^4}{\nu^3} \left\{ (\|\mathbf{R}_K\|_{0,K} + \|\mathbf{f}\|_{0,K}) \|\mathbf{u}_H\|_{\infty,K} + \|\nabla \cdot \mathbf{u}_H\|_{0,K} \right\}^2 \right]^{1/2} \right)$$

where

$$\tilde{\eta}^2 := \sum_{K \in \mathcal{T}_H} \tilde{\eta}_K^2$$

with

$$\tilde{\eta}_K^2 := \|P_K \phi\|_{a,K}^2 + \frac{1}{2} \sum_{F \in \mathcal{E}(K) \cap \mathcal{E}_H} \|P_F \phi\|_{a,F}^2 + \nu \|\nabla \cdot \mathbf{u}_H\|_{0,K}^2,$$

and the positive constants  $C_1$  and  $C_2$  are independent of  $H$ .

**Remark 1.6** Note that the term

$$T := \left( \sum_{K \in \mathcal{T}_H} \frac{H_K^4}{\nu^3} \left\{ (\|\mathbf{R}_K\|_{0,K} + \|\mathbf{f}\|_{0,K}) \|\mathbf{u}_H\|_{\infty,K} + \|\nabla \cdot \mathbf{u}_H\|_{0,K} \right\}^2 \right)^{1/2},$$

appearing in Theorem 1.7, is, asymptotically, a high order term compared to  $\tilde{\eta}$ . In fact, we can see this, for instance, in Figures 1.1– 1.4 where we observe that  $\tilde{\eta}$  is  $\mathcal{O}(h)$  and  $T$  is  $\mathcal{O}(H^2)$ . For this reason we may omit  $T$  in our numerical tests. The behavior of this h.o.t. term is quite similar to  $\left( \sum_{K \in \mathcal{T}_H} H_K^2 \|\mathbf{f} - P_H \mathbf{f}\|_{0,K}^2 \right)^{1/2}$ , with  $P_H \mathbf{f}$  a projection of  $\mathbf{f}$ , which appears in the a posteriori error estimates of the residual type (see Remark 1.8 in [95]).

## 1.5 Numerical validation

In order to validate our a posteriori error estimator we present some numerical tests. In examples 1.5.1 and 1.5.2 we analyze two problems with analytical solution in two and three dimensions, respectively, comparing in each case the exact approximation error with its estimated error  $\tilde{\eta}$ .

Also, as a measure of the quality of our error estimator, we define the so called *effectivity index*, by

$$E_i := \frac{\tilde{\eta}}{\|(\mathbf{u} - \mathbf{u}_H, p - p_H)\|},$$

we expect that  $E_i$  remain bounded as  $H$  goes to 0 through a sequence of uniform refined meshes.

Finally, in examples 1.5.3 and 1.5.4, we address numerical comparisons with some well-documented benchmarks from the literature, namely, 2D driven cavity flow and 3D flow around a cylinder.

The adaptive procedure handles the nonlinearity by a Newton algorithm and uses a structured coarse mesh to start the process. At each step, we solve the LPS problem and compute its corresponding local error estimator  $\tilde{\eta}_K$  for each element  $K \in \mathcal{T}_H$ , and refine those elements accordingly to

$$\tilde{\eta}_K \geq \theta \max\{\tilde{\eta}_{K'} : K' \in \mathcal{T}_H\},$$

where  $\theta \in ]0, 1[$  is a prescribed parameter. Then we evaluate the stopping criterion and decide to finish or go to the next step. In addition, when it comes to adapt meshes, the solution computed in the previous mesh, after an interpolation process on the current mesh [82], is set as the initial guess solution for the Newton iteration method in the current mesh.

In the case  $\nu \ll 1$ , the numerical algorithm demands a continuation strategy to reach the target viscosity. This strategy consists in beginning with a relatively big viscosity value and decreasing it gradually to attain the desired value.

**Remark 1.7** Note that problem (1.1) have homogeneous Dirichlet boundary condition, but in our numerical examples we consider both non homogeneous Dirichlet and Neumann boundary conditions, which are not covered by our theory. The changes necessary to deal with these boundary conditions are: in the case of non homogeneous Dirichlet conditions it appears an extra term in the estimator that measures the error in the approximation of

the exact Dirichlet condition, in general, this is a high order term that can be neglected in the numerical computations. In the case of Neumann boundary conditions it is necessary to change the rhs of the equation and add, to the definition of  $\tilde{\eta}$  in (1.20), the terms  $a(P_F\phi, P_F\phi)$  for the edges  $F$  on the Neumann boundary.

### 1.5.1 Two-dimensional analytic solution

In this example we consider  $\Omega = ]0, 1[^2$  and the boundary conditions such as the exact solution is given by  $\mathbf{u}(x, y) := (u_1(x, y), u_2(x, y))$ , with

$$\begin{aligned} u_1(x, y) &:= 256y^2(y-1)^2x(x-1)(2x-1), \\ u_2(x, y) &:= -u_1(y, x), \end{aligned}$$

and

$$p(x, y) := 150(x-0.5)(y-0.5).$$

For the viscosity we consider the cases:  $\nu = 1, 10^{-2}$ .

The error, a posteriori estimator and effectivity index are shown in Tables 1.1 and 1.2 for  $\nu = 1$  and  $\nu = 10^{-2}$ , respectively. Likewise, the corresponding convergence history for  $\nu = 1$  and  $\nu = 10^{-2}$  is presented in Figures 1.1 and 1.2.

Table 1.1: Exact error, a posteriori error estimator and effectivity index for the 2D example with analytical solution with  $\nu = 1$ .

| $H$      | $\ (u - u_H, p - p_H)\ $ | $\tilde{\eta}$ | $E_i$    |
|----------|--------------------------|----------------|----------|
| 0.031250 | 0.557676                 | 0.523659       | 0.939002 |
| 0.015625 | 0.276208                 | 0.263430       | 0.953736 |
| 0.007813 | 0.137523                 | 0.132090       | 0.960493 |
| 0.003906 | 0.068629                 | 0.066137       | 0.963677 |
| 0.001953 | 0.034284                 | 0.033091       | 0.965216 |

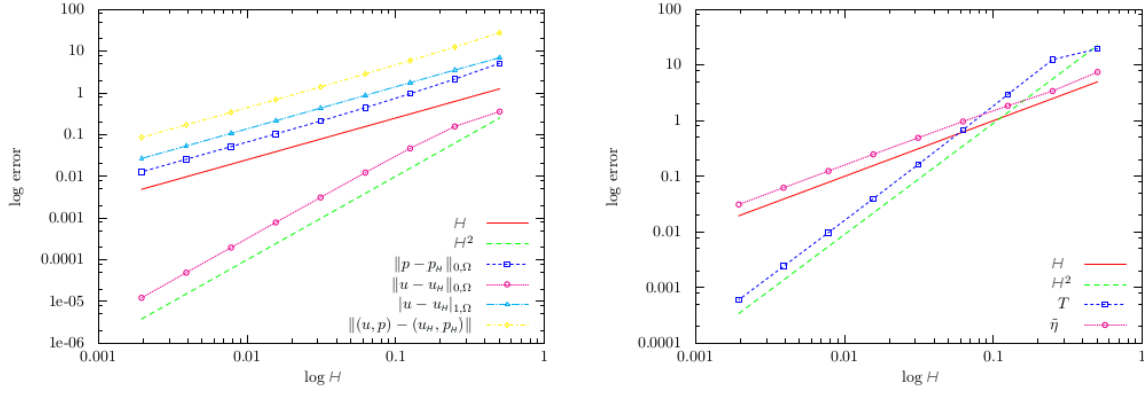


Figure 1.1: Convergence history for the 2D example with analytical solution, case  $\nu = 1$  (left) and the behavior of  $T$  when  $H$  goes to 0 (right).

Table 1.2: Exact error, a posteriori error estimator and effectivity index for the 2D example with analytical solution with  $\nu = 10^{-2}$ .

| $H$      | $\ (u - u_H, p - p_H)\ $ | $\tilde{\eta}$ | $E_i$    |
|----------|--------------------------|----------------|----------|
| 0.031250 | 3.656915                 | 2.163265       | 0.591555 |
| 0.015625 | 1.684914                 | 1.075223       | 0.638147 |
| 0.007813 | 0.811511                 | 0.533646       | 0.657596 |
| 0.003906 | 0.400764                 | 0.266174       | 0.664166 |
| 0.001953 | 0.199667                 | 0.132940       | 0.665810 |

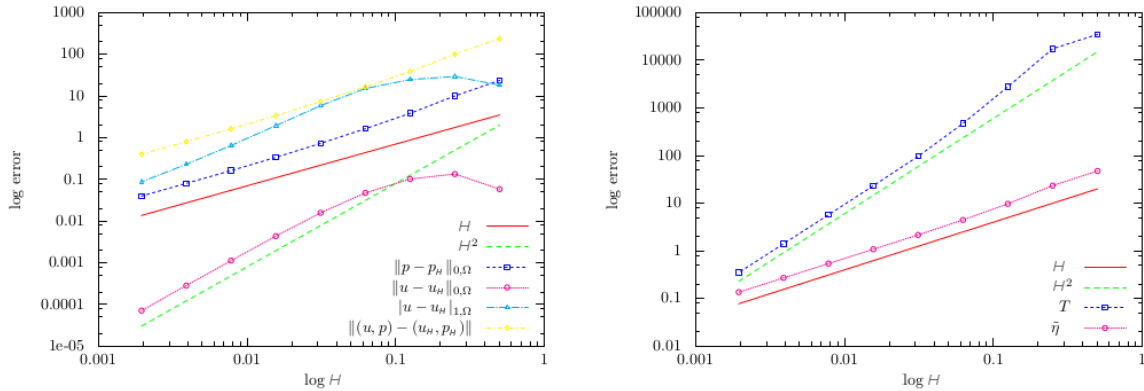


Figure 1.2: Convergence history for the 2D example with analytical solution, case  $\nu = 10^{-2}$  (left) and the behavior of  $T$  when  $H$  goes to 0 (right).

In both cases,  $\nu = 1$  or  $\nu = 10^{-2}$ , we observe a good agreement between the numerical

results and the results predicted by the theory.

### 1.5.2 Three-dimensional analytic solution

We consider  $\Omega := [0, 1]^3$  and choose the data  $\mathbf{f}$  so that the exact solution is given by

$$\mathbf{u}(x, y, z) := (e^x \sin(z), -e^x \sin(z), e^x \cos(z) - e^x \cos(y))$$

and

$$p(x, y) := \frac{-1}{2} e^{2x} + \frac{1}{4} (e^2 - 1).$$

As in the 2D example, we analyze the cases  $\nu = 1, 10^{-2}$ .

In Figures 1.3 and 1.4, we summarize the convergence history of the LPS method with  $\nu = 1$  and  $\nu = 10^{-2}$ , respectively. Also, in Tables 1.3 and 1.4 we show the exact error, a posteriori error estimator and effectivity index for the cases  $\nu = 1$  and  $\nu = 10^{-2}$ .

Table 1.3: Exact error, a posteriori error estimator and effectivity index for the 3D example with analytical solution with  $\nu = 1$ .

| $H$      | $\ (\mathbf{u} - \mathbf{u}_H, p - p_H)\ $ | $\tilde{\eta}$ | $E_i$    |
|----------|--|----------------|----------|
| 0.444081 | 0.544975                                   | 0.438047       | 0.803793 |
| 0.247472 | 0.283073                                   | 0.232354       | 0.820826 |
| 0.143330 | 0.150263                                   | 0.131043       | 0.872088 |
| 0.081658 | 0.080683                                   | 0.072337       | 0.896558 |
| 0.045780 | 0.043711                                   | 0.039629       | 0.906613 |

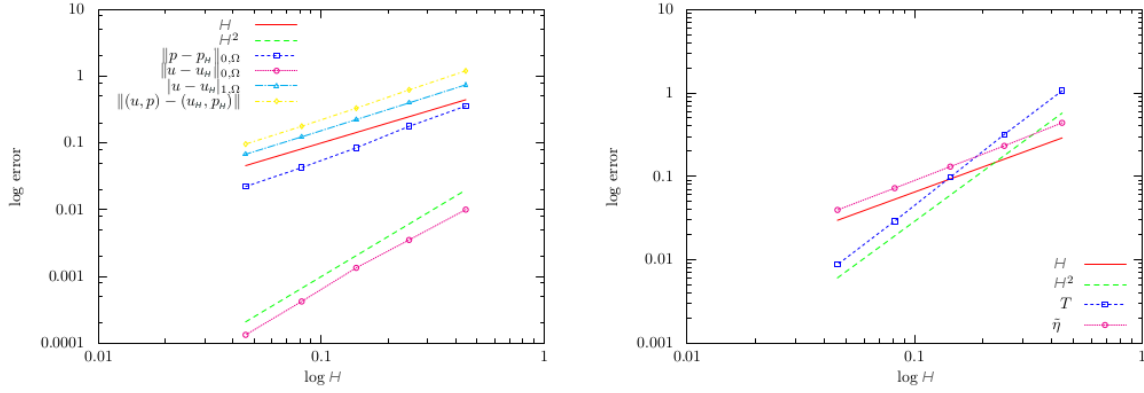


Figure 1.3: Convergence history for the 3D example with analytical solution, case  $\nu = 1$  (left) and the behavior of  $T$  when  $H$  goes to 0 (right).

Table 1.4: Exact error, a posteriori error estimator and effectivity index for the 3D example with analytical solution with  $\nu = 10^{-2}$ .

| $H$       | $\ (\mathbf{u} - \mathbf{u}_H, p - p_H)\ $ | $\tilde{\eta}$ | $E_i$     |
|-----------|--|----------------|-----------|
| 0.2474718 | 2.8269643                                  | 0.4619786      | 0.1634186 |
| 0.1433296 | 1.2279783                                  | 0.2728947      | 0.2222309 |
| 0.0816576 | 0.5090968                                  | 0.1525166      | 0.2995827 |
| 0.0457801 | 0.2144706                                  | 0.0848238      | 0.3955032 |

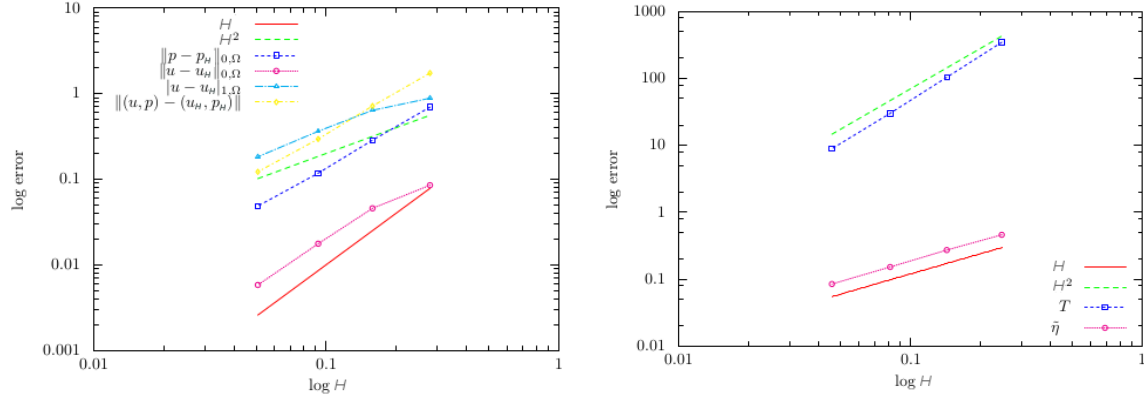


Figure 1.4: Convergence history for the 3D example with analytical solution, case  $\nu = 10^{-2}$  (left) and the behavior of  $T$  when  $H$  goes to 0 (right).

**Remark 1.8** Note that from Tables 1.1–1.2 and Tables 1.3–1.4 we observe that the errors grow when we change  $\nu$  from 1 to  $10^{-2}$ , which means that we have some inrobustness with

respect to  $\nu$ . In our computations for the Stokes problem we observe the same phenomena, this lead us to think that the problem is the lack of robustness of the method related to the pressure in the sense of [71].

### 1.5.3 Two-dimensional lid-driven cavity problem

In this case we considered the well-known 2D cavity problem, where the domain  $\Omega$  is  $]0, 1[ \times ]0, 1[$ ,  $\mathbf{f} = \mathbf{0}$  and the boundary conditions are defined as in Figure 1.5 (we refer the reader to [48, 75, 92] for a complete bibliography on this problem). In our particular case,  $\nu = 1/Re$ , with Reynolds number  $Re = 5,000$ .

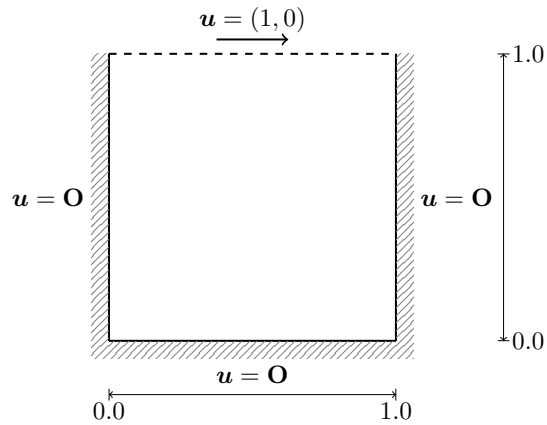


Figure 1.5: Domain and boundary conditions for the driven cavity problem.

The Figure 1.6 depicts the final mesh obtained with our adaptive scheme together the streamlines given by the solution obtained using that mesh. We observe that mesh refinement concentrates mainly around the primary vortex but also we recover secondary vortices in the expected locations.

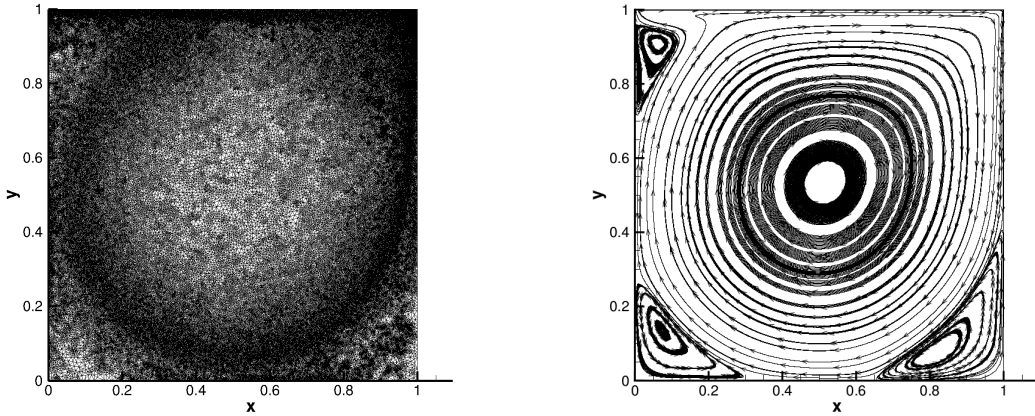


Figure 1.6: Lid-driven cavity problem for  $Re = 5,000$ . Adaptive mesh and streamlines. The mesh has 345,947 elements.

In Table 1.5, we compare our results with the ones obtained from other approaches in the literature. Note that we get similar values compared with others solvers.

| Scheme                                 | $x$    | $y$    |
|--|--------|--------|
| Ghia <i>et al.</i> (1982)              | 0.5117 | 0.5352 |
| Medic & Mohammadi (1999)               | 0.53   | 0.53   |
| LPS $\mathbb{P}_1 \times \mathbb{P}_0$ | 0.5156 | 0.5343 |

Table 1.5: Position of the center of the primary vortex. The LPS results were obtained with the adaptive mesh of Figure 1.6.

#### 1.5.4 Flow around of a circular cylinder

This problem, depicted in Figure 1.7, represents a channel with a cylindrical obstacle. The domain  $\Omega$  is the region  $]0, 2.5[ \times ]0, A[ \times ]0, A[$ , with  $A = 0.41\text{m}$ , without a cylinder of diameter  $D = 0.1\text{ m}$ . The inflow velocity field is

$$\mathbf{u}_p = A^{-4} (16Uyz(A-y)(A-z), 0, 0)^t,$$

with  $U = 0.45\text{ m/s}$ , the fluid viscosity is given by  $\nu = 10^{-3}$  and the right-hand side of the momentum equation vanishes, i.e.  $\mathbf{f} = \mathbf{0}$ . For further details see [63, 83].

The benchmark coefficients to compute are the following three: the pressure difference  $\Delta p$  between the points  $(0.55, 0.2, 0.205)$  and  $(0.45, 0.2, 0.205)$ , and the *drag* and *lift* coeffi-

cients defined as follows:

$$C_{\text{drag}} := \frac{2F_{\text{drag}}}{\rho \bar{u}^2 D A} \quad \text{and} \quad C_{\text{lift}} := \frac{2F_{\text{lift}}}{\rho \bar{u}^2 D A},$$

where  $\rho = 1$  and  $\bar{u} = 0.2$ , are the density of the fluid and the mean inflow, respectively, and

$$F_{\text{drag}} := \int_S \left( \rho \nu \frac{\partial u_t}{\partial \mathbf{n}} n_y - p n_x \right) dS \quad \text{and} \quad F_{\text{lift}} := \int_S \left( \rho \nu \frac{\partial u_t}{\partial \mathbf{n}} n_x - p n_y \right) dS$$

be the *drag* and *lift* forces, respectively. Here  $S$  is the surface of the cylinder,  $\mathbf{n} = (n_x, n_y, n_z)$  the inward pointing unit vector with respect to  $\Omega$ ,  $\mathbf{t}$  a tangential vector on  $S$  and  $u_t = \mathbf{u} \cdot \mathbf{t}$  is the projection of the velocity into the direction  $\mathbf{t}$ .

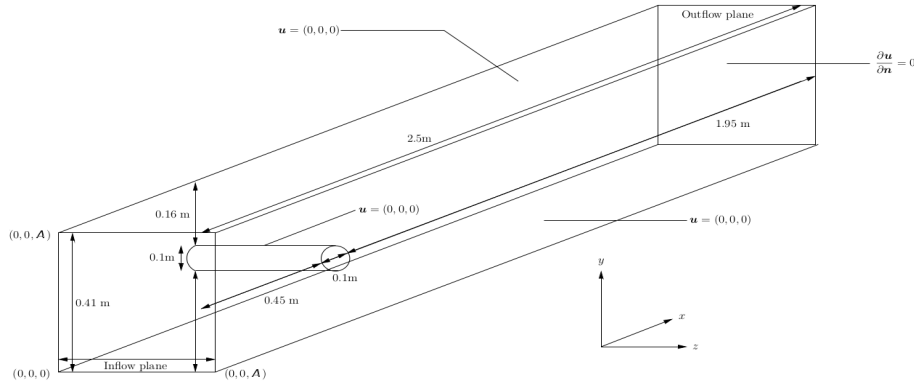


Figure 1.7: Configuration of the cylinder benchmark problem.

The Table 1.6 shows the results from the LPS method obtained from the adaptive meshes. The reference intervals for the three coefficients (see [63]) are:  $C_{\text{drag}} \in [6.05, 6.25]$ ,  $C_{\text{lift}} \in [0.008, 0.01]$  and  $\Delta p \in [0.165, 0.175]$ .

| elements  | $C_{\text{drag}}$ | $C_{\text{lift}}$ | $\Delta p$ |
|-----------|-------------------|-------------------|------------|
| 628,725   | 6.1911            | 0.0173540         | 0.17092    |
| 908,760   | 6.1236            | 0.0078108         | 0.16566    |
| 1,080,148 | 6.1023            | 0.0082491         | 0.17000    |

Table 1.6: The benchmark coefficients  $C_{\text{drag}}$ ,  $C_{\text{lift}}$  and  $\Delta p$ .

In Figure 1.8 we show the final adapted mesh, obtained with our adaptive scheme, and a zoom of a cut made at  $z = 0.205$ . Note, as expected, that most of the refinement is done near the cylinder. To complement the information, in Figure 1.9 we show the streamtracers

of the velocity field and in Figure 1.10 the magnitude of the velocity and the pressure at the cross-section  $z = 0.205$  in the final adapted mesh. Observe that the overall results are in accordance with the expected behavior of the flow (see, for instance, [15, 27]).

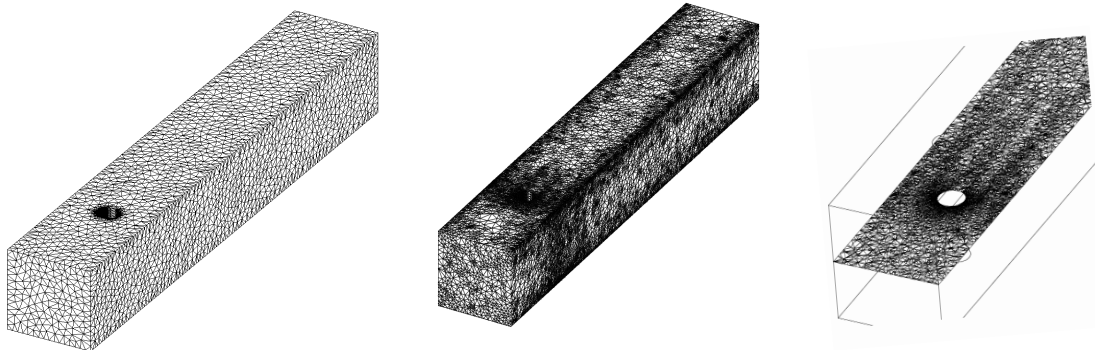


Figure 1.8: Initial mesh (left), final adapted mesh with 1,080,148 elements (center) and a cut through the plane  $z = 0.205$  (right).

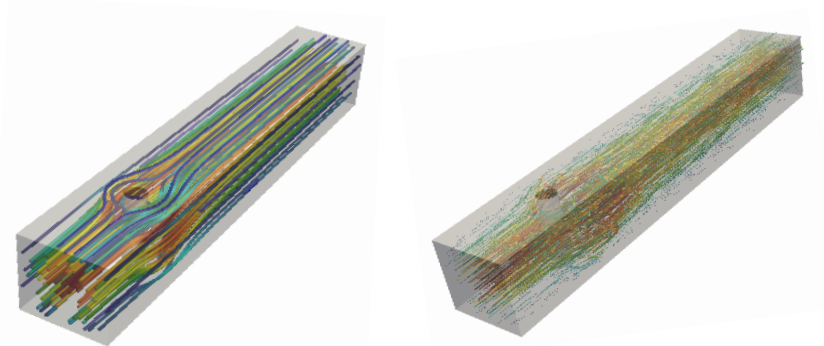


Figure 1.9: Streamtracers (left) and velocity vector field (right).

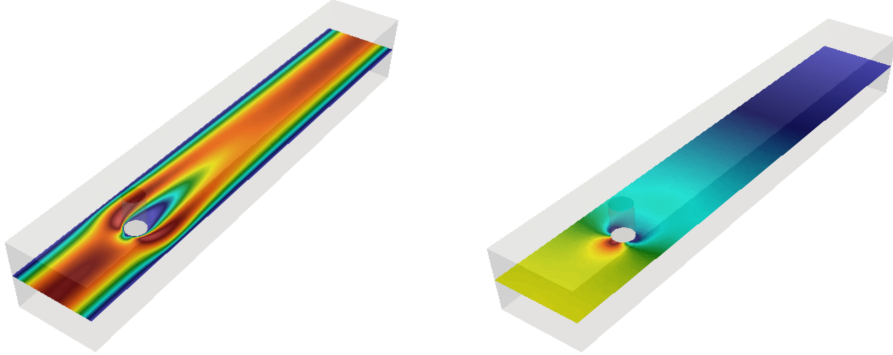


Figure 1.10: Isovalues of the magnitude of the velocity field (left) and of the pressure (right).

**Remark 1.9** *A more accurate approximation of the drag and lift coefficients is presented in [30], where the authors used a  $\mathbb{Q}_2$  approximation joint with an a posteriori error estimator based in the computation of quantities of interest. Note that our estimator is designed with an “energy norm” in mind, then it is not optimal in the sense of the computation of those parameters. On the other hand, a goal oriented estimator is, normally, more expensive to compute due to the cost implied in solving the dual problem.*

## 1.6 Conclusions

In this chapter we adapted the ideas of [9] and [14] to develop an a posteriori error analysis of hierarchical-type for the LPS method, introduced in [15], which approximates the solution of the fully nonlinear incompressible Navier–Stokes equations. Our a posteriori estimator is based on the solution of local problems posed in specific one-dimensional spaces of bubble-like functions, so is easy to implement with low computational cost. In order to study the performance of our a posteriori estimator we presented numerical examples with analytical solutions checking that the effectivity index stays bounded as  $h$  goes to zero, and we tested well known benchmark problems which live outside of the theoretical framework showing that our a posteriori estimator generates a sequence of adapted meshes improving the quality of the numerical solutions even in turbulent regime, as was shown with the lid-driven cavity problem.

## Chapter 2

# On a Multiscale a Posteriori Error Estimator for the Stokes and Brinkman Equations

### 2.1 Introduction

In this chapter we propose and analyze a residual a posteriori error estimator for the Multiscale Hybrid-Mixed (MHM) method for the Stokes and Brinkman equations. The error estimator relies on the multi-level structure of the MHM method and considers two levels of approximation of the method. As a result, the error estimator accounts for a first-level global estimator defined on the skeleton of the partition and second-level contributions from element-wise approximations. The analysis establishes local efficiency and reliability of the complete multiscale estimator. Also, it yields a new face-adaptive strategy on the mesh's skeleton which avoids changing the topology of the global mesh. Specially designed to work on multiscale problems, the present estimator can leverage parallel computers since local error estimators are independent of each other. Academic and realistic multiscale numerical tests assess the performance of the estimator and validate the adaptive algorithms.

This chapter is organized as follows: Section 2.2 introduces the model problem, and Section 2.3 revisits the one and two-level MHM methods proposed in [12], and gives some preliminary results. Section 2.4 presents the multiscale a posteriori error estimator and its analysis. Also, it outlines two adaptive algorithms based on the multi-level structure of the estimator. Three examples assess the theoretical results in Section 2.5.

## 2.2 Model problem and Preliminaries

Let  $\Omega \subset \mathbb{R}^d$ ,  $d \in \{2, 3\}$ , be an open and bounded polytopal domain with boundary  $\partial\Omega$ . The generalized Stokes problem, also called Brinkman problem, consists of finding a velocity  $\mathbf{u} : \Omega \rightarrow \mathbb{R}^d$  and a pressure  $p : \Omega \rightarrow \mathbb{R}$  fields such that

$$\begin{aligned} -\nu \Delta \mathbf{u} + \boldsymbol{\gamma} \mathbf{u} + \nabla p &= \mathbf{f} \quad \text{in } \Omega, \\ \nabla \cdot \mathbf{u} &= 0 \quad \text{in } \Omega, \\ \mathbf{u} &= \mathbf{g} \quad \text{on } \partial\Omega. \end{aligned} \tag{2.1}$$

Here  $\nu \in \mathbb{R}^+$  is the diffusion coefficient,  $\boldsymbol{\gamma} \in L^\infty(\Omega)^{d \times d}$  is a tensor which may contains multiscale features of the media,  $\mathbf{f} \in L^2(\Omega)^d$  is a body force and the function  $\mathbf{g} \in H^{1/2}(\partial\Omega)^d$  satisfies the compatibility condition  $\int_{\partial\Omega} \mathbf{g} \cdot \mathbf{n}_F \, dS = 0$ .

Also, we assume  $\boldsymbol{\gamma}$  is a symmetric and definite positive tensor which is uniformly elliptic, i.e., there exist constants  $\gamma_{\min}, \gamma_{\max} > 0$  such that

$$\gamma_{\min} |\boldsymbol{\xi}|^2 \leq \boldsymbol{\xi}^T \boldsymbol{\gamma}(\mathbf{x}) \boldsymbol{\xi} \leq \gamma_{\max} |\boldsymbol{\xi}|^2, \quad \forall \boldsymbol{\xi} \in \mathbb{R}^d, \forall \mathbf{x} \in \Omega. \tag{2.2}$$

### 2.2.1 Notations

The standard variational mixed formulation of problem (2.1) reads: *Find  $\mathbf{u} \in H^1(\Omega)^d$ , with  $\mathbf{u} = \mathbf{g}$  on  $\partial\Omega$ , and  $p \in L_0^2(\Omega)$  such that*

$$\begin{aligned} a(\mathbf{u}, \mathbf{v}) + b(\mathbf{v}, p) &= (\mathbf{f}, \mathbf{v})_\Omega \quad \text{for all } \mathbf{v} \in H_0^1(\Omega)^d, \\ b(\mathbf{u}, q) &= 0 \quad \text{for all } q \in L_0^2(\Omega), \end{aligned} \tag{2.3}$$

where the bilinear forms  $a(\cdot, \cdot)$  and  $b(\cdot, \cdot)$  are defined by

$$a(\mathbf{w}, \mathbf{v}) := (\nu \nabla \mathbf{w}, \nabla \mathbf{v})_\Omega + (\boldsymbol{\gamma} \mathbf{w}, \mathbf{v})_\Omega \quad \text{and} \quad b(\mathbf{v}, q) := -(\nabla \cdot \mathbf{v}, q)_\Omega, \tag{2.4}$$

for all  $\mathbf{w}, \mathbf{v} \in H^1(\Omega)^d$  and  $q \in L_0^2(\Omega)$ . Problem (2.3) is well-posed (see for instance [49]).

On top of a mesh  $\mathcal{T}_H$ , we define the following spaces

$$\mathbf{V} := H^1(\mathcal{T}_H)^d := \{\mathbf{v} \in L^2(\Omega)^d : \mathbf{v}|_K \in H^1(K)^d \quad \text{for all } K \in \mathcal{T}_H\}, \tag{2.5}$$

$$\boldsymbol{\Lambda} := \left\{ \boldsymbol{\sigma} \mathbf{n}^K|_{\partial K} \in H^{-1/2}(\partial K)^d \quad \text{for all } K \in \mathcal{T}_H : \boldsymbol{\sigma} \in H(\text{div}; \Omega) \right\}, \tag{2.6}$$

and

$$Q := L^2(\Omega). \quad (2.7)$$

We define an inner product on  $\mathbf{V}$  by

$$(\mathbf{u}, \mathbf{v})_{\mathbf{V}} := \frac{1}{d_{\Omega}^2} (\mathbf{u}, \mathbf{v})_{\Omega} + \sum_{K \in \mathcal{T}_H} (\nabla \mathbf{u}, \nabla \mathbf{v})_K \quad \text{for all } \mathbf{u}, \mathbf{v} \in \mathbf{V}.$$

We equip the spaces  $H(\text{div}; \Omega)$ ,  $\mathbf{V}$  and  $\mathbf{V} \times Q$  with the norms,

$$\|\boldsymbol{\sigma}\|_{\text{div}, \Omega}^2 := \sum_{K \in \mathcal{T}_H} (\|\boldsymbol{\sigma}\|_{0,K}^2 + d_{\Omega}^2 \|\nabla \cdot \boldsymbol{\sigma}\|_{0,K}^2), \quad (2.8)$$

$$\|\mathbf{v}\|_{\mathbf{V}}^2 := \sum_{K \in \mathcal{T}_H} \left( d_{\Omega}^{-2} \|\mathbf{v}\|_{0,K}^2 + \|\nabla \mathbf{v}\|_{0,K}^2 \right), \quad (2.9)$$

and

$$\|(\mathbf{v}, q)\|_{\mathbf{V} \times Q}^2 := \|\mathbf{v}\|_{\mathbf{V}}^2 + \|q\|_Q^2, \quad (2.10)$$

respectively, and the space  $\boldsymbol{\Lambda}$  with the quotient norm

$$\|\boldsymbol{\mu}\|_{\boldsymbol{\Lambda}} := \inf_{\substack{\boldsymbol{\sigma} \in H(\text{div}; \Omega) \\ \boldsymbol{\sigma} \mathbf{n}^K = \boldsymbol{\mu} \text{ on } \partial K, K \in \mathcal{T}_H}} \|\boldsymbol{\sigma}\|_{\text{div}, \Omega}. \quad (2.11)$$

For  $\boldsymbol{\mu} \in \boldsymbol{\Lambda}$  and  $\mathbf{v} \in \mathbf{V}$  we define

$$(\boldsymbol{\mu}, \mathbf{v})_{\partial \mathcal{T}_H} := \sum_{K \in \mathcal{T}_H} \langle \boldsymbol{\mu}, \mathbf{v} \rangle_{\partial K}$$

and the following norms in  $H^{-1/2}(\partial D)^d$  and  $H^{1/2}(\partial D)^d$ , respectively,

$$\|\boldsymbol{\mu}\|_{-1/2, \partial D} := \sup_{\mathbf{v} \in H^{1/2}(\partial D)^d} \frac{\langle \boldsymbol{\mu}, \mathbf{v} \rangle_{\partial D}}{\|\mathbf{v}\|_{1/2, \partial D}} \quad \text{and} \quad \|\mathbf{v}\|_{1/2, \partial D} := \inf_{\substack{\mathbf{w} \in H^1(D)^d \\ \mathbf{w} = \mathbf{v} \text{ on } \partial D}} \|\mathbf{w}\|_{1,D}. \quad (2.12)$$

We recall from [11, Lemma 8.3] that the norm (2.11) is equivalent to a dual norm, namely,

$$\frac{\sqrt{2}}{2} \|\boldsymbol{\mu}\|_{\boldsymbol{\Lambda}} \leq \sup_{\mathbf{v} \in \mathbf{V}} \frac{(\boldsymbol{\mu}, \mathbf{v})_{\partial \mathcal{T}_H}}{\|\mathbf{v}\|_{\mathbf{V}}} \leq \|\boldsymbol{\mu}\|_{\boldsymbol{\Lambda}} \quad \text{for all } \boldsymbol{\mu} \in \boldsymbol{\Lambda}. \quad (2.13)$$

Above and hereafter we lighten notation and understand the supremum to be taken over

sets excluding the zero function, even though this is not specifically indicated.

Next, following [11], we replace (2.3) by the following hybrid formulation:  $\text{Find } (\mathbf{u}, p, \boldsymbol{\lambda}, \rho) \in \mathbf{V} \times Q \times \boldsymbol{\Lambda} \times \mathbb{R} \text{ such that}$

$$\left\{ \begin{array}{l} a(\mathbf{u}, \mathbf{v}) + b(\mathbf{v}, p) + (\boldsymbol{\lambda}, \mathbf{v})_{\partial\mathcal{T}_H} = (\mathbf{f}, \mathbf{v})_{\mathcal{T}_H} \quad \text{for all } \mathbf{v} \in \mathbf{V}, \\ b(\mathbf{u}, q) + (\rho, q)_{\Omega} = 0 \quad \text{for all } q \in Q, \\ (\boldsymbol{\mu}, \mathbf{u})_{\partial\mathcal{T}_H} = \langle \boldsymbol{\mu}, \mathbf{g} \rangle_{\partial\Omega} \quad \text{for all } \boldsymbol{\mu} \in \boldsymbol{\Lambda}, \\ (\xi, p)_{\Omega} = 0 \quad \text{for all } \xi \in \mathbb{R}, \end{array} \right. \quad (2.14)$$

and we found that  $(\mathbf{u}, p)$  solution of (2.14) coincides with the solution of (2.3) as shown in [12, Theorem 6]. Above and hereafter, we surcharge the notation  $a(\cdot, \cdot)$  and  $b(\cdot, \cdot)$  to extend them to the space  $\mathbf{V}$  as follows

$$a(\mathbf{w}, \mathbf{v}) := \sum_{K \in \mathcal{T}_H} a_K(\mathbf{w}, \mathbf{v}) \quad \text{with} \quad a_K(\mathbf{w}, \mathbf{v}) := (\nu \nabla \mathbf{w}, \nabla \mathbf{v})_K + (\gamma \mathbf{w}, \mathbf{v})_K,$$

and

$$b(\mathbf{v}, q) := \sum_{K \in \mathcal{T}_H} b_K(\mathbf{v}, q) \quad \text{with} \quad b_K(\mathbf{v}, q) := -(\nabla \cdot \mathbf{v}, q)_K,$$

for all  $\mathbf{w}, \mathbf{v} \in \mathbf{V}$  and  $q \in Q$ .

### 2.2.2 Preliminar results

Let  $\mathbf{V}_0$  be the closed subspace of the Hilbert space  $\mathbf{V}$  defined by

$$\mathbf{V}_0 := \{\mathbf{v} \in \mathbf{V} : a(\mathbf{v}, \mathbf{w}) = 0 \quad \text{for all } \mathbf{w} \in \mathbf{V}\}.$$

Observe that for the Stokes problem ( $\gamma = \mathbf{0}$ )

$$\mathbf{V}_0 = \left\{ \mathbf{v} \in \mathbf{V} : \mathbf{v}|_K \in \mathbb{P}_0(K)^d \text{ for all } K \in \mathcal{T}_H \right\},$$

and  $\mathbf{V}_0 = \{\mathbf{0}\}$  otherwise. As such, we can decompose  $\mathbf{V}$  as follows

$$\mathbf{V} = \mathbf{V}_0 \oplus \mathbf{V}_0^{\perp}, \quad (2.15)$$

where  $\mathbf{V}_0^\perp$  is the orthogonal complement with respect to the inner-product  $(\cdot, \cdot)_{\mathbf{V}}$ . Note that for the Stokes equations ( $\gamma = \mathbf{0}$ ), it is given by

$$\mathbf{V}_0^\perp = \left\{ \mathbf{v} \in \mathbf{V} : \mathbf{v}|_K \in [H^1(K) \cap L_0^2(K)]^d \text{ for all } K \in \mathcal{T}_H \right\},$$

and  $\mathbf{V}_0^\perp = \mathbf{V}$  otherwise. We shall denote by  $\mathbf{V}_0^\perp(K)$ ,  $\mathbf{V}(K)$  and  $Q(K)$  the spaces of vector functions in  $\mathbf{V}_0^\perp$ ,  $\mathbf{V}$  and  $Q$  restricted to  $K$ , respectively. Also, the corresponding restricted norms are denoted by  $\|\cdot\|_{\mathbf{V}(K)}$  and  $\|\cdot\|_{Q(K)}$ , and the local product norm by  $\|\cdot, \cdot\|_{\mathbf{V}(K) \times Q(K)}$ .

The next results shall be intensively used in the rest of this work. Although being a direct consequence of standard saddle-point theory, they may not be easy to find in the literature, and then, we decided to detail them here.

**Theorem 2.1** *There exists a constant  $\alpha > 0$ , independent of  $K$ , such that*

$$\sup_{\mathbf{v} \in \mathbf{V}_0(K)^\perp} \frac{(\nabla \cdot \mathbf{v}, q)_K}{\|\mathbf{v}\|_{\mathbf{V}(K)}} \geq \alpha \|q\|_{Q(K)}$$

for all  $q \in Q(K)$ .

*Proof.* We first consider the Stokes case, that is,

$$\mathbf{V}_0(K)^\perp = [H^1(K) \cap L_0^2(K)]^d.$$

Let  $q \in Q(K)$ . Thanks to the decomposition  $L^2(K) = L_0^2(K) \oplus \mathbb{P}_0(K)$ , it holds  $q = \tilde{q} + q_0$  with  $\tilde{q} \in L_0^2(K)$  and  $q_0 = |K|^{-1} \int_K q \, dx$ . Let  $\tilde{\mathbf{w}} \in H_0^1(K)^d$  be such that

$$\nabla \cdot \tilde{\mathbf{w}} = \tilde{q} \quad \text{in } K, \tag{2.16}$$

satisfying

$$|\tilde{\mathbf{w}}|_{1,K} \leq C_d \frac{H_K}{\rho_K} \|\tilde{q}\|_{0,K}, \tag{2.17}$$

where  $\rho_K$  is the radius of the ball inscribed in  $K$  and  $C_d$  is a positive constant which depends only on  $d$ . The existence of such a function  $\tilde{\mathbf{w}}$  is ensured in [42, Theorem 5.2]. Since we supposed that  $\{\mathcal{T}_H\}_{H>0}$  is shape-regular, there exists  $\sigma_0 > 0$  such that

$$\frac{H_K}{\rho_K} \leq \sigma_0,$$

for all  $K \in \mathcal{T}_H$  and all  $H_K$ , thus from (2.17) we have

$$|\tilde{\mathbf{w}}|_{1,K} \leq C_d \sigma_0 \|\tilde{q}\|_{0,K}. \tag{2.18}$$

Setting

$$\mathbf{w} := \tilde{\mathbf{w}} + \frac{q_0}{d} \mathbf{x} - \frac{1}{|K|} \int_K \left( \tilde{\mathbf{w}} + \frac{q_0}{d} \mathbf{x} \right) dx,$$

from (2.16) we have that

$$\nabla \cdot \mathbf{w} = q \quad \text{in } K, \quad (2.19)$$

and from (2.18)

$$\begin{aligned} |\mathbf{w}|_{1,K} &\leq |\tilde{\mathbf{w}}|_{1,K} + |d^{-1}q_0 \mathbf{x}|_{1,K} \\ &\leq C_d \sigma_0 \|\tilde{q}\|_{0,K} + d^{-1/2} \|q_0\|_{0,K} \\ &\leq \max\{C_d \sigma_0, d^{-1/2}\} \|q\|_{0,K}. \end{aligned} \quad (2.20)$$

In addition, since  $\mathbf{w} \in [H^1(K) \cap L_0^2(K)]^d$ , from [28, Theorem 3.2], we have

$$\|\mathbf{w}\|_{0,K} \leq \frac{H_K}{\pi} |\mathbf{w}|_{1,K}. \quad (2.21)$$

Then, from (2.19), (2.20) and (2.21), we get

$$\begin{aligned} \sup_{\mathbf{v} \in [H^1(K) \cap L_0^2(K)]^d} \frac{(\nabla \cdot \mathbf{v}, q)_K}{\|\mathbf{v}\|_{\mathbf{V}(K)}} &\geq \frac{(\nabla \cdot \mathbf{w}, q)_K}{(d_\Omega^{-2} \|\mathbf{w}\|_{0,K}^2 + |\mathbf{w}|_{1,K}^2)^{1/2}} \\ &\geq \left( \left( \frac{1}{\pi^2} + 1 \right)^{1/2} \max\{C_d \sigma_0, d^{-1/2}\} \right)^{-1} \|q\|_{0,K}. \end{aligned} \quad (2.22)$$

For the Brinkman case, that is  $\mathbf{V}_0(K)^\perp = H^1(K)^d$ , we use (2.22) to obtain

$$\begin{aligned} \sup_{\mathbf{v} \in H^1(K)^d} \frac{(\nabla \cdot \mathbf{v}, q)_K}{\|\mathbf{v}\|_{\mathbf{V}(K)}} &\geq \sup_{\mathbf{v} \in [H^1(K) \cap L_0^2(K)]^d} \frac{(\nabla \cdot \mathbf{v}, q)_K}{\|\mathbf{v}\|_{\mathbf{V}(K)}} \\ &\geq \left( \left( \frac{1}{\pi^2} + 1 \right)^{1/2} \max\{C_d \sigma_0, d^{-1/2}\} \right)^{-1} \|q\|_{0,K} \end{aligned}$$

ending the proof. ■

**Theorem 2.2** *There exists a constant  $\beta > 0$ , independent of  $H_K$ , such that*

$$\sup_{(\mathbf{v}, q) \in \mathbf{V}_0(K)^\perp \times Q(K)} \frac{a_K(\mathbf{w}, \mathbf{v}) + b_K(\mathbf{v}, r) - b_K(\mathbf{w}, q)}{\|(\mathbf{v}, q)\|_{\mathbf{V}(K) \times Q(K)}} \geq \beta \|(\mathbf{w}, r)\|_{\mathbf{V}(K) \times Q(K)}$$

for all  $(\mathbf{w}, r) \in \mathbf{V}_0(K)^\perp \times Q(K)$ .

*Proof.* The result follows from the ellipticity of the bilinear form  $a_K(\cdot, \cdot)$  and Theorem 2.1.

**Remark 2.1** Using Theorem 2.2 and Riesz Representation Theorem, the following global inf-sup condition holds

$$\begin{aligned} \sup_{(\mathbf{v}, q) \in \mathbf{V}_0^\perp \times Q} \frac{a(\mathbf{w}, \mathbf{v}) + b(\mathbf{v}, r) - b(\mathbf{w}, q)}{\|(\mathbf{v}, q)\|_{\mathbf{V} \times Q}} &= \left\{ \sum_{K \in \mathcal{T}_H} \left( \sup_{(\mathbf{v}, q) \in \mathbf{V}_0(K)^\perp \times Q(K)} \frac{a_K(\mathbf{w}, \mathbf{v}) + b_K(\mathbf{v}, r) - b_K(\mathbf{w}, q)}{\|(\mathbf{v}, q)\|_{\mathbf{V}(K) \times Q(K)}} \right)^2 \right\}^{1/2} \\ &\geq \beta \|(\mathbf{w}, r)\|_{\mathbf{V} \times Q} \end{aligned} \quad (2.23)$$

for all  $(\mathbf{w}, r) \in \mathbf{V}_0^\perp \times Q$ , where  $\beta > 0$  is independent of  $H$ .

Associated to the second-level meshes for each  $K \in \mathcal{T}_H$ , we define the standard polynomial bubble functions which shall be used in the proofs. Specifically, let  $b_\tau^K$  and  $b_\zeta^K$  be the bubble functions with support in  $\tau \in \mathcal{T}_h^K$  and  $\omega_\zeta \in \mathcal{E}_h^K$ , respectively, and defined with respect to the barycentric coordinates (see for instance [6, Section 2.3.1] for details). For the sake of completeness, we line up two theorems that summarize the main properties of these functions, observing that their vector versions counterpart are straightforward.

**Theorem 2.3** Let  $K \in \mathcal{T}_H$  and let  $b_\tau^K$  be the element bubble function corresponding to  $\tau \in \mathcal{T}_h^K$ . Then

$$\|v_h\|_{0,\tau}^2 \preceq (b_\tau^K v_h, v_h)_\tau \preceq \|v_h\|_{0,\tau}^2$$

and

$$\|v_h\|_{0,\tau} \preceq \|b_\tau^K v_h\|_{0,\tau} + h_\tau |b_\tau^K v_h|_{1,\tau} \preceq \|v_h\|_{0,\tau}$$

for all  $v_h \in \mathbb{P}_n(\mathcal{T}_h^K)$ ,  $n \geq 0$ .

*Proof.* See [6, Theorem 2.2].

**Theorem 2.4** Let  $K \in \mathcal{T}_H$  and let  $b_\zeta^K$  be the corresponding face bubble function on face  $\zeta \in \mathcal{E}_h^K$  and  $\tau \in \mathcal{T}_h^K$  such that  $\tau$  is in the support of  $b_\zeta^K$ . Then

$$\|v_h\|_{0,\zeta}^2 \preceq (b_\zeta^K v_h, v_h)_\zeta \preceq \|v_h\|_{0,\zeta}^2$$

and

$$h_\tau^{-1/2} \|b_\zeta^K v_h\|_{0,\tau} + h_\tau^{1/2} |b_\zeta^K v_h|_{1,\tau} \preceq \|v_h\|_{0,\zeta}$$

for all  $v_h \in \mathbb{P}_n(\mathcal{T}_h^K)$ ,  $n \geq 0$ .

*Proof.* See [6, Theorem 2.4].

Also, let  $\mathcal{C}_h^K : H^1(K) \rightarrow V_1^K$  be the Clément interpolation operator defined on each  $K \in \mathcal{T}_H$ , where  $V_1^K$  is given by

$$V_1^K := \{v_h \in C^0(K) : v_h \in \mathbb{P}_1(\tau) \text{ for all } \tau \in \mathcal{T}_h^K\}.$$

It verifies the following local stability and approximation properties (cf. [39, 45]):

$$\|\mathcal{C}_h(v)\|_{0,\tau} \preceq \|v\|_{0,\tilde{\omega}_\tau} \quad \forall \tau \in \mathcal{T}_h^K, \quad (2.24)$$

$$\|v - \mathcal{C}_h(v)\|_{0,\tau} \preceq h_\tau |v|_{1,\tilde{\omega}_\tau} \quad \forall \tau \in \mathcal{T}_h^K, \quad (2.25)$$

$$\|v - \mathcal{C}_h(v)\|_{0,\zeta} \preceq h_\zeta^{1/2} |v|_{1,\tilde{\omega}_\zeta} \quad \forall \zeta \in \mathcal{E}_h^K, \quad (2.26)$$

for all  $v \in H^1(K)$ , where  $\tilde{\omega}_\tau$  and  $\tilde{\omega}_\zeta$  are the set of elements  $\tau \in \mathcal{T}_h^K$  sharing at least one vertex with  $\tau$  and  $\zeta$ , respectively. Furthermore, we denote by  $\mathcal{C}_h^K(\mathbf{v})$  the vector function whose components are the Clément interpolation of each component of  $\mathbf{v} \in H^1(K)^d$ .

## 2.3 The MHM method

This section summarizes the main ideas of the MHM method proposed in [12]. The basic idea behind the MHM approach is to leverage the nature of hybrid problem (2.14), and characterize the exact solution regarding the well-posed independent local problems and a face-based global problem which ties everything together. The one- and two-level MHM method results from the discretization of the global (one-level) and local (two-level) problems, respectively.

### 2.3.1 Characterizing the exact solution

Let us consider the following local bilinear form  $B_K : (\mathbf{V}_0^\perp(K) \times Q(K)) \times (\mathbf{V}_0^\perp(K) \times Q(K))$  defined by

$$B_K((\mathbf{w}, r), (\mathbf{v}, q)) := a_K(\mathbf{w}, \mathbf{v}) + b_K(\mathbf{v}, r) - b_K(\mathbf{w}, q) \quad (2.27)$$

for all  $(\mathbf{w}, r), (\mathbf{v}, q) \in \mathbf{V}_0^\perp(K) \times Q(K)$ .

We define the following linear mappings:

- $\mathbf{T} : \Lambda \rightarrow \mathbf{V}_0^\perp \times Q$  such that  $\mathbf{T}\boldsymbol{\mu}|_K := (T^u \boldsymbol{\mu}, T^p \boldsymbol{\mu})$  solves

$$B_K((T^u \boldsymbol{\mu}, T^p \boldsymbol{\mu}), (\mathbf{v}, q)) = -\langle \boldsymbol{\mu}, \mathbf{v} \rangle_{\partial K} \quad \text{for all } (\mathbf{v}, q) \in \mathbf{V}_0^\perp(K) \times Q(K); \quad (2.28)$$

- $\hat{\mathbf{T}} : L^2(\Omega)^d \rightarrow \mathbf{V}_0^\perp \times Q$  such that  $\hat{\mathbf{T}}\mathbf{r}|_K := (\hat{T}^u \mathbf{r}, \hat{T}^p \mathbf{r})$  solves

$$B_K((\hat{T}^u \mathbf{r}, \hat{T}^p \mathbf{r}), (\mathbf{v}, q)) = (\mathbf{r}, \mathbf{v})_K \quad \text{for all } (\mathbf{v}, q) \in \mathbf{V}_0^\perp(K) \times Q(K); \quad (2.29)$$

- $\bar{\mathbf{T}} : \mathbb{R} \rightarrow \mathbf{V}_0^\perp \times Q$  such that  $\bar{\mathbf{T}}\xi|_K := (\bar{T}^u \xi, \bar{T}^p \xi)$  solves

$$B_K((\bar{T}^u \xi, \bar{T}^p \xi), (\mathbf{v}, q)) = -(\xi, q)_K \quad \text{for all } (\mathbf{v}, q) \in \mathbf{V}_0^\perp(K) \times Q(K). \quad (2.30)$$

Owing to decomposition (2.15), and noting that  $a(\mathbf{w}, \mathbf{v}) = 0$  when  $\mathbf{w} \in \mathbf{V}_0$  or  $\mathbf{v} \in \mathbf{V}_0$ , we rewrite (2.14) as the following global-local problem: *Find  $(\mathbf{u}_0, \boldsymbol{\lambda}, \rho) \in \mathbf{V}_0 \times \boldsymbol{\Lambda} \times \mathbb{R}$  such that*

$$\begin{cases} (\boldsymbol{\lambda}, \mathbf{v}_0)_{\partial\mathcal{T}_H} = (\mathbf{f}, \mathbf{v}_0)_{\mathcal{T}_H}, \\ (\boldsymbol{\mu}, \mathbf{u}_0)_{\partial\mathcal{T}_H} + (\boldsymbol{\mu}, T^u \boldsymbol{\lambda})_{\partial\mathcal{T}_H} + (\boldsymbol{\mu}, \bar{T}^u \rho)_{\partial\mathcal{T}_H} = \langle \boldsymbol{\mu}, \mathbf{g} \rangle_{\partial\Omega} - (\boldsymbol{\mu}, \hat{T}^u \mathbf{f})_{\partial\mathcal{T}_H}, \\ (\xi, T^p \boldsymbol{\lambda})_\Omega + (\xi, \bar{T}^p \rho)_\Omega = -(\xi, \hat{T}^p \mathbf{f})_\Omega, \end{cases} \quad (2.31)$$

for all  $(\mathbf{v}_0, \boldsymbol{\mu}, \xi) \in \mathbf{V}_0 \times \boldsymbol{\Lambda} \times \mathbb{R}$ .

Hereafter, we assume that the global problem (2.31) is well-posed. Hence, from the linearity of problems (2.28)-(2.30), we find that the exact  $\mathbf{u}$  and  $p$  can be characterized as follows

$$\mathbf{u} = \mathbf{u}_0 + T^u \boldsymbol{\lambda} + \hat{T}^u \mathbf{f} \quad \text{and} \quad p = T^p \boldsymbol{\lambda} + \hat{T}^p \mathbf{f} \quad (2.32)$$

where we used (see [12]) that  $\rho = 0$ . Next, we prove that operators  $\mathbf{T}$ ,  $\hat{\mathbf{T}}$  and  $\bar{\mathbf{T}}$  are stable with respect to the given data.

**Theorem 2.5** *The operators  $\mathbf{T}$ ,  $\hat{\mathbf{T}}$  and  $\bar{\mathbf{T}}$ , given by (2.28), (2.29) and (2.30), respectively, are well-defined. Moreover, we have that*

$$\begin{aligned} \|\mathbf{T}\boldsymbol{\mu}\|_{\mathbf{V} \times Q} &\leq \|\boldsymbol{\mu}\|_{\boldsymbol{\Lambda}} \quad \text{for all } \boldsymbol{\mu} \in \boldsymbol{\Lambda}, \\ \|\hat{\mathbf{T}}\mathbf{r}\|_{\mathbf{V} \times Q} &\leq \|\mathbf{r}\|_{0,\Omega} \quad \text{for all } \mathbf{r} \in L^2(\Omega)^d, \\ \|\bar{\mathbf{T}}\xi\|_{\mathbf{V} \times Q} &\leq |\xi| \quad \text{for all } \xi \in \mathbb{R}. \end{aligned}$$

*Proof.* From (2.13) and the global inf-sup (2.23) we get

$$\begin{aligned} \|\boldsymbol{T}\boldsymbol{\mu}\|_{\mathbf{V} \times Q} &= \|(T^u \boldsymbol{\mu}, T^p \boldsymbol{\mu})\|_{\mathbf{V} \times Q} \\ &\leq \frac{1}{\beta} \sup_{(\mathbf{v}, q) \in \mathbf{V}_0^\perp \times Q} \frac{a(T^u \boldsymbol{\mu}, \mathbf{v}) + b(\mathbf{v}, T^p \boldsymbol{\mu}) - b(T^u \boldsymbol{\mu}, q)}{\|(\mathbf{v}, q)\|_{\mathbf{V} \times Q}} \\ &= \frac{1}{\beta} \sup_{(\mathbf{v}, q) \in \mathbf{V}_0^\perp \times Q} \frac{-(\boldsymbol{\mu}, \mathbf{v})_{\partial \mathcal{T}_H}}{\|(\mathbf{v}, q)\|_{\mathbf{V} \times Q}} \leq \frac{1}{\beta} \|\boldsymbol{\mu}\|_{\Lambda}, \end{aligned}$$

where  $\beta > 0$  is independent of  $H$ . The proofs of the other two inequalities are analogous.  $\blacksquare$

Note that the solution of the coupled global-local problem (2.28)–(2.31) coincides with the solution of the hybrid problem (2.14).

### 2.3.2 The one-level MHM method

The one-level MHM method stems from the coupled problems (2.28)–(2.31). We search the approximate Lagrange multipliers in the following space

$$\boldsymbol{\Lambda}_H := \{\boldsymbol{\lambda}_H \in \boldsymbol{\Lambda} : \boldsymbol{\lambda}_H|_{\tilde{F}} \in \mathbb{P}_l(\tilde{F})^d, \text{ for all } \tilde{F} \subset \mathcal{T}_{\tilde{H}}(F), \text{ for all } F \in \mathcal{E}_H\}. \quad (2.33)$$

Observe that (2.33) permits discontinuous interpolations on faces which can differ on each  $F \in \mathcal{E}_H$ . See Figure 2.1 for an illustration. We shall denote by  $\boldsymbol{\Lambda}_l^m$  the space when  $\mathcal{T}_{\tilde{H}}(F)$  is composed of  $m$  elements. When  $m = 1$ , we denote  $\boldsymbol{\Lambda}_l^1$  by  $\boldsymbol{\Lambda}_l$ .

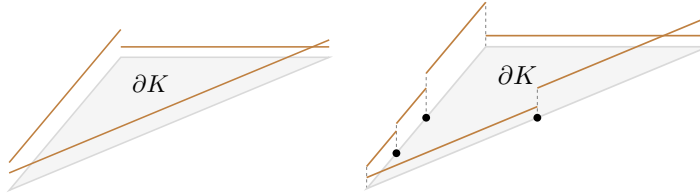


Figure 2.1: Two examples of  $\boldsymbol{\Lambda}_H$  restricted to an element  $K \in \mathcal{E}_H$ .

Replacing  $\boldsymbol{\Lambda}$  by  $\boldsymbol{\Lambda}_H$  uncouples local and global problems as shown in [12]. The multiscale basis functions are computed from (2.28) with the right-hand side replaced by the polynomial base functions on faces, and the degrees of freedom are obtained from the following one-level

MHM method: Find  $(\mathbf{u}_0^H, \boldsymbol{\lambda}_H, \rho_H) \in \mathbf{V}_0 \times \boldsymbol{\Lambda}_H \times \mathbb{R}$  such that

$$\begin{cases} (\boldsymbol{\lambda}_H, \mathbf{v}_0)_{\partial\mathcal{T}_H} = (\mathbf{f}, \mathbf{v}_0)_{\mathcal{T}_H}, \\ (\boldsymbol{\mu}_H, \mathbf{u}_0^H)_{\partial\mathcal{T}_H} + (\boldsymbol{\mu}_H, T^u \boldsymbol{\lambda}_H)_{\partial\mathcal{T}_H} + (\boldsymbol{\mu}_H, \bar{T}^u \rho_H)_{\partial\mathcal{T}_H} = \langle \boldsymbol{\mu}_H, \mathbf{g} \rangle_{\partial\Omega} - (\boldsymbol{\mu}_H, \hat{T}^u \mathbf{f})_{\partial\mathcal{T}_H}, \\ (\xi_H, T^p \boldsymbol{\lambda}_H)_\Omega + (\xi_H, \bar{T}^p \rho_H)_\Omega = -(\xi_H, \hat{T}^p \mathbf{f})_\Omega, \end{cases} \quad (2.34)$$

for all  $\mathbf{v}_0 \in \mathbf{V}_0$ ,  $\boldsymbol{\mu}_H \in \boldsymbol{\Lambda}_H$  and  $\xi_H \in \mathbb{R}$ . Here  $\mathbf{T}$ ,  $\hat{\mathbf{T}}$  and  $\bar{\mathbf{T}}$  are given by (2.28)-(2.30), respectively. Observe that, in the one-level method (2.34), we assume that close formulas are available for the corresponding solutions of local problems (2.28)-(2.30). Thereby, the discrete one-level approximation  $(\mathbf{u}_H, p_H, \rho_H)$  of the exact solutions read

$$\mathbf{u}_H := \mathbf{u}_0^H + T^u \boldsymbol{\lambda}_H + \hat{T}^u \mathbf{f} + \bar{T}^u \rho_H \quad \text{and} \quad p_H := T^p \boldsymbol{\lambda}_H + \hat{T}^p \mathbf{f} + \bar{T}^p \rho_H. \quad (2.35)$$

We remark that the one-level MHM method is non-conform in  $H^1(\Omega)^d$ . Nevertheless, it provides a discrete stress tensor  $\boldsymbol{\sigma}_H$  given by

$$\boldsymbol{\sigma}_H := -\nu \nabla \mathbf{u}_H + p_H \mathbf{I} \quad \text{in } H(\text{div}; \Omega),$$

since  $\boldsymbol{\sigma}_H \mathbf{n}^K|_{\partial K} \in \boldsymbol{\Lambda}_H$  for all  $K \in \mathcal{T}_H$ . Also, the discrete stress tensor  $\boldsymbol{\sigma}_H$  is automatically in equilibrium, in each element  $K \in \mathcal{T}_H$ , i.e.,

$$\int_{\partial K} \boldsymbol{\sigma}_H \mathbf{n}^K d\mathbf{s} = \int_{\partial K} \boldsymbol{\lambda}_H d\mathbf{s} = \int_K \mathbf{f} dx,$$

where we used the first equation in (2.34).

In order to make the MHM method effective, one must provide approximate solutions for the local problems (2.28), (2.29) and (2.30). This is the subject of the next section.

### 2.3.3 The two-level MHM method

We begin selecting local finite dimensional spaces  $\mathbf{V}_h(K) \subset \mathbf{V}_0^\perp(K)$  and  $Q_h(K) \subset Q(K)$ , given by

$$\mathbf{V}_h(K) := \left\{ \mathbf{v}_h \in \mathbf{V}_0^\perp(K) \cap C^0(K)^d : \mathbf{v}_h|_\tau \in \mathbb{P}_k(\tau)^d \text{ for all } \tau \in \mathcal{T}_h^K \right\} \quad (2.36)$$

and

$$Q_h(K) := \left\{ q_h \in Q(K) \cap C^0(K) : q_h|_\tau \in \mathbb{P}_n(\tau) \text{ for all } \tau \in \mathcal{T}_h^K \right\}. \quad (2.37)$$

The corresponding global finite dimensional space are given by

$$\mathbf{V}_h := \bigoplus_{K \in \mathcal{T}_H} \mathbf{V}_h(K) \quad \text{and} \quad Q_h := \bigoplus_{K \in \mathcal{T}_H} Q_h(K). \quad (2.38)$$

The two-level MHM method reads: *Find  $(\mathbf{u}_0^{H,h}, \boldsymbol{\lambda}_{H,h}, \rho_H) \in \mathbf{V}_0 \times \boldsymbol{\Lambda}_H \times \mathbb{R}$  such that*

$$\begin{cases} (\boldsymbol{\lambda}_{H,h}, \mathbf{v}_0)_{\partial\mathcal{T}_H} = (\mathbf{f}, \mathbf{v}_0)_{\mathcal{T}_H}, \\ (\boldsymbol{\mu}_H, \mathbf{u}_0^{H,h})_{\partial\mathcal{T}_H} + (\boldsymbol{\mu}_H, T_h^u \boldsymbol{\lambda}_{H,h})_{\partial\mathcal{T}_H} + (\boldsymbol{\mu}_H, \bar{T}_h^u \rho_H)_{\partial\mathcal{T}_H} = \langle \boldsymbol{\mu}_H, \mathbf{g} \rangle_{\partial\Omega} - (\boldsymbol{\mu}_H, \hat{T}_h^u \mathbf{f})_{\partial\mathcal{T}_H}, \\ (\xi_H, T_h^p \boldsymbol{\lambda}_{H,h})_{\Omega} + (\xi_H, \bar{T}_h^p \rho_H)_{\Omega} = -(\xi_H, \hat{T}_h^p \mathbf{f})_{\Omega}, \end{cases} \quad (2.39)$$

for all  $(\mathbf{v}_0, \boldsymbol{\mu}_H, \xi_H) \in \mathbf{V}_0 \times \boldsymbol{\Lambda}_H \times \mathbb{R}$ .

Operators  $\mathbf{T}_h$ ,  $\bar{\mathbf{T}}_h$  and  $\hat{\mathbf{T}}_h$  are defined such that they approximate  $\mathbf{T}$ ,  $\bar{\mathbf{T}}$  and  $\hat{\mathbf{T}}$  when  $h$  goes to zero. In this work, one adopts the unusual stabilized finite element method (USFEM) proposed in [25] to define  $\mathbf{T}_h$ ,  $\bar{\mathbf{T}}_h$  and  $\hat{\mathbf{T}}_h$ . The USFEM allows using nodal equal-order pair of spaces for the velocity and the pressure variables, i.e., we can set  $k = n$  in (2.36) and (2.37). It is worth to mention that, in its more general version, the MHM method may adopt different order of interpolation spaces in each  $K \in \mathcal{T}_H$  (and even different numerical methods). Here, for the sake of clarity, we adopt the USFEM method with the same degree of interpolation in all elements of the partition.

We recall (see [25] for details) that the USFEM consists of finding  $(\mathbf{u}, p) \in \mathbf{V}_h(K) \times Q_h(K)$  such that

$$\tilde{B}_K((\mathbf{u}, p), (\mathbf{v}, q)) = F_K(\mathbf{v}, q) \quad \text{for all } (\mathbf{v}, q) \in \mathbf{V}_h(K) \times Q_h(K),$$

where

$$\begin{aligned} \tilde{B}_K((\mathbf{u}, p), (\mathbf{v}, q)) := & a_K(\mathbf{u}, \mathbf{v}) + b_K(\mathbf{v}, p) - b_K(\mathbf{u}, q) \\ & - \sum_{\tau \in \mathcal{T}_h^K} \kappa_\tau (-\nu \Delta \mathbf{u} + \boldsymbol{\gamma} \mathbf{u} + \nabla p, -\nu \Delta \mathbf{v} + \boldsymbol{\gamma} \mathbf{v} - \nabla q)_\tau \end{aligned} \quad (2.40)$$

and

$$F_K(\mathbf{v}, q) := (\mathbf{f}, \mathbf{v})_K - \sum_{\tau \in \mathcal{T}_h^K} \kappa_\tau (\mathbf{f}, -\nu \Delta \mathbf{v} + \boldsymbol{\gamma} \mathbf{v} - \nabla q)_\tau.$$

The stabilization parameter is given by

$$\kappa_\tau := \frac{h_\tau^2}{\gamma_{\min} h_\tau^2 \max\{1, \lambda_\tau\} + \frac{4\nu}{m_k}} \quad \text{with} \quad \lambda_\tau := \frac{4\nu}{m_k \gamma_{\min} h_\tau^2}, \quad (2.41)$$

where  $\gamma_{\min}$  is defined in (2.2),  $m_k := \min\{\frac{1}{3}, C_k\}$  and

$$C_k h_\tau^2 \|\Delta \mathbf{v}\|_{0,\tau}^2 \leq \|\nabla \mathbf{v}\|_{0,\tau}^2 \quad \text{for all } \mathbf{v} \in \mathbf{V}_h(K). \quad (2.42)$$

Note that the only unknown constant in the design of the stabilization parameter is  $C_k$ . This constant, depending only on  $d$  and the polynomial degree for the velocity, is tabulated in [53] for some 2D cases. A general way to calculate  $C_k$  numerically is proposed in [46].

Owing to the above definitions, we define the corresponding discrete operators as follows:

- $\mathbf{T}_h : \Lambda_H \rightarrow \mathbf{V}_h \times Q_h$  such that  $\mathbf{T}_h \boldsymbol{\lambda}_{H,h}|_K := (T_h^u \boldsymbol{\lambda}_{H,h}, T_h^p \boldsymbol{\lambda}_{H,h})$  solves

$$\tilde{B}_K((T_h^u \boldsymbol{\lambda}_{H,h}, T_h^p \boldsymbol{\lambda}_{H,h}), (\mathbf{v}_h, q_h)) = -\langle \boldsymbol{\lambda}_{H,h}, \mathbf{v}_h \rangle_{\partial K} \quad \text{for all } (\mathbf{v}_h, q_h) \in \mathbf{V}_h(K) \times Q_h(K); \quad (2.43)$$

- $\hat{\mathbf{T}}_h : L^2(\Omega)^d \rightarrow \mathbf{V}_h \times Q_h$  such that  $\hat{\mathbf{T}}_h \mathbf{f}|_K := (\hat{T}_h^u \mathbf{f}, \hat{T}_h^p \mathbf{f})$  solves

$$\tilde{B}_K((\hat{T}_h^u \mathbf{f}_H, \hat{T}_h^p \mathbf{f}_H), (\mathbf{v}_h, q_h)) = F_K(\mathbf{v}_h, q_h) \quad \text{for all } (\mathbf{v}_h, q_h) \in \mathbf{V}_h(K) \times Q_h(K); \quad (2.44)$$

- $\bar{\mathbf{T}}_h : \mathbb{R} \rightarrow \mathbf{V}_h \times Q_h$  such that  $\bar{\mathbf{T}}_h \rho_H|_K := (\bar{T}_h^u \rho_H, \bar{T}_h^p \rho_H)$  solves

$$\tilde{B}_K((\bar{T}_h^u \rho_H, \bar{T}_h^p \rho_H), (\mathbf{v}_h, q_h)) = -(\rho_H, q_h)_K \quad \text{for all } (\mathbf{v}_h, q_h) \in \mathbf{V}_h(K) \times Q_h(K). \quad (2.45)$$

Operators  $\mathbf{T}_h$ ,  $\hat{\mathbf{T}}_h$  and  $\bar{\mathbf{T}}_h$  are well-defined since the discrete problems (2.43), (2.44) and (2.45) are well-posed from [25]. As a result, the discrete two-level solution  $(\mathbf{u}_{H,h}, p_{H,h}, \rho_H)$  is given through the expressions

$$\mathbf{u}_{H,h} := \mathbf{u}_0^{H,h} + T_h^u \boldsymbol{\lambda}_{H,h} + \hat{T}_h^u \mathbf{f} \quad \text{and} \quad p_{H,h} := T_h^p \boldsymbol{\lambda}_{H,h} + \hat{T}_h^p \mathbf{f}, \quad (2.46)$$

where we used that  $\rho_H = 0$  (c.f. [12]).

**Remark 2.2** By taking  $(\mathbf{v}_h, q_h) = (0, 1_K)$  in equations (2.43), (2.44) and (2.45), the fol-

lowing local conservation property holds for the discrete velocity field  $\mathbf{u}_{H,h}$

$$\int_K \nabla \cdot \mathbf{u}_{H,h} d\mathbf{x} = 0 \quad \text{for all } K \in \mathcal{T}_H, \quad (2.47)$$

and the approximate flux  $\boldsymbol{\lambda}_{H,h}$  is in equilibrium with external forces, i.e.,

$$\int_{\partial K} \boldsymbol{\lambda}_{H,h} d\mathbf{s} = \int_K \mathbf{f} d\mathbf{x} \quad \text{for all } K \in \mathcal{T}_H, \quad (2.48)$$

## 2.4 A posteriori error analysis

This section introduces the multiscale a posteriori error estimator, which is proved to be locally efficient and reliable.

### 2.4.1 The multiscale a posteriori error estimator

This section presents the residual-based error estimator for the MHM method. Given  $F \in \mathcal{E}_H$ , we define a face-residual estimator as follows:

$$\mathbf{R}_F := \begin{cases} -\frac{1}{2} [\![\mathbf{u}_{H,h}]\!] & F \in \mathcal{E}_0, \\ \mathbf{g} - \mathbf{u}_{H,h} & F \in \mathcal{E}_D. \end{cases} \quad (2.49)$$

Thus, we define

$$\eta_{1,F} := \left\{ \sum_{\tilde{F} \in \mathcal{T}_{\tilde{H}}(F)} \eta_{1,\tilde{F}}^2 \right\}^{1/2} \quad (2.50)$$

where

$$\eta_{1,\tilde{F}} := \frac{\|\mathbf{R}_F\|_{0,\tilde{F}}}{H_F^{1/2}}$$

for all  $\tilde{F} \in \mathcal{T}_{\tilde{H}}(F)$ . Owing to previous definitions, the first level a posteriori error estimator reads

$$\eta_1 := \left\{ \sum_{K \in \mathcal{T}_H} \eta_{1,K}^2 \right\}^{1/2}, \quad \text{where} \quad \eta_{1,K}^2 := \sum_{F \subset \partial K} \eta_{1,F}^2. \quad (2.51)$$

To propose a second-level estimator, we first need some notations related to local residuals in each sub-element  $\tau \in \mathcal{T}_h^K$  and on each sub-face  $\zeta \in \mathcal{E}_h^K$ . They are the following:

$$\mathbf{R}_\tau^K := (\nu \Delta \mathbf{u}_{H,h} - \gamma \mathbf{u}_{H,h} - \nabla p_{H,h} + \mathbf{f})|_\tau \quad \text{for all } \tau \in \mathcal{T}_h^K \quad (2.52)$$

and

$$\mathbf{R}_\zeta^K := \begin{cases} \llbracket -\nu \frac{\partial \mathbf{u}_{H,h}}{\partial \mathbf{n}_\zeta^\tau} + p_{H,h} \mathbf{n}_\zeta^\tau \rrbracket & \text{on } \zeta \in \mathcal{E}_0^K \\ -\boldsymbol{\lambda}_{H,h} - \nu \frac{\partial \mathbf{u}_{H,h}}{\partial \mathbf{n}_\zeta^\tau} + p_{H,h} \mathbf{n}_\zeta^\tau & \text{on } \zeta \in \mathcal{E}_h^K \setminus \mathcal{E}_0^K. \end{cases} \quad (2.53)$$

Using previous definitions, the second-level a posteriori error estimator reads as follows

$$\eta_2 := \left\{ \sum_{K \in \mathcal{T}_H} \eta_{2,K}^2 \right\}^{1/2} \quad (2.54)$$

where

$$\eta_{2,K} := \left[ \sum_{\tau \in \mathcal{T}_h^K} [h_\tau^2 \|\mathbf{R}_\tau^K\|_{0,\tau}^2 + \|\nabla \cdot \mathbf{u}_{H,h}\|_{0,\tau}^2] + \sum_{\zeta \in \mathcal{E}_h^K} h_\zeta \|\mathbf{R}_\zeta^K\|_{0,\zeta}^2 \right]^{1/2}.$$

Summing up (2.51) and (2.54), we build an a posteriori error estimator, which includes the first and second level residuals, given by

$$\eta = \eta_1 + \eta_2. \quad (2.55)$$

**Remark 2.3** *The contribution of  $\eta_1$  depends only on the jump of the velocity across the faces of the first-level mesh. It has the same form of the a posteriori estimator introduced in [11] for the Darcy equation. We recall that the error associated to the local problems were not considered in [11], which explains the absence of contribution  $\eta_2$  in [11].*

**Remark 2.4** *Note that  $\eta_2$  behaves asymptotically as a high order term compare to  $\eta$  when  $h \leq H^{\alpha+1}$ , with  $\alpha > 0$ . With such a choice, second-level error estimator  $\eta_2$  may be disregarded in the numerical tests, i.e.,  $\eta = \eta_1$ . As shown in the next section, such a simplified version is also an efficient and reliable a posteriori error estimator for the two-level MHM method.*

#### 2.4.2 Efficiency and reliability

This section proves that the estimator (2.55) is close to the real error. To this end, we need some intermediary estimates which are addressed first.

The first result measures the quality of the second-level approximation with respect to the second-level a posteriori error estimator  $\eta_{2,K}$  in each  $K \in \mathcal{T}_H$ .

**Lemma 2.1** *The following estimate holds*

$$\|((T^u - T_h^u)\boldsymbol{\lambda}_{H,h} + (\hat{T}^u - \hat{T}_h^u)\mathbf{f}, (T^p - T_h^p)\boldsymbol{\lambda}_{H,h} + (\hat{T}^p - \hat{T}_h^p)\mathbf{f})\|_{\mathbf{V}(K) \times Q(K)} \preceq \eta_{2,K}.$$

*Proof.* Recalling from (2.46) that

$$p_{H,h} = T_h^p \boldsymbol{\lambda}_{H,h} + \hat{T}_h^p \mathbf{f}$$

we define

$$\begin{cases} \tilde{\mathbf{u}} := T^u \boldsymbol{\lambda}_{H,h} + \hat{T}^u \mathbf{f}, \\ \tilde{p} := T^p \boldsymbol{\lambda}_{H,h} + \hat{T}^p \mathbf{f}, \\ \tilde{\mathbf{u}}_{H,h} := T_h^u \boldsymbol{\lambda}_{H,h} + \hat{T}_h^u \mathbf{f}, \end{cases}$$

and

$$\begin{cases} e^{\tilde{\mathbf{u}}} := \tilde{\mathbf{u}} - \tilde{\mathbf{u}}_{H,h}, \\ e^{\tilde{p}} := \tilde{p} - p_{H,h}. \end{cases}$$

Let  $\mathbf{v} \in \mathbf{V}(K)$ ,  $q \in Q(K)$  and  $\mathbf{v}_h := \mathcal{C}_h^K(\mathbf{v})$  be the Clément interpolant of  $\mathbf{v}$  on  $K \in \mathcal{T}_h$ . From the definition of the bilinear form  $B_K(\cdot, \cdot)$  given in (2.27), (2.28), (2.29), (2.46) and integration by parts, it holds

$$\begin{aligned} B_K((e^{\tilde{\mathbf{u}}}, e^{\tilde{p}}), (\mathbf{v}, q)) &= a_K(\tilde{\mathbf{u}} - \tilde{\mathbf{u}}_{H,h}, \mathbf{v}) + b_K(\mathbf{v}, \tilde{p} - p_{H,h}) - b_K(\tilde{\mathbf{u}} - \tilde{\mathbf{u}}_{H,h}, q) \\ &= -\langle \boldsymbol{\lambda}_{H,h}, \mathbf{v} \rangle_{\partial K} + (\mathbf{f}, \mathbf{v})_K - [a_K(\mathbf{u}_{H,h}, \mathbf{v}) + b_K(\mathbf{v}, p_{H,h}) - b_K(\mathbf{u}_{H,h}, q)] \\ &= \sum_{\tau \in \mathcal{T}_h^K} [(\mathbf{R}_\tau^K, \mathbf{v})_\tau + (\nabla \cdot \mathbf{u}_{H,h}, q)_\tau] + \sum_{\zeta \in \mathcal{E}_h^K} (\mathbf{R}_\zeta^K, \mathbf{v})_\zeta, \end{aligned} \quad (2.56)$$

thus, replacing  $\mathbf{v}$  by  $\mathbf{v} - \mathbf{v}_h$  in (2.56) and using Cauchy–Schwartz inequality, we get

$$\begin{aligned} B_K((e^{\tilde{\mathbf{u}}}, e^{\tilde{p}}), (\mathbf{v} - \mathbf{v}_h, q)) &\leq \sum_{\tau \in \mathcal{T}_h^K} [\|\mathbf{R}_\tau^K\|_{0,\tau} \|\mathbf{v} - \mathbf{v}_h\|_{0,\tau} + \|\nabla \cdot \mathbf{u}_{H,h}\|_{0,\tau} \|q\|_{0,\tau}] \\ &\quad + \sum_{\zeta \in \mathcal{E}_h^K} \|\mathbf{R}_\zeta^K\|_{0,\zeta} \|\mathbf{v} - \mathbf{v}_h\|_{0,\zeta}. \end{aligned} \quad (2.57)$$

On the other hand, testing (2.56) with  $(\mathbf{v}, q) = (\mathbf{v}_h, 0) \in \mathbf{V}_h \times Q_h$ , we arrive at

$$\begin{aligned} B_K((e^{\tilde{\mathbf{u}}}, e^{\tilde{p}}), (\mathbf{v}_h, 0)) &= a_K(\tilde{\mathbf{u}} - \tilde{\mathbf{u}}_{H,h}, \mathbf{v}_h) + b_K(\mathbf{v}_h, \tilde{p} - p_{H,h}) \\ &= - \sum_{\tau \in \mathcal{T}_h^K} \kappa_\tau (-\nu \Delta \mathbf{u}_{H,h} + \gamma \mathbf{u}_{H,h} + \nabla p_{H,h} - \mathbf{f}, -\nu \Delta \mathbf{v}_h + \gamma \mathbf{v}_h)_\tau \\ &= \sum_{\tau \in \mathcal{T}_h^K} \kappa_\tau (\mathbf{R}_\tau^K, -\nu \Delta \mathbf{v}_h + \gamma \mathbf{v}_h)_\tau. \end{aligned} \quad (2.58)$$

From the definition of  $\kappa_\tau$  (see (2.41)), it is easy to verify that

$$\kappa_\tau \leq \frac{h_\tau^2}{12\nu}, \quad (2.59)$$

thus, using (2.42) and (2.59), we get

$$\begin{aligned} \kappa_\tau \| -\nu \Delta \mathbf{v}_h + \gamma \mathbf{v}_h \|_{0,\tau} &\leq \frac{h_\tau}{C_k 12\nu} \|\nabla \mathbf{v}_h\|_{0,\tau} + \|\gamma\|_\infty \frac{h_\tau^2}{12\nu} \|\mathbf{v}_h\|_{0,\tau} \\ &\preceq h_\tau \{ \|\nabla \mathbf{v}_h\|_{0,\tau} + \frac{1}{d_\Omega} \|\mathbf{v}_h\|_{0,\tau} \}. \end{aligned} \quad (2.60)$$

Then, combining (2.57), (2.58), (2.60), the properties of Clément interpolation operator (2.24)-(2.26) and the mesh regularity, we arrive at

$$\begin{aligned} B_K((e^{\tilde{\mathbf{u}}}, e^{\tilde{p}}), (\mathbf{v}, q)) &= B_K((e^{\tilde{\mathbf{u}}}, e^{\tilde{p}}), (\mathbf{v} - \mathbf{v}_h, q)) + B_K((e^{\tilde{\mathbf{u}}}, e^{\tilde{p}}), (\mathbf{v}_h, 0)) \\ &\preceq \sum_{\tau \in \mathcal{T}_h^K} [\|\mathbf{R}_\tau^K\|_{0,\tau} \|\mathbf{v} - \mathbf{v}_h\|_{0,\tau} + \|\nabla \cdot \mathbf{u}_{H,h}\|_{0,\tau} \|q\|_{0,\tau}] \\ &\quad + \sum_{\zeta \in \mathcal{E}_h^K} \|\mathbf{R}_\zeta^K\|_{0,\zeta} \|\mathbf{v} - \mathbf{v}_h\|_{0,\zeta} + \sum_{\tau \in \mathcal{T}_h^K} h_\tau \|\mathbf{R}_\tau^K\|_{0,\tau} \{ \|\nabla \mathbf{v}_h\|_{0,\tau} + \frac{1}{d_\Omega} \|\mathbf{v}_h\|_{0,\tau} \} \\ &\preceq \sum_{\tau \in \mathcal{T}_h^K} [h_\tau \|\mathbf{R}_\tau^K\|_{0,\tau} |\mathbf{v}|_{1,\tilde{\omega}_\tau} + \|\nabla \cdot \mathbf{u}_{H,h}\|_{0,\tau} \|q\|_{0,\tau}] \\ &\quad + \sum_{\zeta \in \mathcal{E}_h^K} h_\zeta^{1/2} \|\mathbf{R}_\zeta^K\|_{0,\zeta} |\mathbf{v}|_{1,\tilde{\omega}_\zeta} + \sum_{\tau \in \mathcal{T}_h^K} h_\tau \|\mathbf{R}_\tau^K\|_{0,\tau} \{ \|\nabla \mathbf{v}_h\|_{0,\tau} + \frac{1}{d_\Omega} \|\mathbf{v}_h\|_{0,\tau} \} \\ &\preceq \left[ \sum_{\tau \in \mathcal{T}_h^K} [h_\tau^2 \|\mathbf{R}_\tau^K\|_{0,\tau}^2 + \|\nabla \cdot \mathbf{u}_{H,h}\|_{0,\tau}^2] + \sum_{\zeta \in \mathcal{E}_h^K} h_\zeta \|\mathbf{R}_\zeta^K\|_{0,\zeta}^2 \right]^{1/2} \\ &\quad \times \left[ \sum_{\tau \in \mathcal{T}_h^K} [\|\nabla \mathbf{v}\|_{0,\tau}^2 + \frac{1}{d_\Omega^2} \|\mathbf{v}_h\|_{0,\tau}^2 + |\mathbf{v}|_{1,\tilde{\omega}_\tau}^2 + \|q\|_{0,\tau}^2] + \sum_{\zeta \in \mathcal{E}_h^K} |\mathbf{v}|_{1,\tilde{\omega}_\zeta}^2 \right]^{1/2} \\ &\preceq \left[ \sum_{\tau \in \mathcal{T}_h^K} [h_\tau^2 \|\mathbf{R}_\tau^K\|_{0,\tau}^2 + \|\nabla \cdot \mathbf{u}_{H,h}\|_{0,\tau}^2] + \sum_{\zeta \in \mathcal{E}_h^K} h_\zeta \|\mathbf{R}_\zeta^K\|_{0,\zeta}^2 \right]^{1/2} \times \|(\mathbf{v}, q)\|_{\mathbf{V}(K) \times Q(K)}. \end{aligned}$$

Thus, the result follows from the inf-sup condition given in Theorem 2.2. ■

Now, we adapt the ideas of the proof in [11, Lemma 5.1] to include second-level approximations.

**Lemma 2.2** *Let  $\mathbf{u}_{H,h} \in \mathbf{V}_h$  be the discrete solution given by (2.46). Then, there exists*

$\chi \in \mathbf{V}$  satisfying

$$(\boldsymbol{\mu}, \chi)_{\partial\mathcal{T}_H} = \langle \boldsymbol{\mu}, \mathbf{g} \rangle_{\partial\Omega} - (\boldsymbol{\mu}, \mathbf{u}_{H,h})_{\partial\mathcal{T}_H} \quad \text{for all } \boldsymbol{\mu} \in \boldsymbol{\Lambda},$$

such that

$$\|\chi\|_{\mathbf{V}} \leq \eta_1.$$

*Proof.* Let  $(\bar{\chi}, \bar{\xi}) \in \mathbf{V} \times \boldsymbol{\Lambda}$  be the solution of the following problem

$$\begin{aligned} \frac{1}{d_{\Omega}^2} (\bar{\chi}, \mathbf{v})_{\mathcal{T}_H} + (\nabla \bar{\chi}, \nabla \mathbf{v})_{\mathcal{T}_H} + (\bar{\xi}, \mathbf{v})_{\partial\mathcal{T}_H} &= \frac{1}{d_{\Omega}^2} (\mathbf{u}_{H,h}, \mathbf{v})_{\mathcal{T}_H} - \sum_{K \in \mathcal{T}_H} \sum_{\tau \in \mathcal{T}_h^K} (\Delta \mathbf{u}_{H,h}, \mathbf{v})_{\tau} \\ (\boldsymbol{\mu}, \bar{\chi})_{\partial\mathcal{T}_H} &= \langle \boldsymbol{\mu}, \mathbf{g} \rangle_{\partial\Omega} \end{aligned} \quad (2.61)$$

for all  $(\mathbf{v}, \boldsymbol{\mu}) \in \mathbf{V} \times \boldsymbol{\Lambda}$ . From [51] we have that  $\bar{\xi}$  belongs to  $L^2(\mathcal{E}_H)^d$ . Then, there exists  $\boldsymbol{\sigma} \in H(\operatorname{div}; \Omega)$  such that  $\boldsymbol{\sigma} \mathbf{n} = \bar{\xi}$  on  $\mathcal{E}_H$ , and we define  $\tilde{\xi} := \boldsymbol{\sigma} \mathbf{n}_{\zeta}^{\tau}$  on  $\mathcal{E}_h^K$ . Using  $\mathbf{v}|_K \in H^1(K)^d$ , we can rewrite (2.61) as follows

$$\begin{aligned} \frac{1}{d_{\Omega}^2} (\bar{\chi}, \mathbf{v})_{\mathcal{T}_H} + (\nabla \bar{\chi}, \nabla \mathbf{v})_{\mathcal{T}_H} + \sum_{K \in \mathcal{T}_H} \sum_{\tau \in \mathcal{T}_h^K} \langle \tilde{\xi}, \mathbf{v} \rangle_{\partial\tau} &= \frac{1}{d_{\Omega}^2} (\mathbf{u}_{H,h}, \mathbf{v})_{\mathcal{T}_H} - \sum_{K \in \mathcal{T}_H} \sum_{\tau \in \mathcal{T}_h^K} (\Delta \mathbf{u}_{H,h}, \mathbf{v})_{\tau} \\ (\boldsymbol{\mu}, \bar{\chi})_{\partial\mathcal{T}_H} &= \langle \boldsymbol{\mu}, \mathbf{g} \rangle_{\partial\Omega} \end{aligned}$$

for all  $(\mathbf{v}, \boldsymbol{\mu}) \in \mathbf{V} \times \boldsymbol{\Lambda}$ . Now, define  $\chi := \bar{\chi} - \mathbf{u}_{H,h}$  and  $\xi := \tilde{\xi} + \nabla \mathbf{u}_{H,h} \mathbf{n}$ . Then,  $(\chi, \xi) \in H^{3/2}(\mathcal{T}_H)^d \times L^2(\mathcal{E}_H)^d$  and satisfies

$$\begin{aligned} \frac{1}{d_{\Omega}^2} (\chi, \mathbf{v})_{\mathcal{T}_H} + (\nabla \chi, \nabla \mathbf{v})_{\mathcal{T}_H} + (\xi, \mathbf{v})_{\partial\mathcal{T}_H} &= 0 \quad \text{for all } \mathbf{v} \in \mathbf{V}, \\ (\boldsymbol{\mu}, \chi)_{\partial\mathcal{T}_H} &= -(\boldsymbol{\mu}, \mathbf{u}_{H,h})_{\partial\mathcal{T}_H} + \langle \boldsymbol{\mu}, \mathbf{g} \rangle_{\partial\Omega} \quad \text{for all } \boldsymbol{\mu} \in \boldsymbol{\Lambda}. \end{aligned} \quad (2.62)$$

Testing (2.62) with  $(\mathbf{v}, \boldsymbol{\mu}) = (\chi, \xi)$  and using Cauchy–Schwartz inequality, we get

$$\begin{aligned} \|\chi\|_{\mathbf{V}}^2 &= \sum_{K \in \mathcal{T}_H} \left\{ \frac{1}{d_{\Omega}^2} \|\chi\|_{0,K}^2 + \|\nabla \chi\|_{0,K}^2 \right\} = -(\xi, \chi)_{\partial\mathcal{T}_H} = (\xi, \mathbf{u}_{H,h})_{\partial\mathcal{T}_H} - (\xi, \mathbf{g})_{\partial\Omega} \\ &= \sum_{F \in \mathcal{E}_H} \|\xi\|_{0,F} \|[\mathbf{u}_{H,h}]_{0,F} + \sum_{F \in \partial\Omega} \|\xi\|_{0,F} \|\mathbf{g} - \mathbf{u}_{H,h}\|_{0,F} \\ &\leq \left\{ \sum_{F \in \mathcal{E}_H} H_F \|\xi\|_{0,F}^2 \right\}^{1/2} \left\{ \sum_{F \in \mathcal{E}_0} \frac{1}{H_F} \|[\mathbf{u}_{H,h}]_{0,F}^2 + \sum_{F \in \partial\Omega} \frac{1}{H_F} \|\mathbf{g} - \mathbf{u}_{H,h}\|_{0,F}^2 \right\}^{1/2} \\ &= \left\{ \sum_{F \in \mathcal{E}_H} H_F \|\nabla \chi \mathbf{n}\|_{0,F}^2 \right\}^{1/2} \eta_1 \leq \|\chi\|_{\mathbf{V}} \eta_1 \end{aligned}$$

and the result follows.  $\blacksquare$

In what follows, we will use the following local norm

$$\|\mathbf{v}\|_{\mathbf{V}, \omega_F}^2 := \sum_{K \in \omega_F} (H_K^{-2} \|\mathbf{v}\|_{0,K}^2 + \|\nabla \mathbf{v}\|_{0,K}^2),$$

where  $F \in \mathcal{E}_H$ . The next theorem proves a bound for  $\eta_{2,K}$  with respect to the local error.

**Theorem 2.6** *Let  $K \in \mathcal{T}_H$ . For  $\tau \in \mathcal{T}_h^K$ , then it holds*

$$h_\tau \|\mathbf{R}_\tau^K\|_{0,\tau} \preceq [h_\tau \|\mathbf{u} - \mathbf{u}_{H,h}\|_{0,\tau} + |\mathbf{u} - \mathbf{u}_{H,h}|_{1,\tau} + \|p - p_{H,h}\|_{0,\tau}]$$

and

$$\|\nabla \cdot \mathbf{u}_{H,h}\|_{0,\tau} \preceq |\mathbf{u} - \mathbf{u}_{H,h}|_{1,\tau}.$$

Furthermore, for  $\zeta \in \mathcal{E}_0^K$  we have that

$$h_\zeta^{1/2} \|\mathbf{R}_\zeta^K\|_{0,\zeta} \preceq \sum_{\tau \in \omega_\zeta} \left\{ |\mathbf{u} - \mathbf{u}_{H,h}|_{1,\tau} + h_\tau \|\mathbf{u} - \mathbf{u}_{H,h}\|_{0,\tau} + \|p - p_{H,h}\|_{0,\tau} \right\}$$

and, for  $\zeta \in \mathcal{E}_h^K \setminus \mathcal{E}_0^K$  we get

$$h_\zeta^{1/2} \|\mathbf{R}_\zeta^K\|_{0,\zeta} \preceq \sum_{\tau \in \omega_\zeta} \left\{ |\mathbf{u} - \mathbf{u}_{H,h}|_{1,\tau} + h_\tau \|\mathbf{u} - \mathbf{u}_{H,h}\|_{0,\tau} + \|p - p_{H,h}\|_{0,\tau} \right\} + \|\boldsymbol{\lambda} - \boldsymbol{\lambda}_{H,h}\|_{-1/2, \partial K}.$$

Therefore, it holds

$$\eta_{2,K}^2 \preceq \|\mathbf{u} - \mathbf{u}_{H,h}\|_{\mathbf{V}(K)}^2 + \|p - p_{H,h}\|_{Q(K)}^2 + \|\boldsymbol{\lambda} - \boldsymbol{\lambda}_{H,h}\|_{-1/2, \partial K}^2, \quad (2.63)$$

for all  $K \in \mathcal{T}_H$ .

*Proof.* Let  $K \in \mathcal{T}_H$ ,  $\tau \in \mathcal{T}_h^K$  and  $\zeta \in \mathcal{E}_h^K$ . We define  $\mathbf{b}_\tau^K := b_\tau^K \mathbf{R}_\tau^K$  and  $\mathbf{b}_\zeta^K := b_\zeta^K \mathbf{P}_\zeta^K(\mathbf{R}_\zeta^K)$ , where  $\mathbf{P}_\zeta^K : \mathbb{P}_k(\zeta)^d \rightarrow \mathbb{P}_k(\omega_\zeta)^d$  is a extension of functions defined on a face  $\zeta$  to the patch  $\omega_\zeta$ , as in [10, Section 4.1]. Since  $\mathbf{b}_\tau^K|_\tau \in H_0^1(\tau)^d$ , using integration by parts, (2.14) and Theorem 2.3 we obtain

$$\begin{aligned} (\mathbf{R}_\tau^K, \mathbf{b}_\tau^K)_\tau &= (\nu \Delta \mathbf{u}_{H,h} - \boldsymbol{\gamma} \mathbf{u}_{H,h} - \nabla p_{H,h} + \mathbf{f}, \mathbf{b}_\tau^K)_\tau \\ &= (\nu \nabla(\mathbf{u} - \mathbf{u}_{H,h}), \nabla \mathbf{b}_\tau^K)_\tau + (\boldsymbol{\gamma}(\mathbf{u} - \mathbf{u}_{H,h}), \mathbf{b}_\tau^K)_\tau - (\nabla \cdot \mathbf{b}_\tau^K, p - p_{H,h})_\tau \\ &\leq [h_\tau^{-1} |\mathbf{u} - \mathbf{u}_{H,h}|_{1,\tau} + \|\mathbf{u} - \mathbf{u}_{H,h}\|_{0,\tau} + h_\tau^{-1} \|p - p_{H,h}\|_{0,\tau}] \|\mathbf{R}_\tau^K\|_{0,\tau} \end{aligned}$$

and then

$$h_\tau \|\mathbf{R}_\tau^K\|_{0,\tau} \preceq h_\tau \|\mathbf{u} - \mathbf{u}_{H,h}\|_{0,\tau} + |\mathbf{u} - \mathbf{u}_{H,h}|_{1,\tau} + \|p - p_{H,h}\|_{0,\tau}.$$

Using Theorem 2.3 again, we arrive at

$$\begin{aligned} \|\nabla \cdot \mathbf{u}_{H,h}\|_{0,\tau}^2 &\preceq (\nabla \cdot \mathbf{u}_{H,h}, b_\tau^K \nabla \cdot \mathbf{u}_{H,h})_\tau = (\nabla \cdot (\mathbf{u}_{H,h} - \mathbf{u}), b_\tau^K \nabla \cdot \mathbf{u}_{H,h})_\Omega \\ &= (\nabla \cdot (\mathbf{u}_{H,h} - \mathbf{u}), b_\tau^K \nabla \cdot \mathbf{u}_{H,h})_\tau \\ &\preceq |\mathbf{u}_{H,h} - \mathbf{u}|_{1,\tau} \|\nabla \cdot \mathbf{u}_{H,h}\|_{0,\tau} \end{aligned}$$

and hence

$$\|\nabla \cdot \mathbf{u}_{H,h}\|_{0,\tau} \preceq |\mathbf{u} - \mathbf{u}_{H,h}|_{1,\tau}.$$

Now we proceed to bound the term  $h_\zeta^{1/2} \|\mathbf{R}_\zeta^K\|_{0,\zeta}$ . For  $\zeta \in \mathcal{E}_0^K$ , from (2.14) and using Theorem 2.4, we get

$$\begin{aligned} (\mathbf{R}_\zeta^K, \mathbf{b}_\zeta^K)_\zeta &= \sum_{\tau \in \omega_\zeta} \left\{ -(\mathbf{R}_\tau^K, \mathbf{b}_\zeta^K)_\tau + (\nu \nabla(\mathbf{u} - \mathbf{u}_{H,h}), \nabla \mathbf{b}_\zeta^K)_\tau + (\gamma(\mathbf{u} - \mathbf{u}_{H,h}), \mathbf{b}_\zeta^K)_\tau \right. \\ &\quad \left. - (\nabla \cdot \mathbf{b}_\zeta^K, p - p_{H,h})_\tau \right\} \\ &\preceq \sum_{\tau \in \omega_\zeta} \left\{ \|\mathbf{R}_\tau^K\|_{0,\tau} \|\mathbf{b}_\zeta^K\|_{0,\tau} + \nu |\mathbf{u} - \mathbf{u}_{H,h}|_{1,\tau} |\mathbf{b}_\zeta^K|_{1,\tau} + \|\gamma(\mathbf{u} - \mathbf{u}_{H,h})\|_{0,\tau} \|\mathbf{b}_\zeta^K\|_{0,\tau} \right. \\ &\quad \left. + |\mathbf{b}_\zeta^K|_{1,\tau} \|p - p_{H,h}\|_{0,\tau} \right\} \\ &\preceq \sum_{\tau \in \omega_\zeta} \left[ h_\tau^{1/2} \|\mathbf{R}_\tau^K\|_{0,\tau} + h_\tau^{-1/2} |\mathbf{u} - \mathbf{u}_{H,h}|_{1,\tau} + h_\tau^{1/2} \|\mathbf{u} - \mathbf{u}_{H,h}\|_{0,\tau} \right. \\ &\quad \left. + h_\tau^{-1/2} \|p - p_{H,h}\|_{0,\tau} \right] \|\mathbf{R}_\zeta^K\|_{0,\zeta} \end{aligned}$$

and then, from the regularity of the second level meshes, it holds

$$h_\zeta^{1/2} \|\mathbf{R}_\zeta^K\|_{0,\zeta} \preceq \sum_{\tau \in \omega_\zeta} \left\{ h_\tau \|\mathbf{R}_\tau^K\|_{0,\tau} + |\mathbf{u} - \mathbf{u}_{H,h}|_{1,\tau} + h_\tau \|\mathbf{u} - \mathbf{u}_{H,h}\|_{0,\tau} + \|p - p_{H,h}\|_{0,\tau} \right\}.$$

For  $\zeta \in \mathcal{E}_h^K \setminus \mathcal{E}_0^K$ , from (2.14) and the definition of the norm  $\|\cdot\|_{1/2,\partial K}$  in (2.12), and

Theorem 2.4, we get

$$\begin{aligned}
(\mathbf{R}_\zeta^K, \mathbf{b}_\zeta^K)_\zeta &= \sum_{\tau \in \omega_\zeta} \left\{ -(\mathbf{R}_\tau^K, \mathbf{b}_\zeta^K)_\tau + (\nu \nabla(\mathbf{u} - \mathbf{u}_{H,h}), \nabla \mathbf{b}_\zeta^K)_\tau + (\boldsymbol{\gamma}(\mathbf{u} - \mathbf{u}_{H,h}), \mathbf{b}_\zeta^K)_\tau \right. \\
&\quad \left. - (\nabla \cdot \mathbf{b}_\zeta^K, p - p_{H,h})_\tau \right\} + \langle \boldsymbol{\lambda} - \boldsymbol{\lambda}_{H,h}, \mathbf{b}_\zeta^K \rangle_{\partial K} \\
&\leq \sum_{\tau \in \omega_\zeta} \left\{ \|\mathbf{R}_\tau^K\|_{0,\tau} \|\mathbf{b}_\zeta^K\|_{0,\tau} + |\mathbf{u} - \mathbf{u}_{H,h}|_{1,\tau} |\mathbf{b}_\zeta^K|_{1,\tau} + \|\mathbf{u} - \mathbf{u}_{H,h}\|_{0,\tau} \|\mathbf{b}_\zeta^K\|_{0,\tau} \right. \\
&\quad \left. + |\mathbf{b}_\zeta^K|_{1,\tau} \|p - p_{H,h}\|_{0,\tau} \right\} + \|\boldsymbol{\lambda} - \boldsymbol{\lambda}_{H,h}\|_{-1/2,\partial K} \|\mathbf{b}_\zeta^K\|_{1/2,\partial K} \\
&\leq \left[ \sum_{\tau \in \omega_\zeta} \left\{ h_\tau^{1/2} \|\mathbf{R}_\tau^K\|_{0,\tau} + h_\tau^{-1/2} |\mathbf{u} - \mathbf{u}_{H,h}|_{1,\tau} + h_\tau^{1/2} \|\mathbf{u} - \mathbf{u}_{H,h}\|_{0,\tau} \right. \right. \\
&\quad \left. \left. + h_\tau^{-1/2} \|p - p_{H,h}\|_{0,\tau} \right\} + h_\zeta^{-1/2} \|\boldsymbol{\lambda} - \boldsymbol{\lambda}_{H,h}\|_{-1/2,\partial K} \right] \|\mathbf{R}_\zeta^K\|_{0,\tau}.
\end{aligned}$$

Now, from the regularity of the second-level meshes we get

$$\begin{aligned}
h_\zeta^{1/2} \|\mathbf{R}_\zeta^K\|_{0,\zeta} &\leq \sum_{\tau \in \omega_\zeta} \left\{ h_\tau \|\mathbf{R}_\tau^K\|_{0,\tau} + |\mathbf{u} - \mathbf{u}_{H,h}|_{1,\tau} + h_\tau \|\mathbf{u} - \mathbf{u}_{H,h}\|_{0,\tau} \right. \\
&\quad \left. + \|p - p_{H,h}\|_{0,\tau} \right\} + \|\boldsymbol{\lambda} - \boldsymbol{\lambda}_{H,h}\|_{-1/2,\partial K},
\end{aligned}$$

and estimate (2.63) follows. ■

A first equivalence between the real error and the multiscale a posteriori estimator is presented in the next theorem.

**Theorem 2.7** *Let  $(\mathbf{u}, p) \in \mathbf{V} \times Q$  and  $(\mathbf{u}_{H,h}, p_{H,h}) \in \mathbf{V}_h \times Q_h$  be the solutions of continuous and discrete problems given by (2.32) and (2.35), respectively. Then we have that*

$$\|\mathbf{u} - \mathbf{u}_{H,h}\|_{\mathbf{V}} + \|p - p_{H,h}\|_Q + \|\boldsymbol{\lambda} - \boldsymbol{\lambda}_{H,h}\|_{\boldsymbol{\Lambda}} \preceq (\eta_1 + \eta_2) + h.o.t. \quad (2.64)$$

Moreover, for  $F \in \mathcal{E}_H$ , we have that

$$\eta_{1,F} \preceq \|\mathbf{u} - \mathbf{u}_{H,h}\|_{\mathbf{V},\omega_F}. \quad (2.65)$$

*Proof.* We begin by proving the reliability of the estimator. From (2.32) and (2.46), it holds

$$\begin{aligned}
& \|(\mathbf{u}, p) - (\mathbf{u}_{H,h}, p_{H,h})\|_{\mathbf{V} \times Q} \\
&= \|(\mathbf{u}_0 + T^{\mathbf{u}} \boldsymbol{\lambda} + \hat{T}^{\mathbf{u}} \mathbf{f}, T^p \boldsymbol{\lambda} + \hat{T}^p \mathbf{f}) - (\mathbf{u}_0^{H,h} + T_h^{\mathbf{u}} \boldsymbol{\lambda}_{H,h} + \hat{T}_h^{\mathbf{u}} \mathbf{f}, T_h^p \boldsymbol{\lambda}_{H,h} + \hat{T}_h^p \mathbf{f})\|_{\mathbf{V} \times Q} \\
&\leq \|\mathbf{u}_0 - \mathbf{u}_0^{H,h}\|_{\mathbf{V}} + \|(T^{\mathbf{u}} - T_h^{\mathbf{u}})\boldsymbol{\lambda}_{H,h} + (\hat{T}^{\mathbf{u}} - \hat{T}_h^{\mathbf{u}})\mathbf{f}\|_{\mathbf{V}} + \|T^{\mathbf{u}}(\boldsymbol{\lambda} - \boldsymbol{\lambda}_{H,h})\|_{\mathbf{V}} \\
&\quad + \|(T^p - T_h^p)\boldsymbol{\lambda}_{H,h} + (\hat{T}^p - \hat{T}_h^p)\mathbf{f}\|_Q + \|T^p(\boldsymbol{\lambda} - \boldsymbol{\lambda}_{H,h})\|_Q. \tag{2.66}
\end{aligned}$$

Furthermore, given  $\boldsymbol{\mu}_H \in \boldsymbol{\Lambda}_H$  and using (2.31) and (2.39), we obtain

$$\begin{aligned}
-(\boldsymbol{\mu}_H, \mathbf{u}_0 - \mathbf{u}_0^{H,h})_{\partial\mathcal{T}_H} &= (\boldsymbol{\mu}_H, T^{\mathbf{u}} \boldsymbol{\lambda} - T_h^{\mathbf{u}} \boldsymbol{\lambda}_{H,h})_{\partial\mathcal{T}_H} + (\boldsymbol{\mu}_H, \hat{T}^{\mathbf{u}} \mathbf{f} - \hat{T}_h^{\mathbf{u}} \mathbf{f})_{\partial\mathcal{T}_H} \\
&= (\boldsymbol{\mu}_H, T^{\mathbf{u}}(\boldsymbol{\lambda} - \boldsymbol{\lambda}_{H,h}))_{\partial\mathcal{T}_H} + (\boldsymbol{\mu}_H, (T^{\mathbf{u}} - T_h^{\mathbf{u}})\boldsymbol{\lambda}_{H,h} + (\hat{T}^{\mathbf{u}} - \hat{T}_h^{\mathbf{u}})\mathbf{f})_{\partial\mathcal{T}_H} \\
&\leq \|\boldsymbol{\mu}_H\|_{\boldsymbol{\Lambda}} \{ \|T^{\mathbf{u}}(\boldsymbol{\lambda} - \boldsymbol{\lambda}_{H,h})\|_{\mathbf{V}} + \|(T^{\mathbf{u}} - T_h^{\mathbf{u}})\boldsymbol{\lambda}_{H,h} + (\hat{T}^{\mathbf{u}} - \hat{T}_h^{\mathbf{u}})\mathbf{f}\|_{\mathbf{V}} \}.
\end{aligned}$$

Consequently, we get

$$\sup_{\boldsymbol{\mu}_H \in \boldsymbol{\Lambda}_H} \frac{-(\boldsymbol{\mu}_H, \mathbf{u}_0 - \mathbf{u}_0^{H,h})_{\partial\mathcal{T}_H}}{\|\boldsymbol{\mu}_H\|_{\boldsymbol{\Lambda}}} \leq \|T^{\mathbf{u}}(\boldsymbol{\lambda} - \boldsymbol{\lambda}_{H,h})\|_{\mathbf{V}} + \|(T^{\mathbf{u}} - T_h^{\mathbf{u}})\boldsymbol{\lambda}_{H,h} + (\hat{T}^{\mathbf{u}} - \hat{T}_h^{\mathbf{u}})\mathbf{f}\|_{\mathbf{V}}. \tag{2.67}$$

Now, since  $\mathbf{u}_0 - \mathbf{u}_0^{H,h} \in \mathbf{V}_0$ , there exists a matrix function  $\boldsymbol{\sigma}^*$  such that each of its rows belong to the lowest order Raviart–Thomas space, satisfying

$$\nabla \cdot \boldsymbol{\sigma}^* = \mathbf{u}_0 - \mathbf{u}_0^{H,h} \text{ in } \Omega \quad \text{and} \quad \|\boldsymbol{\sigma}^*\|_{\text{div}, \Omega} \leq C \|\mathbf{u}_0 - \mathbf{u}_0^{H,h}\|_{0, \Omega}. \tag{2.68}$$

Defining  $\boldsymbol{\mu}^* := \boldsymbol{\sigma}^* \mathbf{n} \in \boldsymbol{\Lambda}_H$ , and using (2.68), it holds

$$\begin{aligned}
\sup_{\boldsymbol{\mu}_H \in \boldsymbol{\Lambda}_H} \frac{-(\boldsymbol{\mu}_H, \mathbf{u}_0 - \mathbf{u}_0^{H,h})_{\partial\mathcal{T}_H}}{\|\boldsymbol{\mu}_H\|_{\boldsymbol{\Lambda}}} &\geq \frac{(\boldsymbol{\mu}^*, \mathbf{u}_0 - \mathbf{u}_0^{H,h})_{\partial\mathcal{T}_H}}{\|\boldsymbol{\mu}^*\|_{\boldsymbol{\Lambda}}} \geq \frac{(\boldsymbol{\sigma}^* \mathbf{n}, \mathbf{u}_0 - \mathbf{u}_0^{H,h})_{\partial\mathcal{T}_H}}{\|\boldsymbol{\sigma}^*\|_{\text{div}, \Omega}} \\
&= \frac{(\nabla \cdot \boldsymbol{\sigma}^*, \mathbf{u}_0 - \mathbf{u}_0^{H,h})_{\partial\mathcal{T}_H}}{\|\boldsymbol{\sigma}^*\|_{\text{div}, \Omega}} \geq C \|\mathbf{u}_0 - \mathbf{u}_0^{H,h}\|_{0, \Omega} \geq C \|\mathbf{u}_0 - \mathbf{u}_0^{H,h}\|_{\mathbf{V}}. \tag{2.69}
\end{aligned}$$

Using (2.69) in (2.67), and replacing the result in (2.66), and from Lemmas 2.1, using (2.86) and Lemmas 2.4 and 2.5 in the appendix, estimate (2.64) follows.

As for the efficiency of the a posteriori error estimator, we first recall the following scaling

property (cf. [4, Theorem 3.10]): Given  $v \in H^1(K)$ , we have that

$$\|v\|_{0,\partial K} \preceq \left( \frac{1}{H_K} \|v\|_{0,K}^2 + H_K \|\nabla v\|_{0,K}^2 \right)^{1/2}. \quad (2.70)$$

Since  $\mathbf{R}_F \in L^2(F)^d$ ,

$$\|\mathbf{R}_F\|_{0,F}^2 \leq 2(\mathbf{R}_F, [\![\mathbf{u} - \mathbf{u}_{H,h}]\!])_F \leq 2\|\mathbf{R}_F\|_{0,F}\|[\![\mathbf{u} - \mathbf{u}_{H,h}]\!]\|_{0,F}$$

and using (2.70) and the mesh regularity, it holds

$$\begin{aligned} \|\mathbf{R}_F\|_{0,F} &\leq 2\|[\![\mathbf{u} - \mathbf{u}_{H,h}]\!]\|_{0,F} \\ &\preceq \sum_{K \in \omega_F} (H_K^{-1}\|\mathbf{u} - \mathbf{u}_{H,h}\|_{0,K}^2 + H_K \|\nabla(\mathbf{u} - \mathbf{u}_{H,h})\|_{0,K}^2)^{1/2} \\ &\preceq H_F^{1/2} \sum_{K \in \omega_F} (H_K^{-2}\|\mathbf{u} - \mathbf{u}_{H,h}\|_{0,K}^2 + \|\nabla(\mathbf{u} - \mathbf{u}_{H,h})\|_{0,K}^2)^{1/2} \\ &\preceq H_F^{1/2}\|\mathbf{u} - \mathbf{u}_{H,h}\|_{\mathbf{V},\omega_F}, \end{aligned}$$

and the estimate (2.65) follows. ■

We are ready to present the main result of this section.

**Theorem 2.8** *Let  $(\mathbf{u}, p, \boldsymbol{\lambda}) \in \mathbf{V} \times Q \times \boldsymbol{\Lambda}$  and  $(\mathbf{u}_{H,h}, p_{H,h}, \boldsymbol{\lambda}_{H,h}) \in \mathbf{V}_h \times Q_h \times \boldsymbol{\Lambda}_h$  be the solutions of continuous and discrete problems, characterized through (2.32) and (2.35), respectively. Then, we have that*

$$\|\mathbf{u} - \mathbf{u}_{H,h}\|_{\mathbf{V}} + \|p - p_{H,h}\|_Q + \|\boldsymbol{\lambda} - \boldsymbol{\lambda}\|_{\boldsymbol{\Lambda}} \preceq (\eta_1 + \eta_2) + h.o.t. \quad (2.71)$$

Moreover, given  $K \in \mathcal{T}_H$  and  $F \in \mathcal{E}_H$ , we have

$$\eta_{1,F} \preceq \|\mathbf{u} - \mathbf{u}_{H,h}\|_{\mathbf{V},\omega_F} \quad (2.72)$$

and

$$\eta_{2,K} \preceq \|\mathbf{u} - \mathbf{u}_{H,h}\|_{\mathbf{V}(K)} + \|p - p_{H,h}\|_{Q(K)} + \|\boldsymbol{\lambda} - \boldsymbol{\lambda}_{H,h}\|_{-1/2,\partial K}. \quad (2.73)$$

*Proof.* The result is straightforward from Theorem 2.6 and Theorem 2.7. ■

## 2.5 Numerical results

Using the definitions of the error estimators  $\eta_1$  and  $\eta_2$  given in (2.51) and (2.54), respectively, we validate two adaptive refinement algorithms: a classical procedure based on refining the elements of the first level mesh, and a new one based on refining faces which keeps the topology of the first-level mesh untouched.

### 2.5.1 First strategy: Adaptivity by elements

For all  $K \in \mathcal{T}_H$ , we define

$$\eta_K := \eta_{2,K} + \sum_{F \in \mathcal{E}_H \cap \partial K} \eta_{1,F}.$$

The adaptive mesh generation strategy is given in the Algorithm 1.

---

#### **Algorithm 1** : Adaptivity by elements

---

**Require:**  $\theta \in (0, 1)$  and a coarse first-level mesh  $\mathcal{T}_H$ .

- 1: Solve the discrete problem on the current mesh.
  - 2: For each element  $K \in \mathcal{T}_H$ , compute the local error indicator  $\eta_K$ .
  - 3: Mark the elements  $K \in \mathcal{T}_H$  such that  $\eta_K \geq \theta \max_{K \in \mathcal{T}_H} \eta_K$ , and create a new first-level mesh  $\mathcal{T}_H$  refining the marked elements.
  - 4: If the stop criterion is not satisfied, repeat the algorithm.
- 

Note that Algorithm 1 does not induce local mesh refinement in the second-level submeshes. This fact is supported by the numerical experiments that show that second-level meshes may consist only of one element when the first-level mesh diameter goes to zero.

### 2.5.2 Second strategy: Adaptivity by faces

For all  $F \in \mathcal{E}_H$ , we define

$$\eta_F := \eta_{1,F} + \sum_{K \in \omega_F} \eta_{2,K}.$$

---

**Algorithm 2** : Adaptivity by faces

---

**Require:**  $\theta \in (0, 1)$  and a coarse first-level mesh  $\mathcal{T}_H$ .

- 1: Solve the discrete problem on the current mesh.
  - 2: For each  $F \in \mathcal{E}_H$ , compute the local error indicator  $\eta_F$ .
  - 3: Mark the faces  $F \in \mathcal{E}_H$  such that  $\eta_F \geq \theta \max_{F \in \mathcal{E}_H} \eta_F$ , and refine  $\tilde{F} \in \mathcal{T}_{\tilde{H}}(F)$  such that  $\eta_{1,\tilde{F}} = \max_{\tilde{F} \in \mathcal{T}_{\tilde{H}}(F)} \eta_{1,\tilde{F}}$  for each marked  $F$ , and if  $\eta_{1,F} < \sum_{K \in \omega_F} \eta_{2,K}$  also refine the second-level meshes  $\mathcal{T}_h^K$  for  $K \in \omega_F$ .
  - 4: If the stop criterion is not satisfied, repeat the algorithm.
- 

Owing to Algorithm 2, the first-level mesh does not change as the adaptive process runs unlike in the classical mesh adaptation described in Algorithm 1. As a result, only the local problems associated with the elements “touched” by the estimator need to be revisited. This fact leads to a few extra entries go into the global system. Algorithm 2 is particularly attractive for use with real three-dimensional problems since it dramatically decreases the computational cost involved in the adaptive procedure, and avoids three-dimensional global re-meshing.

### 2.5.3 An example with analytical solution

In this example, we consider a Stokes problem with viscosity  $\nu = 1$  and  $\nu = 10^{-2}$  on the unit square domain  $\Omega$ . We chose  $\mathbf{f}$  and  $\mathbf{g}$  such that the exact solution  $\mathbf{u} = (u_1, u_2)$  is given by  $u_1(x, y) := 256y^2(y - 1)^2x(x - 1)(2x - 1)$  and  $u_2(x, y) := -u_1(y, x)$ , and  $p(x, y) := 150(x - 0.5)(y - 0.5)$ .

A typical quantity to measure the quality of an error estimator, is the so-called *effectivity index*,  $E_i$ , defined by  $E_i = \frac{\eta}{\|(\mathbf{u} - \mathbf{u}_{H,h}, p - p_{H,h})\|_{\mathbf{V} \times Q}}$ . In tables 2.1, 2.2, 2.3 and 2.4 we tabulate this index for some different values of  $H$  and using one element as second-level meshes.

We observe that  $\eta_1$  and  $\eta_2$  have, in general, equivalent rates of convergence (see Tables 2.1 and 2.3). However, if one chooses  $h = H^2$  then  $\eta_2$  achieves a higher order of convergence when compare to  $\eta_1$  (see Tables 2.2 and 2.4). This is in accordance with the theory and was announced in Remark 2.4.

| $l$ | $H$  | $\ (\mathbf{u} - \mathbf{u}_{H,h}, p - p_{H,h})\ _{\mathbf{V} \times Q}$ |       | $\eta_1$  |       | $\eta_2$  |       | $E_i$ |
|-----|------|--|-------|-----------|-------|-----------|-------|-------|
|     |      | error  | rate  | error     | rate  | value     | rate  |       |
| 2   | 1/2  | 5.001E-01  | –     | 1.091E-01 | –     | 9.548E+00 | –     | 0.218 |
|     | 1/4  | 6.947E-02  | 2.848 | 1.437E-02 | 2.925 | 1.276E+00 | 2.904 | 0.207 |
|     | 1/8  | 8.663E-03  | 3.003 | 1.780E-03 | 3.013 | 1.557E-01 | 3.034 | 0.205 |
|     | 1/16 | 1.079E-03  | 3.006 | 2.254E-04 | 2.981 | 1.925E-02 | 3.016 | 0.209 |
|     | 1/32 | 1.345E-04  | 3.003 | 2.858E-05 | 2.980 | 2.397E-03 | 3.006 | 0.212 |
| 1   | 1/2  | 8.001E-01  | –     | 4.747E-01 | –     | 5.708E+00 | –     | 0.593 |
|     | 1/4  | 3.516E-01  | 1.186 | 2.000E-01 | 1.247 | 1.818E+00 | 1.651 | 0.569 |
|     | 1/8  | 8.642E-02  | 2.024 | 5.168E-02 | 1.953 | 4.640E-01 | 1.970 | 0.598 |
|     | 1/16 | 2.144E-02  | 2.011 | 1.335E-02 | 1.953 | 1.135E-01 | 2.031 | 0.623 |
|     | 1/32 | 5.365E-03  | 1.998 | 3.418E-03 | 1.965 | 2.787E-02 | 2.027 | 0.637 |
| 0   | 1/2  | 9.719E+00  | –     | 6.203E+00 | –     | 6.187E+00 | –     | 0.638 |
|     | 1/4  | 4.762E+00  | 1.029 | 3.503E+00 | 0.825 | 2.151E+00 | 1.524 | 0.736 |
|     | 1/8  | 2.339E+00  | 1.026 | 2.001E+00 | 0.808 | 1.040E+00 | 1.048 | 0.855 |
|     | 1/16 | 1.148E+00  | 1.027 | 1.064E+00 | 0.911 | 5.189E-01 | 1.003 | 0.927 |
|     | 1/32 | 5.686E-01  | 1.014 | 5.456E-01 | 0.964 | 2.594E-01 | 1.001 | 0.960 |

Table 2.1: History of convergence for the Stokes problem with  $\nu = 1$ ,  $\mathbf{u}_{H,h} \in \mathbb{P}^3(\mathcal{T}_H)^2$ ,  $p_h \in \mathbb{P}^3(\mathcal{T}_H)$  and  $\boldsymbol{\lambda}_{H,h} \in \boldsymbol{\Lambda}_l^1$ .

| $l$ | $H$  | $\ (\mathbf{u} - \mathbf{u}_{H,h}, p - p_{H,h})\ _{\mathbf{V} \times Q}$ |       | $\eta_1$  |       | $\eta_2$  |       | $E_i$ |
|-----|------|--|-------|-----------|-------|-----------|-------|-------|
|     |      | error  | rate  | error     | rate  | value     | rate  |       |
| 2   | 1/2  | 2.993E-01  | –     | 6.850E-02 | –     | 1.562E+00 | –     | 0.229 |
|     | 1/4  | 3.250E-02  | 3.203 | 9.136E-03 | 2.906 | 4.013E-02 | 5.282 | 0.281 |
|     | 1/8  | 3.701E-03  | 3.135 | 1.171E-03 | 2.964 | 1.407E-03 | 4.834 | 0.316 |
|     | 1/16 | 4.480E-04  | 3.046 | 1.515E-04 | 2.951 | 5.545E-05 | 4.665 | 0.338 |
| 1   | 1/2  | 7.746E-01  | –     | 3.523E-01 | –     | 1.803E+00 | –     | 0.455 |
|     | 1/4  | 3.564E-01  | 1.120 | 1.487E-01 | 1.244 | 1.589E-01 | 3.504 | 0.417 |
|     | 1/8  | 8.783E-02  | 2.021 | 3.854E-02 | 1.948 | 1.321E-02 | 3.589 | 0.439 |
|     | 1/16 | 2.178E-02  | 2.012 | 9.941E-03 | 1.955 | 1.054E-03 | 3.647 | 0.456 |
| 0   | 1/2  | 9.720E+00  | –     | 4.387E+00 | –     | 1.370E+00 | –     | 0.451 |
|     | 1/4  | 4.764E+00  | 1.029 | 2.477E+00 | 0.825 | 2.034E-01 | 2.752 | 0.520 |
|     | 1/8  | 2.340E+00  | 1.025 | 1.415E+00 | 0.808 | 3.354E-02 | 2.600 | 0.605 |
|     | 1/16 | 1.148E+00  | 1.027 | 7.524E-01 | 0.911 | 5.439E-03 | 2.625 | 0.655 |

Table 2.2: History convergence for the Stokes problem with  $\nu = 1$ ,  $\mathbf{u}_{H,h} \in \mathbb{P}^3(\mathcal{T}_H)^2$ ,  $p_h \in \mathbb{P}^3(\mathcal{T}_H)$  and  $\boldsymbol{\lambda}_{H,h} \in \boldsymbol{\Lambda}_l^1$ . Here  $h = H^2$ .

| $l$ | $H$  | $\ (\mathbf{u} - \mathbf{u}_{H,h}, p - p_{H,h})\ _{\mathbf{V} \times Q}$ |       | $\eta_1$  |       | $\eta_2$  |       | $E_i$ |
|-----|------|--|-------|-----------|-------|-----------|-------|-------|
|     |      | error  | rate  | error     | rate  | value     | rate  |       |
| 2   | 1/2  | 4.365E-01  | —     | 7.712E-02 | —     | 2.306E-01 | —     | 0.705 |
|     | 1/4  | 6.190E-02  | 2.818 | 1.016E-02 | 2.925 | 2.776E-02 | 3.055 | 0.613 |
|     | 1/8  | 7.709E-03  | 3.005 | 1.259E-03 | 3.013 | 3.255E-03 | 3.092 | 0.586 |
|     | 1/16 | 9.593E-04  | 3.006 | 1.594E-04 | 2.981 | 3.981E-04 | 3.032 | 0.581 |
|     | 1/32 | 1.197E-04  | 3.003 | 2.021E-05 | 2.980 | 4.943E-05 | 3.009 | 0.582 |
| 1   | 1/2  | 5.342E+01  | —     | 2.717E+01 | —     | 8.219E+00 | —     | 0.662 |
|     | 1/4  | 1.350E+01  | 1.985 | 6.936E+00 | 1.970 | 2.106E+00 | 1.964 | 0.670 |
|     | 1/8  | 3.388E+00  | 1.994 | 1.746E+00 | 1.990 | 5.313E-01 | 1.987 | 0.672 |
|     | 1/16 | 8.483E-01  | 1.998 | 4.378E-01 | 1.996 | 1.333E-01 | 1.995 | 0.673 |
|     | 1/32 | 2.122E-01  | 1.999 | 1.096E-01 | 1.998 | 3.338E-02 | 1.998 | 0.674 |
| 0   | 1/2  | 4.889E+02  | —     | 2.842E+02 | —     | 6.531E+00 | —     | 0.595 |
|     | 1/4  | 2.793E+02  | 0.808 | 1.828E+02 | 0.637 | 3.267E+00 | 0.999 | 0.666 |
|     | 1/8  | 1.505E+02  | 0.892 | 1.097E+02 | 0.736 | 1.634E+00 | 1.000 | 0.740 |
|     | 1/16 | 7.748E+01  | 0.958 | 5.918E+01 | 0.891 | 8.170E-01 | 1.000 | 0.774 |
|     | 1/32 | 3.913E+01  | 0.985 | 3.048E+01 | 0.957 | 4.085E-01 | 1.000 | 0.789 |

Table 2.3: History of convergence for the Stokes problem with  $\nu = 10^{-2}$ ,  $\mathbf{u}_{H,h} \in \mathbb{P}^3(\mathcal{T}_H)^2$ ,  $p_h \in \mathbb{P}^3(\mathcal{T}_H)$  and  $\boldsymbol{\lambda}_{H,h} \in \Lambda_l^1$ .

| $l$ | $H$  | $\ (\mathbf{u} - \mathbf{u}_{H,h}, p - p_{H,h})\ _{\mathbf{V} \times Q}$ |       | $\eta_1$  |       | $\eta_2$  |       | $E_i$ |
|-----|------|--|-------|-----------|-------|-----------|-------|-------|
|     |      | error  | rate  | error     | rate  | value     | rate  |       |
| 2   | 1/2  | 2.254E-01  | —     | 6.850E-02 | —     | 3.861E-02 | —     | 0.475 |
|     | 1/4  | 2.663E-02  | 3.082 | 9.136E-03 | 2.906 | 1.090E-03 | 5.146 | 0.384 |
|     | 1/8  | 3.147E-03  | 3.081 | 1.171E-03 | 2.964 | 3.866E-05 | 4.818 | 0.384 |
|     | 1/16 | 3.878E-04  | 3.020 | 1.515E-04 | 2.951 | 1.520E-06 | 4.668 | 0.395 |
| 1   | 1/2  | 5.147E+01  | —     | 2.932E+01 | —     | 3.404E+00 | —     | 0.636 |
|     | 1/4  | 1.308E+01  | 1.976 | 7.526E+00 | 1.962 | 2.941E-01 | 3.533 | 0.598 |
|     | 1/8  | 3.288E+00  | 1.992 | 1.895E+00 | 1.990 | 2.404E-02 | 3.613 | 0.584 |
|     | 1/16 | 8.237E-01  | 1.997 | 4.750E-01 | 1.996 | 1.945E-03 | 3.627 | 0.579 |
| 0   | 1/2  | 4.890E+02  | —     | 2.843E+02 | —     | 2.561E+00 | —     | 0.587 |
|     | 1/4  | 2.795E+02  | 0.807 | 1.826E+02 | 0.638 | 4.074E-01 | 2.652 | 0.655 |
|     | 1/8  | 1.506E+02  | 0.892 | 1.096E+02 | 0.736 | 6.476E-02 | 2.653 | 0.728 |
|     | 1/16 | 7.752E+01  | 0.958 | 5.913E+01 | 0.890 | 1.039E-02 | 2.640 | 0.763 |

Table 2.4: History of convergence for the Stokes problem with  $\nu = 10^{-2}$ ,  $\mathbf{u}_{H,h} \in \mathbb{P}^3(\mathcal{T}_H)^2$ ,  $p_h \in \mathbb{P}^3(\mathcal{T}_H)$  and  $\boldsymbol{\lambda}_{H,h} \in \Lambda_l^1$ . Here  $h = H^2$ .

#### 2.5.4 The 2D lid-driven cavity problem

We consider the well-known 2D cavity problem for the Stokes ( $\boldsymbol{\gamma} = \mathbf{0}$ ) and Brinkman ( $\boldsymbol{\gamma} = 10^4 \mathbf{I}$ ) problems with  $\nu = 1$ . In Figures 2.2 and 2.3, we show the meshes obtained by the two versions of the adaptive algorithms looking for  $\mathbf{u}_h \in \mathbb{P}^2(K)^2$ ,  $p_h \in \mathbb{P}^2(K)$  and

$\lambda_{H,h} \in \Lambda_0$ . Higher polynomial degrees does not change conclusions and then they are not presented.

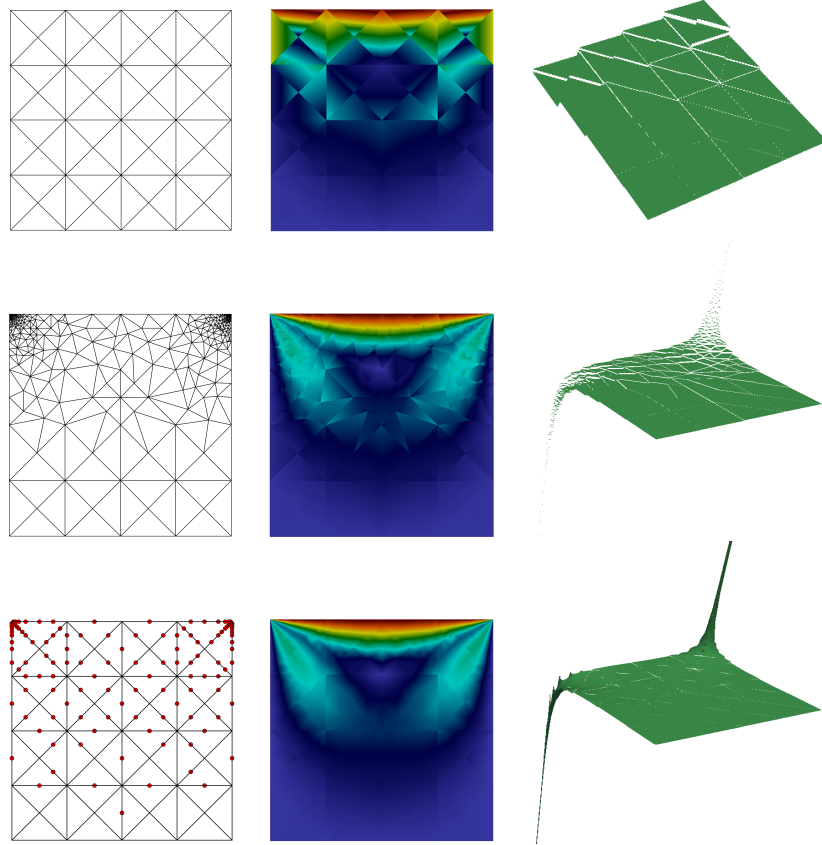


Figure 2.2: Lid-driven cavity problem for the Stokes equation with  $\mathbf{u}_h \in \mathbb{P}^2(K)^2, p_h \in \mathbb{P}^2(K), \lambda_{H,h} \in \Lambda_0$  and  $\nu = 1$ . Second and third rows correspond, respectively, to the final step of the adaptive procedure by elements (6,216 dof) and adaptive procedure by faces (912 dof), and the first row shows the start step in both adaptive procedures. Second and third columns represent the magnitude of the velocity and pressure, respectively.

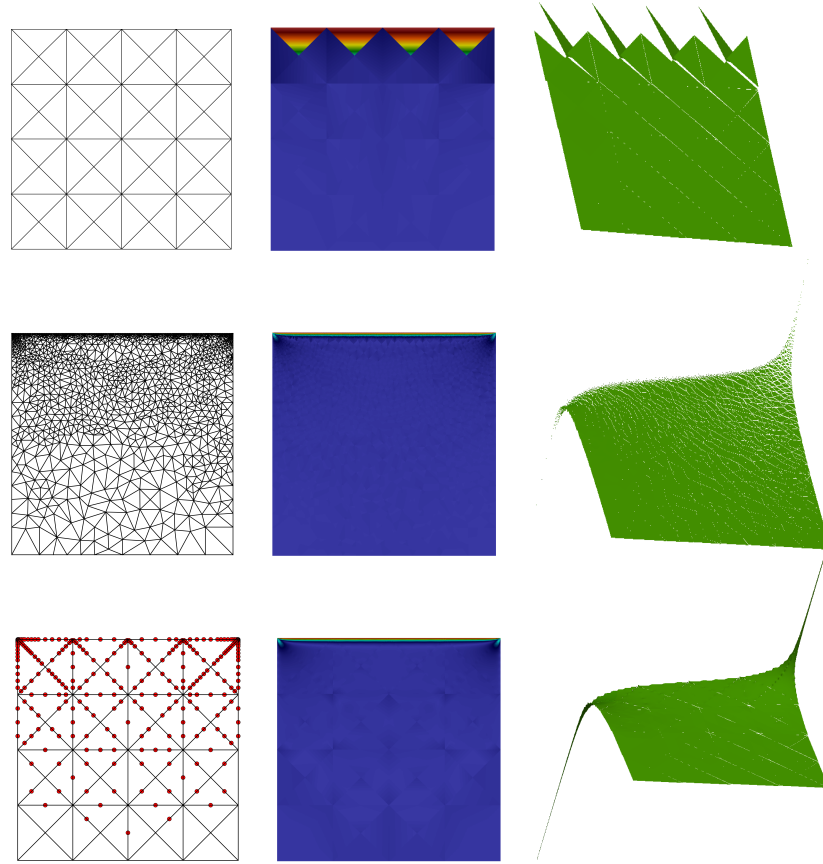


Figure 2.3: Lid-driven cavity problem for the Brinkman equation with  $\mathbf{u}_h \in \mathbb{P}^2(K)^2$ ,  $p_h \in \mathbb{P}^2(K)$ ,  $\boldsymbol{\lambda}_{H,h} \in \boldsymbol{\Lambda}_0$ ,  $\nu = 1$  and  $\gamma = 10^4 \mathbf{I}$ . Second and third rows correspond, respectively, to the final step of the adaptive procedure by elements (32,337 dof) and adaptive procedure by faces (786 dof), and the first row shows the start step in both adaptive procedures. Second and third columns represent the magnitude of the velocity and pressure, respectively.

As expected, in the cavity problem for Stokes and Brinkman, the adaptive algorithms refine the upper part of the domain, where the solution has boundary layers and/or singularities. Note that Algorithm 2 requires less degrees of freedom than Algorithm 1 to get good numerical results.

### 2.5.5 A highly heterogeneous case

This numerical test illustrates the capacity of the MHM method to simulate fluid flow in a highly heterogeneous porous media. The domain is  $\Omega := [0, 1200] \times [0, 2200]$  with boundary conditions given in Figure 2.4. We adopt a heterogeneous isotropic coefficient  $\gamma$  obtained from the 85th layer of the SPE10 project [38] (second dataset). The domain represents a

quite realistic prototype of a reservoir. Here, we adopt the following version of the Brinkman model

$$-\nu \Delta \mathbf{u} + \gamma \mathbf{u} + \nabla p = \mathbf{0} \quad \text{in } \Omega, \quad \nabla \cdot \mathbf{u} = 0 \quad \text{in } \Omega,$$

with  $\nu = 0.3$  and  $\gamma = (0.3/\kappa) \mathbf{I}$ , where  $\mathbf{I}$  stands for the identity tensor. The permeability  $\kappa$  is depicted in Figure 2.4. The reference solution is calculated using the USFEM scheme of [25] using a uniform mesh of 1,081,344 triangles. The  $\mathbb{P}_1(\tau)^d \times \mathbb{P}_1(\tau)$  element is adopted to approximate the velocity and pressure variables. As such, the total number of degrees of freedom is 1,625,283. As for the MHM solution, we select  $\mathbf{u}_h \in \mathbb{P}^3(K)^2$ ,  $p_h \in \mathbb{P}^3(K)$  and  $\boldsymbol{\lambda}_{H,h} \in \boldsymbol{\Lambda}_1$ .

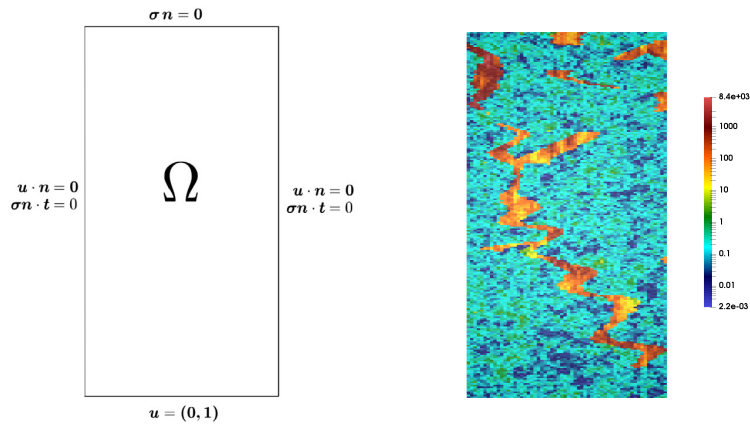


Figure 2.4: Boundary conditions (left) and the permeability  $\kappa$  (right) in logarithmic scale.

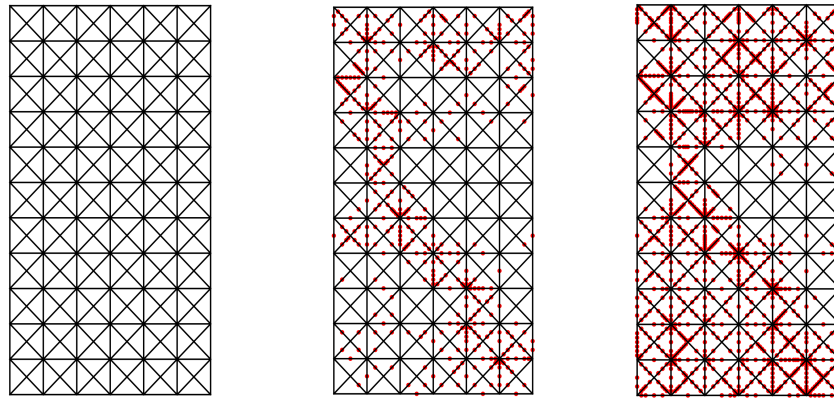


Figure 2.5: Initial mesh (left) with 1,652 dof, an intermediate adapted mesh (center) with 3,352 dof and the final adapted mesh (right) with 7,800 dof.

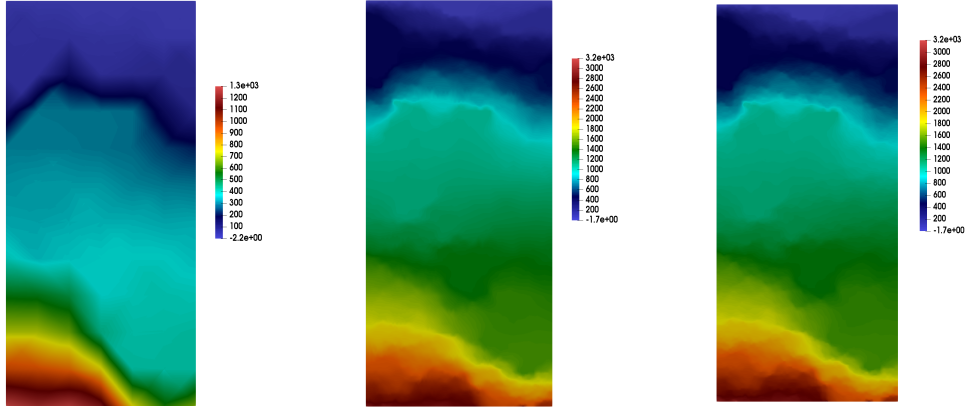


Figure 2.6: Isolines of the pressure corresponding (from left to right) to the solution using the initial mesh (1,652 dofs), the adaptive one (7,800 dofs), and the reference solution (1,625,283 dofs), respectively.

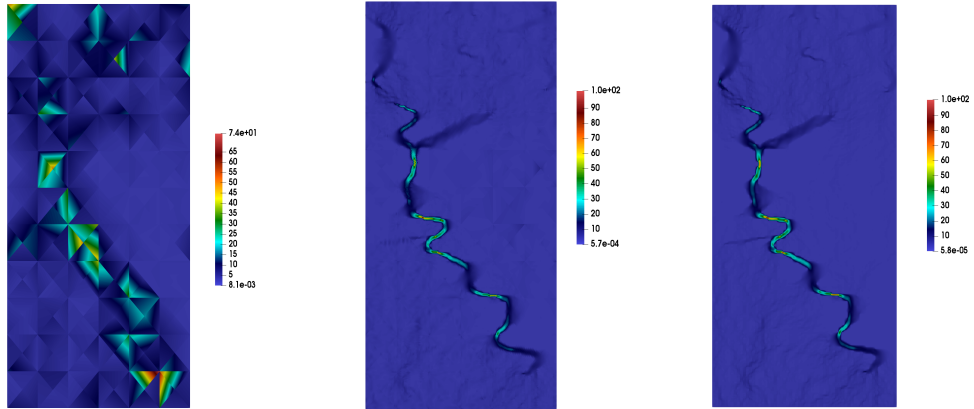


Figure 2.7: Magnitude of velocity corresponding (from left to right) to the solution using the initial mesh (1,652 dofs), the adaptive one (7,800 dofs), and the reference solution (1,625,283 dofs), respectively.

We observe that the solution of the MHM method using the adaptive strategy given by the Algorithm 2 is very close to the reference solution, and captures the heterogeneity of the reservoir clearly with the advantage of using considerably less degrees of freedom.

## 2.6 Appendix: Some technical lemmas

This section presents some technical results needed in the proof of Theorems 2.6 and 2.7.

**Lemma 2.3** *Let  $\boldsymbol{\lambda} \in \Lambda$  and  $\boldsymbol{\lambda}_{H,h} \in \Lambda_H$  be the solutions of problems (2.31) and (2.39), respectively. Then*

$$\int_K T^p(\boldsymbol{\lambda} - \boldsymbol{\lambda}_{H,h}) \, d\mathbf{x} = 0,$$

in the Stokes case ( $\boldsymbol{\gamma} = \mathbf{0}$ ), and

$$\left| \int_K T^p(\boldsymbol{\lambda} - \boldsymbol{\lambda}_{H,h}) \, d\mathbf{x} \right| \preceq H_K |K|^{1/2} \eta_{2,K}$$

otherwise.

*Proof.* Let  $\mathbf{w} := \frac{1}{d} \left( \mathbf{x} - \frac{1}{|K|} \int_K \mathbf{x} \, dx \right)$ . Noticing that  $\mathbf{w} \in [H^1(K) \cap L_0^2(K)]^d$ ,  $\nabla \cdot \mathbf{w} = 1$ , and  $\nabla \mathbf{w} = \frac{1}{d} \mathbf{I}$ , and testing (2.28) and (2.43) with  $(\mathbf{w}, 0)$ , we get

$$\begin{aligned} \int_K T^p \boldsymbol{\lambda}_{H,h} \, d\mathbf{x} &= (T^p \boldsymbol{\lambda}_{H,h}, \nabla \cdot \mathbf{w})_K = (\nu \nabla T^u \boldsymbol{\lambda}_{H,h}, \nabla \mathbf{w})_K + (\gamma T^u \boldsymbol{\lambda}_{H,h}, \mathbf{w})_K + \langle \boldsymbol{\lambda}_{H,h}, \mathbf{w} \rangle_{\partial K} \\ &= \frac{\nu}{d} \int_K \nabla \cdot T^u \boldsymbol{\lambda}_{H,h} \, d\mathbf{x} + (\gamma T^u \boldsymbol{\lambda}_{H,h}, \mathbf{w})_K + \langle \boldsymbol{\lambda}_{H,h}, \mathbf{w} \rangle_{\partial K} \\ &= (\gamma T^u \boldsymbol{\lambda}_{H,h}, \mathbf{w})_K + \langle \boldsymbol{\lambda}_{H,h}, \mathbf{w} \rangle_{\partial K} \\ &= \frac{\nu}{d} \int_K \nabla \cdot T_h^u \boldsymbol{\lambda}_{H,h} \, d\mathbf{x} + (\gamma T^u \boldsymbol{\lambda}_{H,h}, \mathbf{w})_K + \langle \boldsymbol{\lambda}_{H,h}, \mathbf{w} \rangle_{\partial K} \\ &= (\nu \nabla T_h^u \boldsymbol{\lambda}_{H,h}, \nabla \mathbf{w})_K + (\gamma T^u \boldsymbol{\lambda}_{H,h}, \mathbf{w})_K + \langle \boldsymbol{\lambda}_{H,h}, \mathbf{w} \rangle_{\partial K} \\ &= (T_h^p \boldsymbol{\lambda}_{H,h}, \nabla \cdot \mathbf{w})_K + (\gamma (T^u - T_h^u) \boldsymbol{\lambda}_{H,h}, \mathbf{w})_K \\ &\quad + \sum_{\tau \in \mathcal{T}_h^K} \kappa_\tau (-\nu \Delta T_h^u \boldsymbol{\lambda}_{H,h} + \gamma T_h^u \boldsymbol{\lambda}_{H,h} + \nabla T_h^p \boldsymbol{\lambda}_{H,h}, \gamma \mathbf{w})_\tau \\ &= \int_K T_h^p \boldsymbol{\lambda}_{H,h} \, d\mathbf{x} + (\gamma (T^u - T_h^u) \boldsymbol{\lambda}_{H,h}, \mathbf{w})_K \\ &\quad + \sum_{\tau \in \mathcal{T}_h^K} \kappa_\tau (-\nu \Delta T_h^u \boldsymbol{\lambda}_{H,h} + \gamma T_h^u \boldsymbol{\lambda}_{H,h} + \nabla T_h^p \boldsymbol{\lambda}_{H,h}, \gamma \mathbf{w})_\tau. \end{aligned} \tag{2.74}$$

Proceeding in a similar way but now with the equations (2.29) and (2.44), we arrive that

$$\begin{aligned}
\int_K \hat{T}^p \mathbf{f} \, d\mathbf{x} &= (\hat{T}^p \mathbf{f}, \nabla \cdot \mathbf{w})_K = (\nu \nabla \hat{T}^u \mathbf{f}, \nabla \mathbf{w})_K + (\gamma \hat{T}^u \mathbf{f}, \mathbf{w})_K - (\mathbf{f}, \mathbf{w})_K \\
&= \frac{\nu}{d} \int_K \nabla \cdot \hat{T}^u \mathbf{f} \, d\mathbf{x} + (\gamma \hat{T}^u \mathbf{f}, \mathbf{w})_K - (\mathbf{f}, \mathbf{w})_K = (\gamma \hat{T}^u \mathbf{f}, \mathbf{w})_K - (\mathbf{f}, \mathbf{w})_K \\
&= \frac{\nu}{d} \int_K \nabla \cdot \hat{T}_h^u \mathbf{f} \, d\mathbf{x} + (\gamma \hat{T}_h^u \mathbf{f}, \mathbf{w})_K - (\mathbf{f}, \mathbf{w})_K \\
&= (\nu \nabla \hat{T}_h^u \mathbf{f}, \nabla \mathbf{w})_K + (\gamma \hat{T}_h^u \mathbf{f}, \mathbf{w})_K - (\mathbf{f}, \mathbf{w})_K \\
&= (\hat{T}_h^p \mathbf{f}, \nabla \cdot \mathbf{w})_K + (\gamma (\hat{T}^u - \hat{T}_h^u) \mathbf{f}, \mathbf{w})_K \\
&\quad + \sum_{\tau \in \mathcal{T}_h^K} \kappa_\tau (-\nu \Delta \hat{T}_h^u \mathbf{f} + \gamma \hat{T}_h^u \mathbf{f} + \nabla \hat{T}_h^p \mathbf{f} - \mathbf{f}, \gamma \mathbf{w})_\tau \\
&= \int_K \hat{T}_h^p \mathbf{f} \, d\mathbf{x} + (\gamma (\hat{T}^u - \hat{T}_h^u) \mathbf{f}, \mathbf{w})_K \\
&\quad + \sum_{\tau \in \mathcal{T}_h^K} \kappa_\tau (-\nu \Delta \hat{T}_h^u \mathbf{f} + \gamma \hat{T}_h^u \mathbf{f} + \nabla \hat{T}_h^p \mathbf{f} - \mathbf{f}, \gamma \mathbf{w})_\tau
\end{aligned} \tag{2.75}$$

and then, from (2.74), (2.75) and the third equations in (2.31) and (2.39), it holds

$$\begin{aligned}
\int_K T^p (\boldsymbol{\lambda} - \boldsymbol{\lambda}_{H,h}) \, d\mathbf{x} &= \int_K T^p \boldsymbol{\lambda} \, d\mathbf{x} - \int_K T^p \boldsymbol{\lambda}_{H,h} \, d\mathbf{x} = - \int_K \hat{T}^p \mathbf{f} \, d\mathbf{x} - \int_K T^p \boldsymbol{\lambda}_{H,h} \, d\mathbf{x} \\
&= - \int_K \hat{T}^p \mathbf{f} \, d\mathbf{x} - \left[ \int_K T_h^p \boldsymbol{\lambda}_{H,h} \, d\mathbf{x} + (\gamma (T^u - T_h^u) \boldsymbol{\lambda}_{H,h}, \mathbf{w})_K \right. \\
&\quad \left. + \sum_{\tau \in \mathcal{T}_h^K} \kappa_\tau (-\nu \Delta T_h^u \boldsymbol{\lambda}_{H,h} + \gamma T_h^u \boldsymbol{\lambda}_{H,h} + \nabla T_h^p \boldsymbol{\lambda}_{H,h}, \gamma \mathbf{w})_\tau \right] \\
&= - \int_K \hat{T}_h^p \mathbf{f} \, d\mathbf{x} - (\gamma (\hat{T}^u - \hat{T}_h^u) \mathbf{f}, \mathbf{w})_K \\
&\quad - \sum_{\tau \in \mathcal{T}_h^K} \kappa_\tau (-\nu \Delta \hat{T}_h^u \mathbf{f} + \gamma \hat{T}_h^u \mathbf{f} + \nabla \hat{T}_h^p \mathbf{f} - \mathbf{f}, \gamma \mathbf{w})_\tau \\
&\quad - \left[ \int_K T_h^p \boldsymbol{\lambda}_{H,h} \, d\mathbf{x} + (\gamma (T^u - T_h^u) \boldsymbol{\lambda}_{H,h}, \mathbf{w})_K \right. \\
&\quad \left. + \sum_{\tau \in \mathcal{T}_h^K} \kappa_\tau (-\nu \Delta T_h^u \boldsymbol{\lambda}_{H,h} + \gamma T_h^u \boldsymbol{\lambda}_{H,h} + \nabla T_h^p \boldsymbol{\lambda}_{H,h}, \gamma \mathbf{w})_\tau \right] \\
&= - (\gamma (T^u - T_h^u) \boldsymbol{\lambda}_{H,h}, \mathbf{w})_K - (\gamma (\hat{T}^u - \hat{T}_h^u) \mathbf{f}, \mathbf{w})_K \\
&\quad + \sum_{\tau \in \mathcal{T}_h^K} \kappa_\tau (-\nu \Delta u_{H,h} + \gamma u_{H,h} + \nabla p_{H,h} - \mathbf{f}, \gamma \mathbf{w})_\tau \\
&= - (\gamma (T^u - T_h^u) \boldsymbol{\lambda}_{H,h}, \mathbf{w})_K - (\gamma (\hat{T}^u - \hat{T}_h^u) \mathbf{f}, \mathbf{w})_K + \sum_{\tau \in \mathcal{T}_h^K} \kappa_\tau (\mathbf{R}_\tau^K, \gamma \mathbf{w})_\tau.
\end{aligned} \tag{2.76}$$

Observe that for the Stokes problem ( $\boldsymbol{\gamma} = \mathbf{0}$ ), equation (2.76) vanishes and the result follows. For the Brinkman case, applying Cauchy–Schwartz’s inequality, Lemma 2.1, using (2.59) and recalling from [28, Theorem 3.2] that, since  $\mathbf{w} \in [H^1(K) \cap L_0^2(K)]^d$  and the convexity of  $K$ , we have that

$$\|\mathbf{w}\|_{0,K} \leq \frac{H_K}{\pi} |\mathbf{w}|_{1,K} = \frac{1}{d\pi} H_K |K|^{1/2}$$

the result follows. ■

The second auxiliary result establishes bounds for the local pressure associated to the error  $\boldsymbol{\lambda} - \boldsymbol{\lambda}_{H,h}$  in terms of its velocity counterpart.

**Lemma 2.4** *Let  $\boldsymbol{\lambda} \in \boldsymbol{\Lambda}$  and  $\boldsymbol{\lambda}_{H,h} \in \boldsymbol{\Lambda}_H$  be the solutions of problems (2.31) and (2.39), respectively. Then, we have that*

$$\|T^p(\boldsymbol{\lambda} - \boldsymbol{\lambda}_{H,h})\|_{Q(K)} \preceq \|T^u(\boldsymbol{\lambda} - \boldsymbol{\lambda}_{H,h})\|_{\mathbf{V}(K)}$$

for the Stokes problem, and

$$\|T^p(\boldsymbol{\lambda} - \boldsymbol{\lambda}_{H,h})\|_{Q(K)} \preceq \|T^u(\boldsymbol{\lambda} - \boldsymbol{\lambda}_{H,h})\|_{\mathbf{V}(K)} + H_K \eta_{2,K}$$

for the Brinkman problem.

*Proof.* Let  $\boldsymbol{\mu} := \boldsymbol{\lambda} - \boldsymbol{\lambda}_{H,h}$  and consider the Stokes case. From Lemma 2.3, the function  $T^p \boldsymbol{\mu} \in L_0^2(K)$  and then there exists  $\tilde{\mathbf{w}} \in H_0^1(K)^d$  such that

$$\nabla \cdot \tilde{\mathbf{w}} = T^p \boldsymbol{\mu} \quad \text{in } K, \tag{2.77}$$

satisfying

$$|\tilde{\mathbf{w}}|_{1,K} \preceq \|T^p \boldsymbol{\mu}\|_{0,K}. \tag{2.78}$$

Next, defined  $\mathbf{w} := \tilde{\mathbf{w}} - \frac{1}{|K|} \tilde{\mathbf{w}} \in \mathbf{V}_0^\perp(K)$ . From the first equation of (2.31) and (2.39), and the local problems (2.28) and (2.29), it holds

$$\begin{aligned} 0 &= -\langle \boldsymbol{\mu}, \tilde{\mathbf{w}} \rangle_{\partial K} = -\langle \boldsymbol{\mu}, \mathbf{w} \rangle_{\partial K} \\ &= a_K(T^u \boldsymbol{\mu}, \mathbf{w}) + b_K(\mathbf{w}, T^p \boldsymbol{\mu}) = a_K(T^u \boldsymbol{\mu}, \tilde{\mathbf{w}}) + b_K(\tilde{\mathbf{w}}, T^p \boldsymbol{\mu}). \end{aligned} \tag{2.79}$$

Hence, from (2.77), (2.78), (2.79), and Cauchy–Schwartz’s inequality, we get

$$\|T^p \boldsymbol{\mu}\|_{Q(K)}^2 = (T^p \boldsymbol{\mu}, \nabla \cdot \tilde{\mathbf{w}})_K = -b_K(\tilde{\mathbf{w}}, T^p \boldsymbol{\mu}) = a_K(T^u \boldsymbol{\mu}, \tilde{\mathbf{w}}) \preceq \|T^p \boldsymbol{\mu}\|_{Q(K)} \|T^u \boldsymbol{\mu}\|_{\mathbf{V}(K)}$$

and the result follows.

Now, we proceed to the Brinkman case following the proof for the Stokes one. First, we notice that  $T^p \boldsymbol{\mu}$  is not necessarily an element of  $L_0^2(K)$ . Then, we decompose

$$T^p \boldsymbol{\mu} = \tilde{q} + q_0 \quad \text{where} \quad \tilde{q} \in L_0^2(K) \text{ and } q_0 = \frac{1}{|K|} \int_K T^p \boldsymbol{\mu} \, dx, \quad (2.80)$$

and pick  $\tilde{\mathbf{w}} \in H_0^1(K)^d$  such that

$$\nabla \cdot \tilde{\mathbf{w}} = \tilde{q} \quad \text{in } K, \quad (2.81)$$

and

$$|\tilde{\mathbf{w}}|_{1,K} \preceq \|\tilde{q}\|_{0,K}. \quad (2.82)$$

Also, from (2.80) it holds

$$\|\tilde{q}\|_{Q(K)} \leq \|T^p \boldsymbol{\mu}\|_{Q(K)}. \quad (2.83)$$

From local problems (2.28) and (2.29), we arrive at

$$0 = -\langle \boldsymbol{\mu}, \tilde{\mathbf{w}} \rangle_{\partial K} = a_K(T^u \boldsymbol{\mu}, \tilde{\mathbf{w}}) + b_K(\tilde{\mathbf{w}}, T^p \boldsymbol{\mu}) \quad (2.84)$$

and then, from (2.81), (2.82), (2.84), Cauchy–Schwartz’s inequality, (2.83) and Lemma 2.3, we get

$$\begin{aligned} \|T^p \boldsymbol{\mu}\|_{Q(K)}^2 &= (T^p \boldsymbol{\mu}, \tilde{q})_K + (T^p \boldsymbol{\mu}, q_0)_K = (T^p \boldsymbol{\mu}, \nabla \cdot \tilde{\mathbf{w}})_K + (T^p \boldsymbol{\mu}, q_0)_K \\ &= -b_K(\tilde{\mathbf{w}}, T^p \boldsymbol{\mu}) + (T^p \boldsymbol{\mu}, q_0)_K = a_K(T^u \boldsymbol{\mu}, \tilde{\mathbf{w}}) + (T^p \boldsymbol{\mu}, q_0)_K \\ &\preceq \|T^u \boldsymbol{\mu}\|_{\mathbf{V}(K)} \|\tilde{q}\|_{Q(K)} + \|T^p \boldsymbol{\mu}\|_{Q(K)} \|q_0\|_{Q(K)} \\ &\preceq \|T^u \boldsymbol{\mu}\|_{\mathbf{V}(K)} \|T^p \boldsymbol{\mu}\|_{Q(K)} + \|T^p \boldsymbol{\mu}\|_{Q(K)} \|q_0\|_{Q(K)} \\ &= (\|T^u \boldsymbol{\mu}\|_{\mathbf{V}(K)} + \|q_0\|_{0,K}) \|T^p \boldsymbol{\mu}\|_{Q(K)} \preceq (\|T^u \boldsymbol{\mu}\|_{\mathbf{V}(K)} + H_K \eta_{2,K}) \|T^p \boldsymbol{\mu}\|_{Q(K)} \end{aligned}$$

and the result follows. ■

Now, we detail an intermediate error estimate for the local velocity associated to  $\boldsymbol{\lambda} - \boldsymbol{\lambda}_{H,h}$  with respect to  $\eta_1$  and  $\eta_2$ .

**Lemma 2.5** *Let  $\boldsymbol{\lambda} \in \boldsymbol{\Lambda}$  and  $\boldsymbol{\lambda}_{H,h} \in \boldsymbol{\Lambda}_H$  be the solutions of problems (2.31) and (2.39), respectively. The following estimates hold*

$$\|T^u(\boldsymbol{\lambda} - \boldsymbol{\lambda}_{H,h})\|_{\mathbf{V}} \preceq \begin{cases} \eta_1 + \eta_2 & \text{if } \boldsymbol{\gamma} = \mathbf{0}, \\ \eta_1 + \eta_2 + H\{(\eta_1 + \eta_2)\eta_2\}^{1/2} & \text{otherwise.} \end{cases}$$

*Proof.* Let  $\boldsymbol{\mu} = \boldsymbol{\lambda} - \boldsymbol{\lambda}_{H,h}$ . From (2.2), using  $(T^p \boldsymbol{\mu}, \nabla \cdot T^u \boldsymbol{\mu})_{\mathcal{T}_H} = 0$  and (2.28), we obtain that

$$-(\boldsymbol{\mu}, T^u \boldsymbol{\mu})_{\partial \mathcal{T}_H} = \sum_{K \in \mathcal{T}_H} B_K((T^u \boldsymbol{\mu}, T^p \boldsymbol{\mu}), (T^u \boldsymbol{\mu}, 0)) \geq C \|T^u \boldsymbol{\mu}\|_{\mathbf{V}}^2, \quad (2.85)$$

where  $C$  depends only on  $\nu$ ,  $\gamma_{\max}$  and  $d_\Omega$ . Using  $(\boldsymbol{\mu}, \mathbf{v}_0)_{\partial \mathcal{T}_H} = 0$ , for all  $\mathbf{v}_0 \in \mathbf{V}_0$ , and from (2.2), (2.13), (2.28) and the orthogonality between functions in  $\mathbf{V}$  and  $\mathbf{V}_0^\perp$ , it holds

$$\begin{aligned} \frac{\sqrt{2}}{2} \|\boldsymbol{\mu}\|_{\boldsymbol{\Lambda}} &\leq \sup_{\mathbf{v} \in \mathbf{V}} \frac{(\boldsymbol{\mu}, \mathbf{v})_{\partial \mathcal{T}_H}}{\|\mathbf{v}\|_{\mathbf{V}}} = \sup_{\mathbf{v}_0 \in \mathbf{V}_0, \mathbf{v}_0^\perp \in \mathbf{V}_0^\perp} \frac{(\boldsymbol{\mu}, \mathbf{v}_0^\perp)_{\partial \mathcal{T}_H}}{\|\mathbf{v}_0 + \mathbf{v}_0^\perp\|_{\mathbf{V}}} \\ &\leq \sup_{\mathbf{v}_0^\perp \in \mathbf{V}_0^\perp} \frac{(\boldsymbol{\mu}, \mathbf{v}_0^\perp)_{\partial \mathcal{T}_H}}{\|\mathbf{v}_0^\perp\|_{\mathbf{V}}} = \sup_{\mathbf{v}_0^\perp \in \mathbf{V}_0^\perp} \frac{-B((T^u \boldsymbol{\mu}, T^p \boldsymbol{\mu}), (\mathbf{v}_0^\perp, 0))}{\|\mathbf{v}_0^\perp\|_{\mathbf{V}}} \\ &\preceq \|T^u \boldsymbol{\mu}\|_{\mathbf{V}} + \|T^p \boldsymbol{\mu}\|_Q. \end{aligned}$$

Thus, from Lemma 2.4 we get

$$\|\boldsymbol{\mu}\|_{\boldsymbol{\Lambda}} \preceq \begin{cases} \|T^u \boldsymbol{\mu}\|_{\mathbf{V}} & \text{if } \boldsymbol{\gamma} = \mathbf{0}, \\ \|T^u \boldsymbol{\mu}\|_{\mathbf{V}} + H \eta_2 & \text{otherwise.} \end{cases} \quad (2.86)$$

Now, using again  $(\boldsymbol{\mu}, \mathbf{u}_0)_{\partial \mathcal{T}_H} = (\boldsymbol{\mu}, \mathbf{u}_0^{H,h})_{\partial \mathcal{T}_H} = 0$ , from (2.32), (2.46) and Lemmas 2.1 and 2.2, we obtain

$$\begin{aligned} -(\boldsymbol{\mu}, T^u \boldsymbol{\mu})_{\partial \mathcal{T}_H} &= -(\boldsymbol{\mu}, T^u(\boldsymbol{\lambda} - \boldsymbol{\lambda}_{H,h}))_{\partial \mathcal{T}_H} = -(\boldsymbol{\mu}, \mathbf{u}_0 + T^u \boldsymbol{\lambda} + \hat{T}^u \mathbf{f} - (T^u \boldsymbol{\lambda}_{H,h} + \hat{T}^u \mathbf{f}))_{\partial \mathcal{T}_H} \\ &= -(\boldsymbol{\mu}, \mathbf{u})_{\partial \mathcal{T}_H} + (\boldsymbol{\mu}, T^u \boldsymbol{\lambda}_{H,h} + \hat{T}^u \mathbf{f})_{\partial \mathcal{T}_H} \\ &= -\langle \boldsymbol{\mu}, \mathbf{g} \rangle_{\partial \Omega} + (\boldsymbol{\mu}, \mathbf{u}_0^{H,h} + T_h^u \boldsymbol{\lambda}_{H,h} + \hat{T}_h^u \mathbf{f} + (T^u - T_h^u) \boldsymbol{\lambda}_{H,h} + (\hat{T}^u - \hat{T}_h^u) \mathbf{f})_{\partial \mathcal{T}_H} \\ &= -\langle \boldsymbol{\mu}, \mathbf{g} \rangle_{\partial \Omega} + (\boldsymbol{\mu}, \mathbf{u}_{H,h})_{\partial \mathcal{T}_H} + (\boldsymbol{\mu}, (T^u - T_h^u) \boldsymbol{\lambda}_{H,h} + (\hat{T}^u - \hat{T}_h^u) \mathbf{f})_{\partial \mathcal{T}_H} \\ &= -(\boldsymbol{\mu}, \chi)_{\partial \mathcal{T}_H} + (\boldsymbol{\mu}, (T^u - T_h^u) \boldsymbol{\lambda}_{H,h} + (\hat{T}^u - \hat{T}_h^u) \mathbf{f})_{\partial \mathcal{T}_H} \\ &\leq (\|\chi\|_{\mathbf{V}} + \|(T^u - T_h^u) \boldsymbol{\lambda}_{H,h} + (\hat{T}^u - \hat{T}_h^u) \mathbf{f}\|_{\mathbf{V}}) \|\boldsymbol{\mu}\|_{\boldsymbol{\Lambda}} \\ &\preceq (\eta_1 + \|(T^u - T_h^u) \boldsymbol{\lambda}_{H,h} + (\hat{T}^u - \hat{T}_h^u) \mathbf{f}\|_{\mathbf{V}}) \|\boldsymbol{\mu}\|_{\boldsymbol{\Lambda}} \\ &\preceq (\eta_1 + \eta_2) \|\boldsymbol{\mu}\|_{\boldsymbol{\Lambda}}. \end{aligned} \quad (2.87)$$

Hence, for the Stokes equations ( $\boldsymbol{\gamma} = \mathbf{0}$ ) we use (2.85), (2.86) and (2.87) to get the desired

result. For the Brinkman equation, we use again (2.85), (2.86) and (2.87), to obtain that

$$\begin{aligned}\|T^u \boldsymbol{\mu}\|_{\mathbf{V}}^2 &\leq (\eta_1 + \eta_2)(\|T^u \boldsymbol{\mu}\|_{\mathbf{V}} + H^2 \eta_2) \\ &\leq (\eta_1 + \eta_2)^2 + \frac{1}{2} \|T^u \boldsymbol{\mu}\|_{\mathbf{V}}^2 + (\eta_1 + \eta_2) H^2 \eta_2,\end{aligned}$$

thus

$$\|T^u \boldsymbol{\mu}\|_{\mathbf{V}} \leq (\eta_1 + \eta_2) + H\{(\eta_1 + \eta_2)\eta_2\}^{1/2},$$

and the result follows.  $\blacksquare$

## 2.7 Conclusion

Intrinsically attached to the design of the MHM method, the a posteriori error estimator proposed in this work accounts for the multi-level approximations of the method. We restricted the numerical analysis to the first and second level MHM methods for the Stokes and Brinkman equations, for which we proved that the estimator is locally efficient and reliable in the natural norms. The results are, up to our knowledge, the first to address the impact of two-levels of approximation in a multiscale finite element method for the Stokes operator. As a result, the multiscale a posteriori error estimator yielded novel adaptivity strategies which drive first-level meshes as well as (independent) elementwise second level meshes. Fluid flow problems in highly heterogeneous validated the underlying multi-level adaptative algorithms. We showed that the MHM method on such first- and second-level adapted meshes preserves the accuracy of the velocity and pressure fields on coarse global meshes. The missing scales are upscaled through base functions computed in parallel.

## Chapter 3

# A Multiscale Hybrid-Mixed Method for a nonlinear-Stokes problem in glaciology

In this chapter, we derive a new Multiscale Hybrid-Mixed (MHM) finite element method for the non-linear Stokes problem that models a glacier. It is widely accepted that glaciers behave like an incompressible non-Newtonian fluid, modeled by the Stokes equations with nonlinear rheology (see, e.g., [29, 41, 50]). A glacier is a significant, perennial accumulation of crystalline ice, snow, rock, sediment, and often liquid water that originates on land and moves down slope under the influence of its weight and gravity. Due to its size and complexity, it is imperative to have efficient numerical methods that allow us to handle the problem. The finite element method allows us to work with complex geometries and the physical boundary conditions of the model. An additional virtue of the MHM method is the capability of running in parallel on computational clusters providing the computing power for large-scale simulations.

The non-linearity of the problem is solved using Picard's iteration and, for the linear problem resulting from this process, we use the linear MHM technique used in Chapter 2.

This chapter is organized as follows: In Section 3.1 we present some preliminary results also, in Section 3.1.1 we present the Picard method to handle the non-linearity of the problem. In Sections 3.2 and 3.3 we detail the one and two-level MHM method, respectively. Finally, in Section 3.5 we present numerical experiments to verify that the proposed method approximates the solution of a glacier model properly.

### 3.1 Model problem and preliminaries

We consider the following problem: *Find a velocity  $\mathbf{u} : \Omega \rightarrow \mathbb{R}^d$  and a pressure  $p : \Omega \rightarrow \mathbb{R}$  such that*

$$\begin{cases} \nabla \cdot (-\nu(|\mathbf{D}(\mathbf{u})|) \mathbf{D}(\mathbf{u}) + p \mathbf{I}) = \mathbf{f} & \text{in } \Omega, \\ \nabla \cdot \mathbf{u} = 0 & \text{in } \Omega, \\ \mathbf{u} = \mathbf{g} & \text{on } \partial\Omega, \end{cases} \quad (3.1)$$

where the operator  $\mathbf{D}$  represents the gradient

$$\mathbf{D}(\mathbf{v}) = \nabla \mathbf{v}$$

or the strain tensor

$$\mathbf{D}(\mathbf{v}) = \boldsymbol{\varepsilon}(\mathbf{v}).$$

The known data are the given Dirichlet boundary condition  $\mathbf{g} \in L^2(\partial\Omega)^d$ , the body force  $\mathbf{f} = \rho_{\text{ice}} g \hat{\mathbf{k}}$ , where  $\rho_{\text{ice}}$  is the density of the ice,  $g$  is the gravitational constant and  $\hat{\mathbf{k}}$  is a unit vector orthogonal to the surface of the earth. In addition, the viscosity  $\nu : \mathbb{R}^+ \rightarrow \mathbb{R}$  is given by the Glen's law

$$\nu(|\mathbf{D}(\mathbf{u})|) = \frac{\alpha}{2} |\mathbf{D}(\mathbf{u})|^{\beta-2} \quad (3.2)$$

where  $\beta \in (1, 2]$  and the function  $\alpha(\mathbf{x}) \in L^\infty(\Omega)$  are given, with  $0 < \alpha_0 \leq \alpha(\mathbf{x})$  for some  $\alpha_0$ . In (3.1) we are considering only Dirichlet boundary conditions in the boundary for lighten up the notation, but later we will detail the appropriate boundary conditions.

The standard variational mixed formulation of problem (3.1) reads: *Find  $\mathbf{u} \in H^1(\Omega)^d$ , with  $\mathbf{u} = \mathbf{g}$  on  $\partial\Omega$ , and  $p \in L_0^2(\Omega)$  such that*

$$\begin{aligned} a(\mathbf{u}, \mathbf{v}) + b(\mathbf{v}, p) &= (\mathbf{f}, \mathbf{v})_\Omega \quad \text{for all } \mathbf{v} \in H_0^1(\Omega)^d, \\ b(\mathbf{u}, q) &= 0 \quad \text{for all } q \in L_0^2(\Omega), \end{aligned} \quad (3.3)$$

where the  $a(\cdot, \cdot)$  and  $b(\cdot, \cdot)$  are defined by

$$a(\mathbf{w}, \mathbf{v}) := (\mu(|\mathbf{D}(\mathbf{w})|) \mathbf{D}(\mathbf{w}), \mathbf{D}(\mathbf{v}))_\Omega \quad \text{and} \quad b(\mathbf{v}, q) := -(\nabla \cdot \mathbf{v}, q)_\Omega, \quad (3.4)$$

for all  $\mathbf{w}, \mathbf{v} \in H^1(\Omega)^d$  and  $q \in L_0^2(\Omega)$ . The well-posedness of the problem (3.3) is well known (see for instance [40]).

As in the previous chapter, we replace (3.3) by its hybrid formulation counterpart, i.e.,

find  $(\mathbf{u}, p, \boldsymbol{\lambda}, \rho) \in \mathbf{V} \times Q \times \boldsymbol{\Lambda} \times \mathbb{R}$  such that

$$\left\{ \begin{array}{ll} a(\mathbf{u}, \mathbf{v}) + b(\mathbf{v}, p) + (\boldsymbol{\lambda}, \mathbf{v})_{\partial\mathcal{T}_H} = (\mathbf{f}, \mathbf{v})_{\mathcal{T}_H} & \text{for all } \mathbf{v} \in \mathbf{V}, \\ b(\mathbf{u}, q) + (\rho, q)_\Omega = 0 & \text{for all } q \in Q, \\ (\boldsymbol{\mu}, \mathbf{u})_{\partial\mathcal{T}_H} = \langle \boldsymbol{\mu}, \mathbf{g} \rangle_{\partial\Omega} & \text{for all } \boldsymbol{\mu} \in \boldsymbol{\Lambda}, \\ (\xi, p)_\Omega = 0 & \text{for all } \xi \in \mathbb{R}, \end{array} \right. \quad (3.5)$$

where the spaces  $\mathbf{V}$ ,  $Q$  and  $\boldsymbol{\Lambda}$  are those defined in (2.5), (2.7) and (2.6), respectively.

Above and hereafter, we surcharge the notation  $a(\cdot, \cdot)$  and  $b(\cdot, \cdot)$  to extend them to the space  $\mathbf{V}$  as follows

$$a(\mathbf{w}, \mathbf{v}) := \sum_{K \in \mathcal{T}_H} a_K(\mathbf{w}, \mathbf{v}) \quad \text{with} \quad a_K(\mathbf{w}, \mathbf{v}) := (\mu(|\mathbf{D}(\mathbf{w})|) \mathbf{D}(\mathbf{w}), \mathbf{D}(\mathbf{v}))_K, \quad (3.6)$$

and

$$b(\mathbf{v}, q) := \sum_{K \in \mathcal{T}_H} b_K(\mathbf{v}, q) \quad \text{with} \quad b_K(\mathbf{v}, q) := -(\nabla \cdot \mathbf{v}, q)_K, \quad (3.7)$$

for all  $\mathbf{w}, \mathbf{v} \in \mathbf{V}$  and  $q \in Q$ . Note that here the operators  $a(\cdot, \cdot)$  and  $a_K(\cdot, \cdot)$  have a difference with respect to the ones defined on Chapter 2 because the viscosity is dependent on the velocity.

### 3.1.1 Picard iteration for the solution of the nonlinear system

To solve the nonlinear system (3.1), i.e. in the case  $\beta \neq 2$ , we apply the Picard iteration. Starting with a given velocity  $\mathbf{u}^0$ , we determine  $(\mathbf{u}^{j+1}, p^{j+1})$  solving the systems

$$\begin{aligned} \nabla \cdot (-\mu(|\mathbf{D}(\mathbf{u})^j|) \mathbf{D}(\mathbf{u})^{j+1} + \nabla p^{j+1}) &= \mathbf{f} \quad \text{in } \Omega, \\ \nabla \cdot \mathbf{u}^{j+1} &= 0 \quad \text{in } \Omega, \\ \mathbf{u}^{j+1} &= \mathbf{g} \quad \text{on } \partial\Omega \end{aligned} \quad (3.8)$$

for  $j = 0, 1, \dots$ . This procedure continues until a stopping criterion is satisfied. The stopping criteria for the numerical scheme will be specified in the Algorithm 3.

Note that for each  $j$  the system (3.8) becomes linear, and then, we use the method presented in Chapter 2.

For lighten up the presentation, from now on we denote  $\mathbf{u}^* := \mathbf{u}^j$ , which corresponds to a known value in each Picard iteration, and overwrite the unknowns in (3.8) as  $\mathbf{u} := \mathbf{u}^{j+1}$  and  $p := p^{j+1}$ . This allows us to write the problem (3.5) as follows: find  $(\mathbf{u}, p, \boldsymbol{\lambda}, \rho) \in$

$\mathbf{V} \times Q \times \Lambda \times \mathbb{R}$  such that

$$\left\{ \begin{array}{ll} a^*(\mathbf{u}, \mathbf{v}) + b(\mathbf{v}, p) + (\boldsymbol{\lambda}, \mathbf{v})_{\partial\mathcal{T}_H} = (\mathbf{f}, \mathbf{v})_{\mathcal{T}_H} & \text{for all } \mathbf{v} \in \mathbf{V}, \\ b(\mathbf{u}, q) + (\rho, q)_\Omega = 0 & \text{for all } q \in Q, \\ (\boldsymbol{\mu}, \mathbf{u})_{\partial\mathcal{T}_H} = \langle \boldsymbol{\mu}, \mathbf{g} \rangle_{\partial\Omega} & \text{for all } \boldsymbol{\mu} \in \Lambda, \\ (\xi, p)_\Omega = 0 & \text{for all } \xi \in \mathbb{R}, \end{array} \right. \quad (3.9)$$

where

$$a^*(\mathbf{u}, \mathbf{v}) := \sum_{K \in \mathcal{T}_H} a_K^*(\mathbf{u}, \mathbf{v}) \quad \text{with} \quad a_K^*(\mathbf{u}, \mathbf{v}) := (\mu(|\mathbf{D}(\mathbf{u}^*)|) \mathbf{D}(\mathbf{u}), \mathbf{D}(\mathbf{v}))_K. \quad (3.10)$$

Note that in (3.9) the viscosity depends only on the solution in the previous step, and thus (3.9) is a linear problem. Now, inspired in the previous chapter, we propose a numerical method to approximate the non-linear problem.

Let  $\mathbf{V}_0$  be the closed subspace of the Hilbert space  $\mathbf{V}$  defined by

$$\mathbf{V}_0 := \{\mathbf{v} \in \mathbf{V} : a^*(\mathbf{v}, \mathbf{w}) = 0 \quad \text{for all } \mathbf{w} \in \mathbf{V}\}.$$

Note that for  $\mathbf{D}(\cdot) = \nabla(\cdot)$  we get

$$\mathbf{V}_0 = \left\{ \mathbf{v} \in \mathbf{V} : \mathbf{v}|_K \in \mathbb{P}_0(K)^d \quad \text{for all } K \in \mathcal{T}_H \right\},$$

and for  $\mathbf{D}(\cdot) = \varepsilon(\cdot)$  we get

$$\mathbf{V}_0 = \{\mathbf{v} \in \mathbf{V} : \varepsilon(\mathbf{v}) = \mathbf{0} \quad \text{for all } K \in \mathcal{T}_H\},$$

which corresponds to the space of piecewise rigid body modes. It is easy to prove that  $\mathbf{V}_0$  may be characterized as follow: when  $d = 2$

$$\mathbf{v}(\mathbf{x}) = \begin{pmatrix} a_1 \\ a_2 \end{pmatrix} + b \begin{pmatrix} x_2 \\ -x_1 \end{pmatrix}$$

for  $\mathbf{x} = (x_1, x_2) \in K$  with  $a_1, a_2, b \in \mathbb{P}_0(K)$ , and when  $d = 3$

$$\mathbf{v}(\mathbf{x}) = \mathbf{a} + \mathbf{b} \times \mathbf{x}$$

for  $\mathbf{x} \in K$  with  $\mathbf{a}, \mathbf{b} \in \mathbb{P}_0(K)^3$ .

We point out that the only difference between both options for  $\mathbf{D}$  is the space  $\mathbf{V}_0$ ,

affecting only the computational implementation, but not the analysis. This way,

$$\mathbf{V} = \mathbf{V}_0 \oplus \mathbf{V}_0^\perp, \quad (3.11)$$

where  $\mathbf{V}_0^\perp$  stands for the orthogonal complement with respect to the inner-product  $(\cdot, \cdot)_\mathbf{V}$ .

We define the following local operators:

- $\mathbf{T} : \Lambda \rightarrow \mathbf{V} \times Q$  with  $\mathbf{T}\boldsymbol{\mu} := (T^u \boldsymbol{\mu}, T^p \boldsymbol{\mu})$  such that  $T^u \boldsymbol{\mu}|_K$  and  $T^p \boldsymbol{\mu}|_K$  is the unique solution of the local problem

$$\begin{cases} a_K^*(T^u \boldsymbol{\mu}, \mathbf{w}) + b_K(\mathbf{w}, T^p \boldsymbol{\mu}) = -\langle \boldsymbol{\mu}, \mathbf{w} \rangle_{\partial K} & \text{for all } \mathbf{w} \in \mathbf{V}_0^\perp(K), \\ b_K(T^u \boldsymbol{\mu}, q) = 0 & \text{for all } q \in Q(K); \end{cases} \quad (3.12)$$

- $\hat{\mathbf{T}} : L^2(\Omega)^d \rightarrow \mathbf{V}_0^\perp \times Q$  with  $\hat{\mathbf{T}}\mathbf{r} := (\hat{T}^u \mathbf{r}, \hat{T}^p \mathbf{r})$  such that  $\hat{T}^u \mathbf{r}|_K$  and  $\hat{T}^p \mathbf{r}|_K$  is the unique solution of the local problem

$$\begin{cases} a_K^*(\hat{T}^u \mathbf{r}, \mathbf{w}) + b_K(\mathbf{w}, \hat{T}^p \mathbf{r}) = (\mathbf{r}, \mathbf{w})_K & \text{for all } \mathbf{w} \in \mathbf{V}_0^\perp(K), \\ b_K(\hat{T}^u \mathbf{r}, q)_K = 0 & \text{for all } q \in Q(K); \end{cases} \quad (3.13)$$

- $\bar{\mathbf{T}} : \mathbb{R} \rightarrow \mathbf{V}_0^\perp \times Q$  with  $\bar{\mathbf{T}}\xi := (\bar{T}^u \xi, \bar{T}^p \xi)$  such that  $\bar{T}^u \xi|_K$  and  $\bar{T}^p \xi|_K$  is the unique solution of the local problem

$$\begin{cases} a_K^*(\bar{T}^u \xi, \mathbf{w}) + b_K(\mathbf{w}, \bar{T}^p \xi) = 0 & \text{for all } \mathbf{w} \in \mathbf{V}_0^\perp(K), \\ b_K(\bar{T}^u \xi, q) = -(\xi, q)_K & \text{for all } q \in Q(K). \end{cases} \quad (3.14)$$

Owing to decomposition (3.11), and noting that  $a^*(\mathbf{w}, \mathbf{v}) = 0$  when  $\mathbf{w} \in \mathbf{V}_0$  or  $\mathbf{v} \in \mathbf{V}_0$ , we may rewrite (3.9) as the following global-local problem: *Find  $(\mathbf{u}_0, \boldsymbol{\lambda}, \rho) \in \mathbf{V}_0 \times \Lambda \times \mathbb{R}$  such that*

$$\begin{cases} (\boldsymbol{\lambda}, \mathbf{v}_0)_{\partial \mathcal{T}_H} = (\mathbf{f}, \mathbf{v}_0)_{\mathcal{T}_H}, \\ (\boldsymbol{\mu}, \mathbf{u}_0)_{\partial \mathcal{T}_H} + (\boldsymbol{\mu}, T^u \boldsymbol{\lambda})_{\partial \mathcal{T}_H} + (\boldsymbol{\mu}, \bar{T}^u \rho)_{\partial \mathcal{T}_H} = \langle \boldsymbol{\mu}, \mathbf{g} \rangle_{\partial \Omega} - (\boldsymbol{\mu}, \hat{T}^u \mathbf{f})_{\partial \mathcal{T}_H}, \\ (\xi, T^p \boldsymbol{\lambda})_\Omega + (\xi, \bar{T}^p \rho)_\Omega = -(\xi, \hat{T}^p \mathbf{f})_\Omega, \end{cases} \quad (3.15)$$

for all  $(\mathbf{v}_0, \boldsymbol{\mu}, \xi) \in \mathbf{V}_0 \times \Lambda \times \mathbb{R}$ .

Note that Problem (3.15) is the same as (2.31), and the non-linearity is manifested only on the local problems (3.12), (3.13) and (3.14).

The coupled global-local problem (3.12), (3.13), (3.14) and (3.15) is equivalent, in the

sense that its solutions coincide, with the hybrid formulation (3.9). Owing to the linearity of problem (3.15), the solution decomposes as follow

$$\mathbf{u} = \mathbf{u}_0 + T^{\mathbf{u}} \boldsymbol{\lambda} + \hat{T}^{\mathbf{u}} \mathbf{f} + \bar{T}^{\mathbf{u}} \rho \quad \text{and} \quad p = T^p \boldsymbol{\lambda} + \hat{T}^p \mathbf{f} + \bar{T}^p \rho. \quad (3.16)$$

**Remark 3.1** Following [12] we can prove that  $\rho = 0$ . Hence, the solution of (3.15), given by (3.16), reduces to

$$\mathbf{u} := \mathbf{u}_0 + T^{\mathbf{u}} \boldsymbol{\lambda} + \hat{T}^{\mathbf{u}} \mathbf{f} \quad \text{and} \quad p := T^p \boldsymbol{\lambda} + \hat{T}^p \mathbf{f}. \quad (3.17)$$

## 3.2 The one-level MHM method

The one-level MHM method stems from the coupled problems (3.15), (3.12), (3.13) and (3.14). We search the approximate Lagrange multipliers in the space

$$\boldsymbol{\Lambda}_H := \{\boldsymbol{\lambda}_H \in \boldsymbol{\Lambda} : \boldsymbol{\lambda}_H|_{\tilde{F}} \in \mathbb{P}_l(\tilde{F})^d, \text{ for all } \tilde{F} \subset \mathcal{T}_{\tilde{H}}(F), \text{ for all } F \in \mathcal{E}_H\}, \quad (3.18)$$

the same space (2.33) used for the linear Stokes problem. Replacing  $\boldsymbol{\Lambda}$  by  $\boldsymbol{\Lambda}_H$  allows for finding solutions to (3.12) in terms of basis functions and (3.13) and gives rise to a one-level MHM method in the form of (3.15). In this section we assume that the corresponding local problems are computed exactly, i.e, a closed formula for the multiscale basis functions is available.

Specifically, the solution of (3.15) is approximate by  $(\mathbf{u}_0^H, \boldsymbol{\lambda}_H, \rho_H) \in \mathbf{V}_0 \times \boldsymbol{\Lambda}_H \times \mathbb{R}$  which is the solution to the one-level MHM method

$$\left\{ \begin{array}{l} (\boldsymbol{\lambda}_H, \mathbf{v}_0)_{\partial\mathcal{T}_H} = (\mathbf{f}, \mathbf{v}_0)_{\mathcal{T}_H}, \\ (\boldsymbol{\mu}_H, \mathbf{u}_0^H)_{\partial\mathcal{T}_H} + (\boldsymbol{\mu}_H, T^{\mathbf{u}} \boldsymbol{\lambda}_H)_{\partial\mathcal{T}_H} + (\boldsymbol{\mu}_H, \bar{T}^{\mathbf{u}} \rho_H)_{\partial\mathcal{T}_H} = \langle \boldsymbol{\mu}_H, \mathbf{g} \rangle_{\partial\Omega} - (\boldsymbol{\mu}_H, \hat{T}^{\mathbf{u}} \mathbf{f})_{\partial\mathcal{T}_H}, \\ (\xi_H, T^p \boldsymbol{\lambda}_H)_{\Omega} + (\xi_H, \bar{T}^p \rho_H)_{\Omega} = -(\xi_H, \hat{T}^p \mathbf{f})_{\Omega}, \end{array} \right. \quad (3.19)$$

for all  $\mathbf{v}_0 \in \mathbf{V}_0$ ,  $\boldsymbol{\mu} \in \boldsymbol{\Lambda}_H$  and  $\xi_H \in \mathbb{R}$ . Here  $\mathbf{T}$ ,  $\hat{\mathbf{T}}$  and  $\bar{\mathbf{T}}$  are given in (3.12), (3.13) and (3.14), respectively.

Thus, due to linearity of discrete problem (3.19), its solution  $(\mathbf{u}_H, p_H, \rho_H)$  is given through the expressions

$$\mathbf{u}_H := \mathbf{u}_0^H + T^{\mathbf{u}} \boldsymbol{\lambda}_H + \hat{T}^{\mathbf{u}} \mathbf{f} + \bar{T}^{\mathbf{u}} \rho_H \quad \text{and} \quad p_H := T^p \boldsymbol{\lambda}_H + \hat{T}^p \mathbf{f} + \bar{T}^p \rho_H, \quad (3.20)$$

and then, the MHM method is non-conform in  $H^1(\Omega)^d$ . Note that the one-level MHM

method assumes that exact solution of local problems are known, which generally will not be possible. For this reason, we must consider an approximation of the solution of the local problems, which are explained in the next section.

### 3.3 The two-level MHM method

Until here, to lighten up notation and to present the method in a similar way as in Chapter 2, we have only considered the problem with Dirichlet boundary conditions. Since we are interested in to apply the method to a problem with mixed boundary conditions, following we detail both cases: when the boundary conditions are only Dirichlet, and when the boundary conditions are mixed.

To the two-level MHM method, we select the following local finite spaces

$$\mathbf{V}_h(K) := \left\{ \mathbf{v}_h \in \mathbf{V}_0^\perp(K) \cap C^0(K)^d : \mathbf{v}_h|_\tau \in \mathbb{P}_k(\tau)^d \text{ for all } \tau \in \mathcal{T}_h^K \right\} \quad (3.21)$$

and

$$Q_h(K) := \left\{ q_h \in Q(K) \cap C^0(K) : q_h|_\tau \in \mathbb{P}_n(\tau) \text{ for all } \tau \in \mathcal{T}_h^K \right\}, \quad (3.22)$$

and the global finite dimensional space

$$\mathbf{V}_h := \bigoplus_{K \in \mathcal{T}_H} \mathbf{V}_h(K) \quad \text{and} \quad Q_h := \bigoplus_{K \in \mathcal{T}_H} Q_h(K). \quad (3.23)$$

As in Chapter 2, for  $\mathbf{T}_h$ ,  $\bar{\mathbf{T}}_h$  and  $\hat{\mathbf{T}}_h$  we adopt the unusual stabilized finite element method USFEM proposed in [25], but now in its nonlinear version, and adopting the same degree of interpolation in all elements of the partition, that is,  $k = n$  in (3.21) and (3.22).

We recall from [25] that the unusual finite element method reads: *Find  $(\mathbf{u}, p) \in \mathbf{V}_h(K) \times Q_h(K)$  such that*

$$B_K^*(\mathbf{u}, p; \mathbf{v}, q) = F_K^*(\mathbf{v}, q) \quad \text{for all } (\mathbf{v}, q) \in \mathbf{V}_h(K) \times Q_h(K),$$

where

$$\begin{aligned} B_K^*(\mathbf{u}, p; \mathbf{v}, q) := & a_K^*(\mathbf{u}, \mathbf{v}) + b_K(\mathbf{v}, p) - b_K(\mathbf{u}, q) \\ & - \sum_{\tau \in \mathcal{T}_h^K} (-\nabla \cdot (\mu(|\mathbf{D}(\mathbf{u}^*)|) \mathbf{D}(\mathbf{u}) - p \mathbf{I}) \kappa_\tau, -\nabla \cdot (\mu(|\mathbf{D}(\mathbf{u}^*)|) \mathbf{D}(\mathbf{v}) + q \mathbf{I}))_\tau \end{aligned} \quad (3.24)$$

and

$$F_K^*(\mathbf{v}, q) := (\mathbf{f}, \mathbf{v})_K - \sum_{\tau \in \mathcal{T}_h^K} (\mathbf{f}, -\nabla \cdot (\mu(|\mathbf{D}(\mathbf{u}^*)|) \mathbf{D}(\mathbf{v}) + q \mathbf{I}))_\tau. \quad (3.25)$$

The stabilization parameter is given by

$$\kappa_\tau := \frac{m_k h_\tau^2}{4 \mu(|\mathbf{D}(\mathbf{u}^*)|)}, \quad (3.26)$$

where  $m_k := \min \left\{ \frac{1}{3}, C_k \right\}$  and  $C_k$  is a constant satisfying (2.42). This way, the stabilization parameter  $\kappa_\tau$  can be easily calculated. Owing to the definition above, we define the corresponding discrete operators as follows:

- $\mathbf{T}_h : \Lambda_H \rightarrow \mathbf{V}_h \times Q_h$  such that  $\mathbf{T}_h \boldsymbol{\lambda}_{H,h}|_K := (T_h^u \boldsymbol{\lambda}_{H,h}, T_h^p \boldsymbol{\lambda}_{H,h})$  solves

$$B_K^*(T_h^u \boldsymbol{\lambda}_{H,h}, T_h^p \boldsymbol{\lambda}_{H,h}; \mathbf{v}_h, q_h) = -\langle \boldsymbol{\lambda}_{H,h}, \mathbf{v}_h \rangle_{\partial K} \quad \text{for all } (\mathbf{v}_h, q_h) \in \mathbf{V}_h(K) \times Q_h(K), \quad (3.27)$$

- $\hat{\mathbf{T}}_h : L^2(\Omega)^d \rightarrow \mathbf{V}_h \times Q_h(K)$  such that  $\hat{\mathbf{T}}_h \mathbf{f}|_K := (\hat{T}_h^u \mathbf{f}, \hat{T}_h^p \mathbf{f})$  solves

$$B_K^*(\hat{T}_h^u \mathbf{f}, \hat{T}_h^p \mathbf{f}; \mathbf{v}_h, q_h) = F_K^*(\mathbf{v}_h, q_h) \quad \text{for all } (\mathbf{v}_h, q_h) \in \mathbf{V}_h(K) \times Q_h(K), \quad (3.28)$$

- $\bar{\mathbf{T}}_h : \mathbb{R} \rightarrow \mathbf{V}_h \times Q_h$  such that  $\bar{\mathbf{T}}_h \rho_H|_K := (\bar{T}_h^u \rho_H, \bar{T}_h^p \rho_H)$  solves

$$B_K^*(\bar{T}_h^u \rho_H, \bar{T}_h^p \rho_H; \mathbf{v}_h, q_h) = -(\rho_H, q_h)_K \quad \text{for all } (\mathbf{v}_h, q_h) \in \mathbf{V}_h(K) \times Q_h(K).$$

### 3.3.1 The two-level MHM method for a problem with only Dirichlet boundary conditions

The two-level MHM method reads: *Find  $(\mathbf{u}_0^{H,h}, \boldsymbol{\lambda}_{H,h}, \rho_H) \in \mathbf{V}_0 \times \Lambda_H \times \mathbb{R}$  such that*

$$\begin{cases} (\boldsymbol{\lambda}_{H,h}, \mathbf{v}_0)_{\partial \mathcal{T}_H} = (\mathbf{f}, \mathbf{v}_0)_{\mathcal{T}_H}, \\ (\boldsymbol{\mu}_H, \mathbf{u}_0^{H,h})_{\partial \mathcal{T}_H} + (\boldsymbol{\mu}_H, T_h^u \boldsymbol{\lambda}_{H,h})_{\partial \mathcal{T}_H} + (\boldsymbol{\mu}_H, \bar{T}_h^u \rho_H)_{\partial \mathcal{T}_H} = \langle \boldsymbol{\mu}_H, \mathbf{g} \rangle_{\partial \Omega} - (\boldsymbol{\mu}_H, \hat{T}_h^u \mathbf{f})_{\partial \mathcal{T}_H}, \\ (\xi_H, T_h^p \boldsymbol{\lambda}_{H,h})_\Omega + (\xi_H, \bar{T}_h^p \rho_H)_\Omega = -(\xi_H, \hat{T}_h^p \mathbf{f})_\Omega, \end{cases} \quad (3.29)$$

for all  $(\mathbf{v}_0, \boldsymbol{\mu}_H, \xi_H) \in \mathbf{V}_0 \times \Lambda_H \times \mathbb{R}$ , where the operators  $T_h^u$ ,  $\hat{T}_h^u$  and  $\bar{T}_h^u$  are those defined in (3.27), (3.28) and (3.3), respectively. Note that the skeleton problem for the linear problem (Problem (2.39)) and the skeleton problem for the non-linear problem (Problem (3.29)) are

the same.

As a result, the discrete two-level solution  $(\mathbf{u}_{H,h}, p_{H,h}, \rho_H)$  is given through the expressions

$$\mathbf{u}_{H,h} := \mathbf{u}_0^{H,h} + T_h^{\mathbf{u}} \boldsymbol{\lambda}_{H,h} + \hat{T}_h^{\mathbf{u}} \mathbf{f} + \bar{T}_h^{\mathbf{u}} \rho_H \quad \text{and} \quad p_{H,h} := T_h^p \boldsymbol{\lambda}_{H,h} + \hat{T}_h^p \mathbf{f} + \bar{T}_h^p \rho_H. \quad (3.30)$$

**Remark 3.2** As in the continuous case (Remark 3.1), following [12], we have that  $\rho_H = 0$ . Hence, the solution of (3.29), given by (3.30), can be characterized as

$$\mathbf{u}_{H,h} := \mathbf{u}_0^{H,h} + \hat{T}_h^{\mathbf{u}} \boldsymbol{\lambda}_{H,h} + \hat{T}_h^{\mathbf{u}} \mathbf{f} \quad \text{and} \quad p_{H,h} := \hat{T}_h^p \boldsymbol{\lambda}_{H,h} + \hat{T}_h^p \mathbf{f}. \quad (3.31)$$

### 3.3.2 The two-level MHM method for a problema with mixed boundary conditions

Now we consider the problem (3.1) with Dirichlet and Neumann boundary conditions, i.e., we consider the problem:

$$\begin{aligned} \nabla \cdot (-\mu(|\mathbf{D}(\mathbf{u})|) \mathbf{D}(\mathbf{u}) + \nabla p) &= \mathbf{f} \quad \text{in } \Omega, \\ \nabla \cdot \mathbf{u} &= 0 \quad \text{in } \Omega, \\ \mathbf{u} &= \mathbf{g}_D \quad \text{on } \partial\Omega_D, \\ -\mu(|\mathbf{D}(\mathbf{u})|) \nabla \mathbf{u} + p \mathbf{I} &= \mathbf{g}_N \quad \text{on } \partial\Omega_N, \end{aligned} \quad (3.32)$$

with  $\partial\Omega_N \neq \emptyset$ , and  $\mathbf{g}_D \in L^2(\Omega_D)^d$  and  $\mathbf{g}_N \in L^2(\Omega_N)^d$ . Since the Neumann boundary conditions will be essentials, they are imposed explicitly on the solution, and then, the approximate Lagrange multipliers will belong to space

$$\boldsymbol{\Lambda}_H := \{\boldsymbol{\lambda}_H \in \boldsymbol{\Lambda} : \boldsymbol{\lambda}_H|_{\tilde{F}} \in \mathbb{P}_l(\tilde{F})^d, \text{ for all } \tilde{F} \subset \mathcal{T}_{\tilde{H}}(F), \text{ for all } F \in \mathcal{E}_H, \text{ and } \boldsymbol{\lambda}_H|_{\partial\Omega_N} = \mathbf{g}_N\}. \quad (3.33)$$

It is easy to see that when we consider Neumann boundary conditions the pressure belongs to  $L^2(\Omega)$  instead of  $L_0^2(\Omega)$ , and then the unknown  $\rho$ , corresponding to the Lagrange multiplier for the pressure, and its corresponding test function in (3.29) do not appear. Then, proceeding as before, the two-level MHM method for the problem with mixed boundary conditions reads: *Find  $(\mathbf{u}_0^{H,h}, \boldsymbol{\lambda}_{H,h}) \in \mathbf{V}_0 \times \boldsymbol{\Lambda}_H$  such that*

$$\left\{ \begin{array}{l} (\boldsymbol{\lambda}_{H,h}, \mathbf{v}_0)_{\partial\mathcal{T}_H} = (\mathbf{f}, \mathbf{v}_0)_{\mathcal{T}_H}, \\ (\boldsymbol{\mu}_H, \mathbf{u}_0^{H,h})_{\partial\mathcal{T}_H} + (\boldsymbol{\mu}_H, T_h^{\mathbf{u}} \boldsymbol{\lambda}_{H,h})_{\partial\mathcal{T}_H} = \int_{\partial\Omega_D} \boldsymbol{\mu}_H \cdot \mathbf{g}_D - (\boldsymbol{\mu}_H, \hat{T}_h^{\mathbf{u}} \mathbf{f})_{\partial\mathcal{T}_H}, \end{array} \right. \quad (3.34)$$

for all  $(\boldsymbol{v}_0, \boldsymbol{\mu}_H) \in \mathbf{V}_0 \times \boldsymbol{\Lambda}_H$ , and where the operators  $T_h^{\boldsymbol{u}}$  and  $\hat{T}_h^{\boldsymbol{u}}$  are those defined in (3.27) and (3.28), respectively. As a result, the discrete two-level solution  $(\boldsymbol{u}_{H,h}, p_{H,h})$  is given through the expressions

$$\boldsymbol{u}_{H,h} := \boldsymbol{u}_0^{H,h} + T_h^{\boldsymbol{u}} \boldsymbol{\lambda}_{H,h} + \hat{T}_h^{\boldsymbol{u}} \boldsymbol{f} \quad \text{and} \quad p_{H,h} := T_h^p \boldsymbol{\lambda}_{H,h} + \hat{T}_h^p \boldsymbol{f}. \quad (3.35)$$

### 3.4 Numerical algorithm for the MHM method for a problem with mixed boundary conditions

In this section we provide the underlying algorithm for the MHM method for the problem with mixed boundary condition, described in Section 3.3.2. The case of the problem with Dirichlet boundary condition only is analogous.

Let  $\{\boldsymbol{\psi}_1, \boldsymbol{\psi}_2, \dots, \boldsymbol{\psi}_{m_\lambda}\}$  and  $\{\boldsymbol{\phi}_1, \boldsymbol{\phi}_2, \dots, \boldsymbol{\phi}_{m_0}\}$  be a basis for  $\boldsymbol{\Lambda}_H$  and  $\mathbf{V}_0$ , respectively, where  $m_\lambda := \dim(\boldsymbol{\Lambda}_H)$  and  $m_0 := \dim(\mathbf{V}_0)$ . Then, there exist real numbers  $\lambda_1, \lambda_2, \dots, \lambda_{m_\lambda}$  and  $u_0^1, u_0^2, \dots, u_0^{m_0}$  such that

$$\boldsymbol{\lambda}_{H,h} = \sum_{j=1}^{m_\lambda} \lambda_j \boldsymbol{\psi}_j \quad \text{and} \quad \boldsymbol{u}_0^{H,h} = \sum_{j=1}^{m_0} u_0^j \boldsymbol{\phi}_j.$$

For  $j = 1, 2, \dots, m_\lambda$ , let  $(\boldsymbol{\eta}_{j,h}^{\boldsymbol{u}}, \eta_{j,h}^p) \in \mathbf{V}_h(K) \times Q_h(K)$  be the solution of the USFEM formulations (3.27), and (3.28), respectively, i.e.,  $(\boldsymbol{\eta}_{j,h}^{\boldsymbol{u}}, \eta_{j,h}^p)$  is the solution of

$$B_K^*(\boldsymbol{\eta}_{j,h}^{\boldsymbol{u}}, \eta_{j,h}^p; \boldsymbol{v}_h, q_h) = -\langle \boldsymbol{\psi}_j, \boldsymbol{v}_h \rangle_{\partial K} \quad \text{for all } (\boldsymbol{v}_h, q_h) \in \mathbf{V}_h(K) \times Q_h(K).$$

Note that, thanks to the linearity of  $B_K^*$  (c.f. (3.24)),

$$\hat{T}_h^{\boldsymbol{u}} \boldsymbol{\lambda}_{H,h} = \sum_{j=1}^{m_\lambda} \lambda_j \boldsymbol{\eta}_{j,h}^{\boldsymbol{u}} \quad \text{and} \quad \hat{T}_h^p \boldsymbol{\lambda}_{H,h} = \sum_{j=1}^{m_\lambda} \lambda_j \eta_{j,h}^p.$$

We can rewrite (3.34) as the linear system,

$$\begin{bmatrix} \mathcal{A} & \mathcal{C}^T \\ \mathcal{C} & \mathbf{0} \end{bmatrix} \begin{bmatrix} \vec{\boldsymbol{\lambda}} \\ \vec{\boldsymbol{u}}_0 \end{bmatrix} = \begin{bmatrix} \mathbf{F} \\ \mathbf{G} \end{bmatrix}, \quad (3.36)$$

with  $\vec{\boldsymbol{\lambda}}^T = (\lambda_1, \dots, \lambda_{m_\lambda}) \in \mathbb{R}^{m_\lambda}$  and  $\vec{\boldsymbol{u}}_0^T = (u_0^1, \dots, u_0^{m_0}) \in \mathbb{R}^{m_0}$ . Note that the matrix in

(3.36) has a size  $(m_\lambda + m_0) \times (m_\lambda + m_0)$ , and its components are given by

$$\begin{aligned}\mathcal{A} &= (a_{ij}) \in \mathbb{R}^{m_\lambda \times m_\lambda} && \text{with } a_{ij} := (\psi_i, \boldsymbol{\eta}_{j,h}^u)_{\partial\mathcal{T}_H}, \quad 1 \leq i, j \leq m_\lambda, \\ \mathcal{C} &= (c_{ij}) \in \mathbb{R}^{m_0 \times m_\lambda} && \text{with } c_{ij} := (\psi_j, \phi_i)_{\partial\mathcal{T}_H}, \quad 1 \leq i \leq m_0 \quad \text{and} \quad 1 \leq j \leq m_\lambda.\end{aligned}$$

The entries of the global right-hand side are

$$\begin{aligned}\mathbf{F} &= (f_i) \in \mathbb{R}^{m_\lambda} && \text{with } f_i := \int_{\partial\Omega_D} \psi_i \cdot \mathbf{g} - (\psi_i, \hat{T}_h^u \mathbf{f})_{\partial\mathcal{T}_H}, \quad 1 \leq i \leq m_\lambda, \\ \mathbf{G} &= (g_i) \in \mathbb{R}^{m_0} && \text{with } g_i := (\mathbf{f}, \phi_i)_{\mathcal{T}_H}, \quad 1 \leq i \leq m_0.\end{aligned}$$

We recall that for the problem (3.34) with mixed boundary condition, described in Section 3.3.2, since the Neumann boundary condition is essential, i.e., the value of  $\boldsymbol{\lambda}_{H,h}$  on  $\partial\Omega_N$  is known, we must impose them in the system (3.36), for example, in a strongly way.

Let  $\{\boldsymbol{\xi}_1^K, \boldsymbol{\xi}_2^K, \dots, \boldsymbol{\xi}_{m_{h,K}}^K\}$  and  $\{q_1^K, q_2^K, \dots, q_{l_{h,K}}^K\}$  basis of the local spaces  $\mathbf{V}_h(K)$  and  $Q_h(K)$ , respectively, where  $m_{h,K} := \dim(\mathbf{V}_h(K))$  and  $l_{h,K} := \dim(Q_h(K))$ . For each  $j = 1, \dots, m_\lambda$  we define the following vector:

$$\mathbf{S}_{j,K} = (s_i) \in \mathbb{R}^{m_{h,K}} \quad \text{with } s_i := -\langle \psi_j, \boldsymbol{\xi}_i^K \rangle_{\partial K}, \quad 1 \leq i \leq m_\lambda.$$

Also, let  $\mathbf{F}_{h,K} \in \mathbb{R}^{m_{h,K}+l_{h,K}}$  be the local right-hand side vector given by the stabilized linear form  $F_K^*(\cdot)$  defined in (3.25) and  $\mathbf{B}_{h,K} \in \mathbb{R}^{(m_{h,K}+l_{h,K}) \times (m_{h,K}+l_{h,K})}$  the local stiffness matrix given by the stabilized bilinear form  $B_K^*(\cdot; \cdot)$  defined in (3.24). They are both computed using the subspace  $\mathbf{V}_h(K) \times Q_h(K)$ . We denote by  $\mathbf{I}^u \in \mathbb{R}^{m_{h,K} \times m_{h,K}}$  and  $\mathbf{I}^p \in \mathbb{R}^{l_{h,K} \times l_{h,K}}$  the identity matrices,  $\mathbf{0}^u \in \mathbb{R}^{l_{h,K} \times m_{h,K}}$  and  $\mathbf{0}^p \in \mathbb{R}^{m_{h,K} \times l_{h,K}}$  the rectangular matrices composed of zeros, and

$$\mathbf{P}_K^u := \begin{bmatrix} \mathbf{I}^u \\ \mathbf{0}^u \end{bmatrix} \in \mathbb{R}^{(m_{h,K}+l_{h,K}) \times m_{h,K}} \quad \text{and} \quad \mathbf{P}_K^p := \begin{bmatrix} \mathbf{0}^p \\ \mathbf{I}^p \end{bmatrix} \in \mathbb{R}^{(m_{h,K}+l_{h,K}) \times l_{h,K}}.$$

---

**Algorithm 3** MHM algorithm for the problem with mixed boundary conditions

**Require:** A positive real number tol (the tolerance) and an initial solution  $(\mathbf{u}_{H,h}^*, p_{H,h}^*)$ .

- 1: **for** For each  $K \in \mathcal{T}_H$  **do**
- 2:     For each  $\psi_j$  defined on  $\partial K$  solve

$$\mathbf{B}_{h,K} X_{j,K} = \mathbf{P}_K^u S_{j,K}$$

- 3:     Solve

$$\mathbf{B}_{h,K} Y_K = \mathbf{F}_{h,K}$$

- 4:     For each  $\psi_i$  defined on  $\partial K$ , and  $\phi_i$  defined on  $K$ , compute

$$\mathbf{F}^K = (f_i^K), \quad f_i^K := \int_{\partial K \cap \partial \Omega_D} \psi_i \cdot \mathbf{g} - \int_{\partial K} \psi_i \cdot \mathbf{B}_{h,K}^{-1} \mathbf{F}_{h,K} Y_K$$

- 5:     For each  $\phi_i$ , defined on  $K$ , compute

$$\mathbf{G}^K = (g_i^K), \quad g_i^K := -(\mathbf{f}, \phi_i)_K$$

- 6:     Assemble  $\mathbf{F}^K$  and  $\mathbf{G}^K$  into  $\mathbf{F}$  and  $\mathbf{G}$ .

- 7: **end for**

- 8: Solve the global problem

$$\begin{bmatrix} A & \mathcal{C}^T \\ \mathcal{C} & \mathbf{0} \end{bmatrix} \begin{bmatrix} \vec{\lambda} \\ \vec{u}_0 \end{bmatrix} = \begin{bmatrix} \mathbf{F} \\ \mathbf{G} \end{bmatrix}$$

$$\mathbf{u}_{H,h} = \sum_{i=1}^{m_0} u_0^i \phi_i + \sum_{i=1}^{m_\lambda} \lambda_i \left\{ \sum_{K \in \mathcal{T}_H} \sum_{j=1}^{m_{h,K}} X_{i,K}^j \xi_j^K \right\} + \sum_{K \in \mathcal{T}_H} \sum_{j=1}^{m_{h,K}} Y_{i,K}^j \xi_j^K$$

$$p_{H,h} = \sum_{i=1}^{m_\lambda} \lambda_i \left\{ \sum_{K \in \mathcal{T}_H} \sum_{j=m_{h,K}+1}^{m_{h,K}+l_{h,K}} X_{i,K}^j q_j^K \right\} + \sum_{K \in \mathcal{T}_H} \sum_{j=m_{h,K}+1}^{m_{h,K}+l_{h,K}} Y_{i,K}^j q_j^K$$

$$\boldsymbol{\sigma}_{H,h} = -\nu \nabla \mathbf{u}_{H,h} + p_{H,h} \mathbf{I}$$

- 9: Consider the following stopping criteria:

$$\frac{\|(\mathbf{u}_{H,h}, p_{H,h}) - (\mathbf{u}_{H,h}^*, p_{H,h}^*)\|_{\mathbf{V} \times Q}}{\|(\mathbf{u}_{H,h}, p_{H,h})\|_{\mathbf{V} \times Q}} < \text{tol}. \quad (3.37)$$

If (3.37) holds, then return  $\mathbf{u}_{H,h}$  and  $p_{H,h}$  and stop the algorithm. Else, define  $\mathbf{u}_{H,h}^* = \mathbf{u}_{H,h}$  and  $p_{H,h}^* = p_{H,h}$  and repeat the algorithm from the Line 1.

---

### 3.5 Numerical experiments

In this section we simulate standardized 2D tests for glacier models from [79] and [64]. We assume that the glacier is only bounded by two faces: the interface between the atmosphere and the ice sheet (top), and the interface between the bedrock and the ice sheet (bottom). Then, for the top boundary, we assume Neumann boundary condition and for the bottom Dirichlet boundary condition, both equal to zero. For the other two boundaries, we assume periodic conditions, a typical consideration in this context, meaning that whatever exists in the right side of the ice sheet enters in its left side (see, e.g., [64]). One way to apply the periodic boundary conditions, which we use here, is to solve the problem over an elongated domain on left and right, with the same boundary conditions than the original problem, except for the lateral boundaries, where it is imposed zero Dirichlet boundary conditions for the velocity (see, e.g., [64]). Then, we solve the problem in a domain three times larger than the original, reporting the results only on the original domain. In the following examples we report the results for the case  $\mathbf{D}(\cdot) = \varepsilon(\cdot)$ . The physical parameters considered are in Table 3.1.

Table 3.1: Physical parameters for the glaciari model.

| Symbol              | Constant                    | Value          | Units                          |
|---------------------|-----------------------------|----------------|--------------------------------|
| $A$                 | Ice-flow parameter          | 100            | $\text{MPa}^{-n}\text{a}^{-1}$ |
| $\rho_{\text{ice}}$ | Ice density                 | 9.03721418E-19 | $\text{Kg Km}^{-3}$            |
| $g$                 | Gravitational constant      | 9.81           | $\text{m s}^{-2}$              |
| $n$                 | Exponent in Glen's flow law | 3              |                                |
|                     | Seconds per year            | 31556926       | $\text{s a}^{-1}$              |

With the values given in Table 3.1, we may calculate the Glen's law parameters (3.2)  $\alpha = A^{-1/n}$  and  $\beta = 4/3$ , and the source term  $\mathbf{f} = \rho_{\text{ice}} g \hat{\mathbf{k}}$ .

#### 3.5.1 First example

For this example, we consider a gently sloping ice flow with an incline  $\theta = 0.1^\circ$  with a no-slip boundary condition at the base and periodic boundary conditions at the terminus. The horizontal length of the domain is 10km. In the Figure 3.1 we show the numerical solution applying the MHM method with  $\mathbf{u}_h \in \mathbb{P}^3(K)^2$ ,  $p_h \in \mathbb{P}^3(K)$  and  $\boldsymbol{\lambda}_{H,h} \in \boldsymbol{\Lambda}_1^1$  and, in order to compare our numerical results, in the Figure 3.2 we present the solution using the well-known  $P^2/P^1$  stable method (see, e.g., [45]). The mesh for the  $P^2/P^1$  method is

the same first-level mesh for the MHM method with 3077 elements. For the MHM method we show the figures only for the case  $\mathbf{u}_h \in \mathbb{P}^3(K)^2$ ,  $p_h \in \mathbb{P}^3(K)$  and  $\boldsymbol{\lambda}_{H,h} \in \boldsymbol{\Lambda}_1^1$ , because in other cases the plots are very similar.

**Remark 3.3** *The numerical tests with  $\mathbf{D}(\cdot) = \nabla(\cdot)$  behaves properly when the following condition holds*

$$k \geq \begin{cases} l + 1 & \text{when } l \text{ is even and,} \\ l + 2 & \text{when } l \text{ is odd;} \end{cases} \quad (3.38)$$

where  $k$ ,  $n$  and  $l$  are the degrees of the polynomials that define the finite element spaces  $\mathbf{V}_h$ ,  $Q_h$  and  $\boldsymbol{\Lambda}_l$ , respectively, remembering that we chose  $k = n$  (cf. (2.5), (2.7) and (2.6)). We recall that (3.38) is a sufficient condition to ensure the existence and uniqueness of the solution of the second-level MHM method for the linear Stokes problem (see [12]), and then our numerical results for the non-linear case are in accordance with the previous works. But for the case  $\mathbf{D}(\cdot) = \varepsilon(\cdot)$ , the numerical results suggest that, besides (3.38), it is required that  $l \neq 0$ . The mathematical analysis for our non-linear scheme will be addressed in future work.

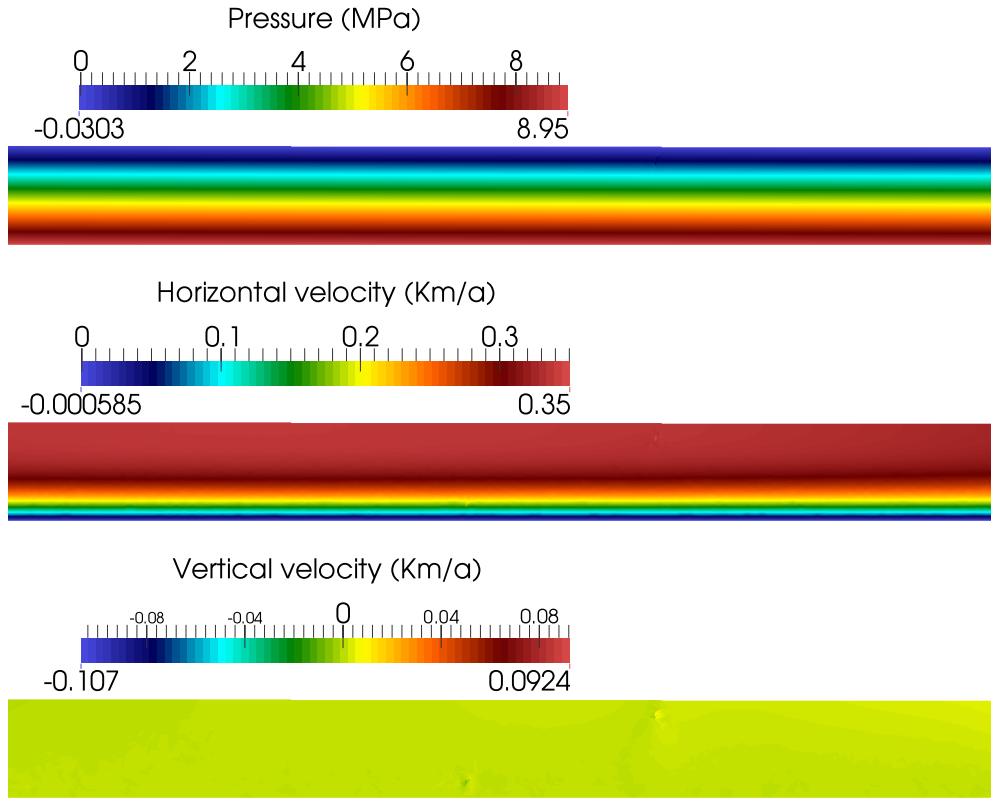


Figure 3.1: Solution of Example 3.5.2 with the MHM method with  $\mathbf{u}_h \in \mathbb{P}^3(K)^2$ ,  $p_h \in \mathbb{P}^3(K)$  and  $\boldsymbol{\lambda}_{H,h} \in \boldsymbol{\Lambda}_1^1$ , using a first-level mesh with 3077 elements, considering the physical parameters given in Table 3.1 and an incline of  $\alpha = 0.1^\circ$ .

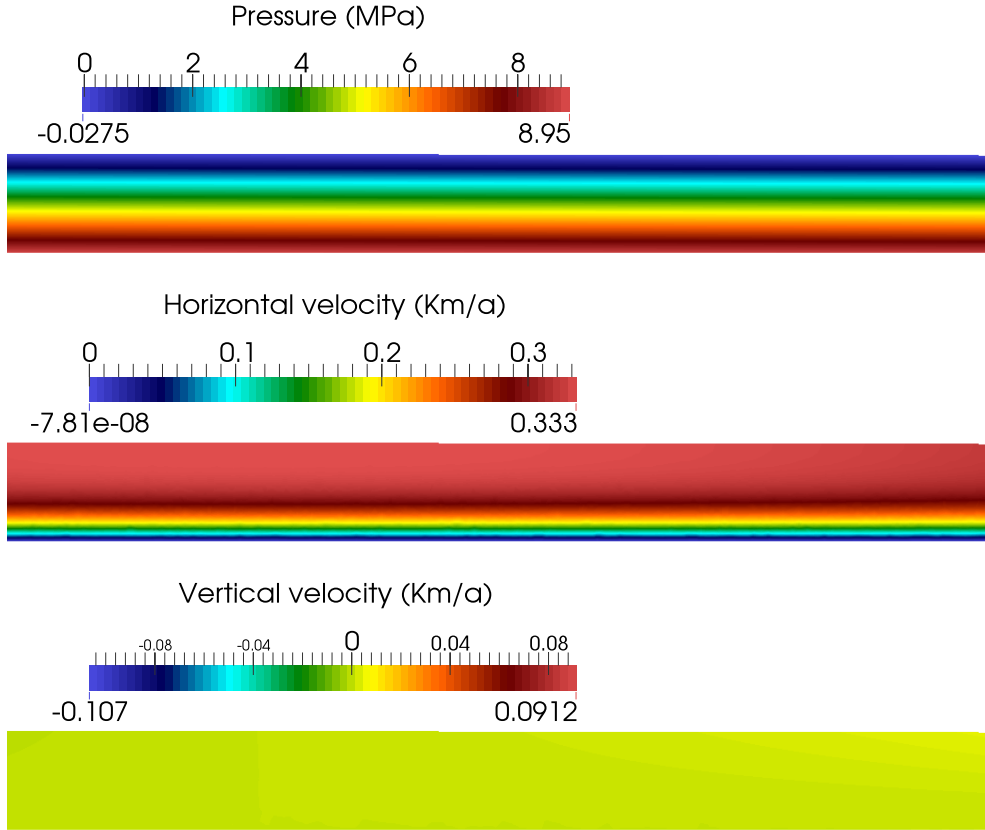


Figure 3.2: Solution of Example 3.5.2 using a  $P^2/P^1$  scheme considering a mesh with 9232 elements, considering the physical parameters given in Table 3.1 and an incline of  $\alpha = 0.1^\circ$ .

### 3.5.2 Second example

Similar to the previous example, we consider a gently sloping ice flow with incline  $\theta = 0.5^\circ$  with periodic boundary conditions at the terminus, but now over a sinusoidal rippled bedrock with no-slip boundary conditions at the base. The horizontal length of the domain is also 10km.

The Figure 3.3 show the numerical solution for the MHM method with  $\mathbf{u}_h \in \mathbb{P}^3(K)^2$ ,  $p_h \in \mathbb{P}^3(K)$  and  $\boldsymbol{\lambda}_{H,h} \in \boldsymbol{\Lambda}_1^1$  and, in order to compare the numerical results of our method, in Figure 3.4 we present the solution of using the well-known  $P^2/P^1$  stable method (see, e.g., [45]). The mesh for the  $P^2/P^1$  method is the same first-level mesh for the MHM method with 4434 elements. For the MHM method we show the figures only for case  $\mathbf{u}_h \in \mathbb{P}^3(K)^2$ ,  $p_h \in \mathbb{P}^3(K)$  and  $\boldsymbol{\lambda}_{H,h} \in \boldsymbol{\Lambda}_1^1$ , because in other cases the plots are very close.

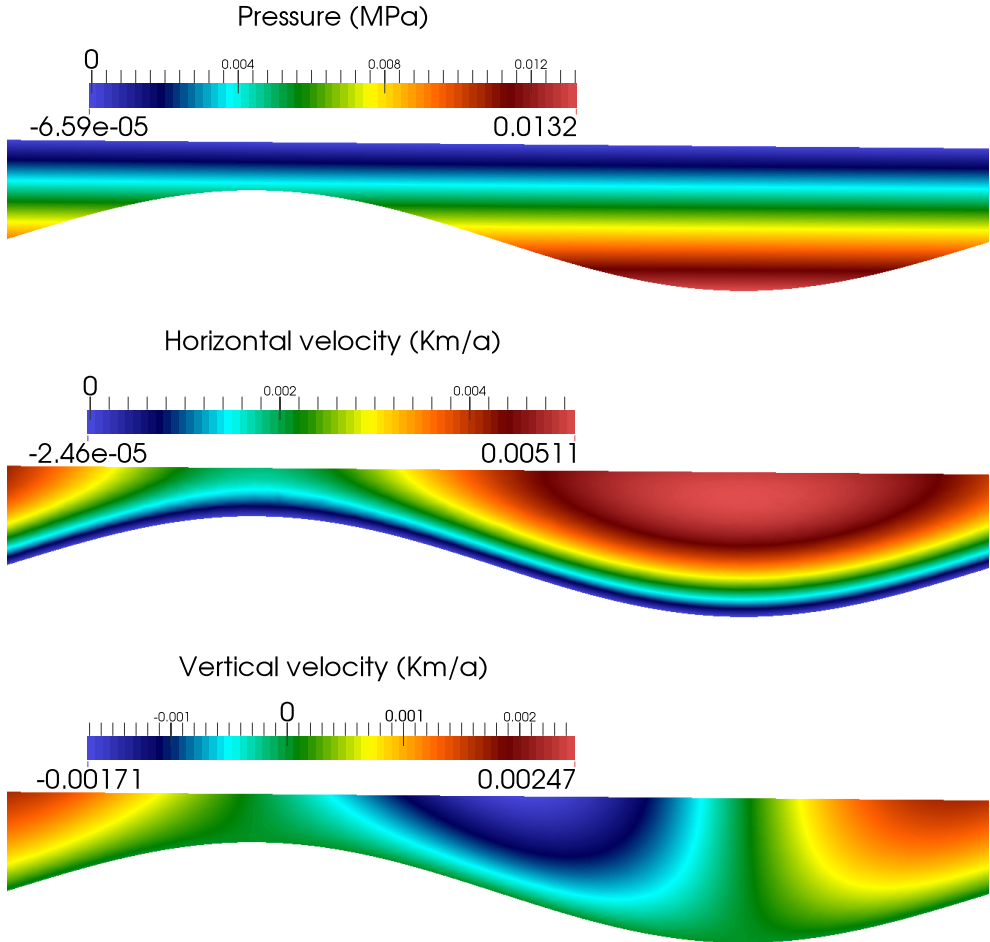


Figure 3.3: Solution of Example 3.5.2 using the MHM method with  $\mathbf{u}_{H,h} \in \mathbb{P}^3(K)^2$ ,  $p_{H,h} \in \mathbb{P}^3(K)$  and  $\boldsymbol{\lambda}_{H,h} \in \Lambda_1^1$ , considering the physical parameters given in Table 3.1 with an incline of  $\alpha = 0.5^\circ$ , and a mesh with 4434 elements.

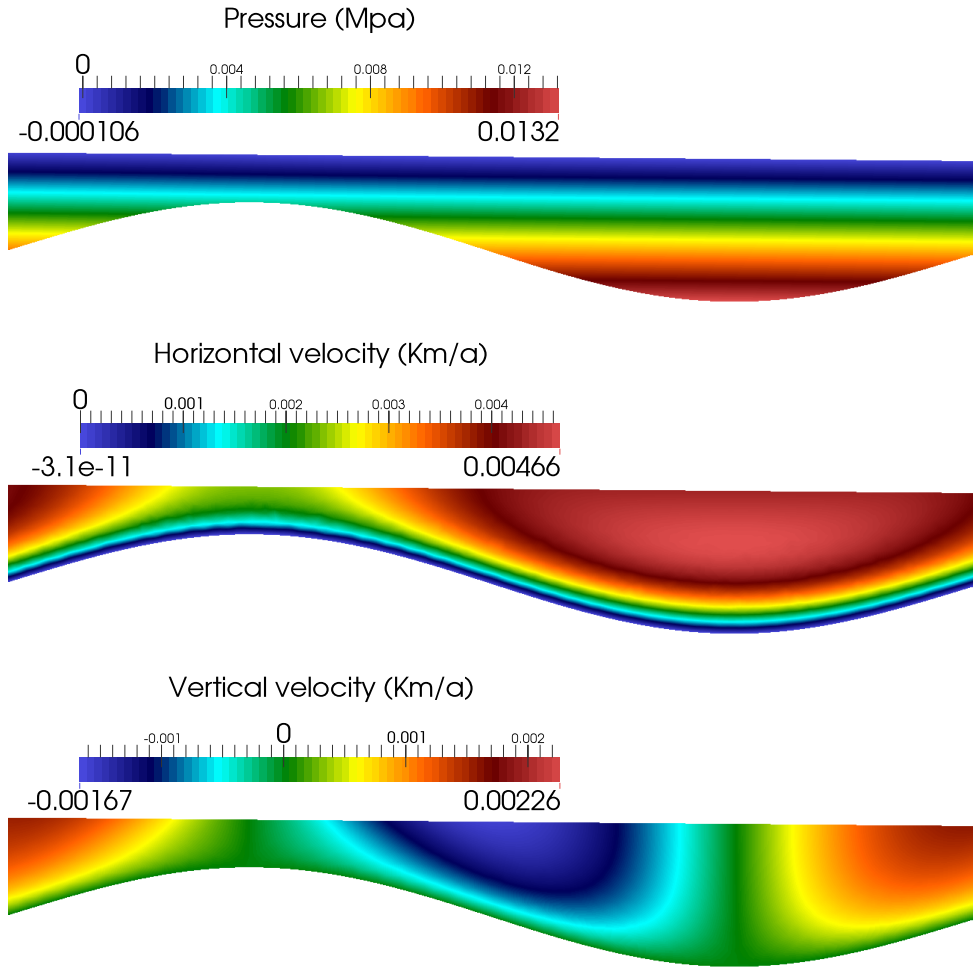


Figure 3.4: Solution of Example 3.5.2 using the  $P^2/P^1$  finite element spaces, considering the physical parameters given in Table 3.1 with an incline of  $\alpha = 0.5^\circ$ , and a mesh with 4434 elements.

We see in both examples that the numerical results using the MHM scheme are very close with the well known  $P^2/P^1$  scheme, with the additional advantage that the MHM method can capture the multiscale behavior of the problems using coarse meshes and other characteristic naturals in the geological context, like the presence of cracks. Furthermore, due to the size of the geological domains, the virtue of running in parallel of the MHM method is specifically relevant.

### 3.6 Conclusion

In this chapter, we proposed a new numerical strategy to apply the MHM for the non-linear Stokes problem with mixed boundary conditions, which models the behavior of a glacier. The numerical method was tested in a glacier model with realistic parameters, verifying that the solutions are physically correct. Our results suggest that the MHM method is a promising technique in the context of glaciology, because, in addition to the properties inherited by the finite element method, it has other virtues, such as being able to be implemented naturally in parallel, which is very relevant due to the size of the domains in this context, especially in 3D. The remaining rigorous mathematical analysis and more numerical tests are a future work.

# Conclusiones y trabajo futuro

## Conclusiones

1. En el Capítulo 1 adaptamos las ideas de [9] y [14] para desarrollar un análisis de error a posteriori -de tipo jerárquico- para el método LPS introducido en [15], que aproxima la solución de las ecuaciones de Navier–Stokes no lineales incompresibles. Nuestro estimador de error a posteriori está basado en la solución de problemas locales puestos en espacios de funciones burbujas específicos de una dimensión, fáciles de calcular y de bajo costo computacional. Para estudiar el desempeño de este estimador a posteriori presentamos ejemplos numéricos con soluciones analíticas verificando que el índice de efectividad permanece acotado cuando  $h$  tiende a cero, y probamos también el problema de referencia bien conocido de la cavidad, el cual está fuera del marco teórico, mostrando que nuestro estimador a posteriori genera secuencias de mallas adaptadas que van mejorando la calidad de las soluciones numéricas incluso en régimen turbulento.
2. En el Capítulo 2 proponemos y analizamos una nueva estrategia de error a posteriori especialmente diseñada para el método MHM. El estimador de error a posteriori propuesto considera las aproximaciones multiescala del método. Desarrollamos el análisis numérico para el primer y segundo nivel del método MHM para las ecuaciones de Stokes y Brinkman probando que el estimador es localmente eficiente y confiable en las normas naturales. El resultado, hasta donde sabemos, es el primero que que considera el impacto de la aproximación del segundo nivel en un método de elementos finitos con un operador de Stokes. Como resultado, el estimador de error multiescala produce una novedosa estrategia de adaptividad que considera la malla de primer nivel así como también las mallas del segundo nivel. Validamos los resultados con problemas de fluidos con flujos altamente heterogéneos. Mostramos que el método MHM en su adaptividad de primer y segundo niveles preserva la precisión de la velocidad y presión en mallas globales gruesas. Las multiples escalas son capturadas a través de

funciones calculadas de manera paralela.

3. En el Capítulo 3 proponemos una nueva estrategia numérica para aplicar el método MHM a problemas no lineales, y la aplicamos a un problema de Stokes no lineal con condiciones de borde mixtas, el cual modela el comportamiento de glaciares. Hasta donde sabemos, ésta es la primera metodología propuesta en la literatura que permite aplicar el método MHM a problemas no lineales. El método fue testeado con parámetros realistas en un modelo de un glaciar verificando que las soluciones obtenidas son las físicamente esperadas.

## Trabajo futuro

Lo novedoso del método MHM deja abierta la posibilidad de múltiples ramas para investigar a partir del trabajo de esta tesis.

1. Extender los métodos presentados al régimen no estacionario.
2. Completar el análisis numérico del método MHM aplicado al problema de Stokes no lineal presentado en el Capítulo 3, y enviarlo para su publicación.
3. Basados en el esquema numérico para problemas no lineales propuesto en el Capítulo 3, proponer un esquema MHM para las ecuaciones de Navier–Stokes, y desarrollar su análisis de error a priori y a posteriori.
4. Continuar con el análisis de modelos de glaciares más completos, por ejemplo, modelos que consideren la deformación debido a la temperatura, efectos del clima, derretimiento, grietas y canales.
5. Extender el código desarrollado para el método MHM al caso 3D, donde se aproveche el paralelismo natural del método.
6. Proponer y analizar un esquema de elementos finitos estabilizados para estudiar modelos de materiales elásticos y viscoelásticos. En particular, nos interesa su aplicación en la modelación de procesos de subducción de placas tectónicas [35, 100]. Sobre este tema, aunque no está documentado en esta tesis, ya tenemos resultados numéricos prometedores.
7. Utilizando el algoritmo desarrollado en 6 para aproximar la solución del segundo nivel, proponer un esquema del tipo MHM para las ecuaciones de viscoelasticidad. Debido a la naturaleza del problema geológico que modela (grandes dominios y presencia de

grietas) intuimos que el método MHM es una herramienta prometedora para este contexto.

# Concluding remarks and future work

## Concluding remarks

1. In Chapter 1 we adapted the ideas of [9] and [14] to develop an a posteriori error analysis of hierarchical-type for the LPS method, introduced in [15], which approximates the solution of the fully non-linear incompressible Navier–Stokes equations. Our a posteriori estimator is based on the solution of local problems posed in specific one-dimensional spaces of bubble-like functions so it is easy to implement with a low computational cost. In order to study the performance of our a posteriori estimator we presented numerical examples with analytical solutions checking that the effectiveness index stays bounded as  $h$  goes to zero, and we tested well-known benchmark problems which live outside of the theoretical framework showing that our a posteriori estimator generates a sequence of adapted meshes improving the quality of the numerical solutions even in the turbulent regime, as was shown with the lid-driven cavity problem.
2. In Chapter 2 we proposed and analyzed a new a posteriori error strategy specially designed for the MHM method. The a posteriori error estimator proposed accounts for the multi-level approximations of the method. We accounts for the numerical analysis to the first and second level MHM methods for the Stokes and Brinkman equations, for which we proved that the estimator is locally efficient and reliable in the natural norms. The results are, up to our knowledge, the first to address the impact of two-levels of approximation in a multiscale finite element method for the Stokes operator. As a result, the multiscale a posteriori error estimator yielded novel adaptivity strategies that drive first-level meshes as well as (independent) elementwise second level meshes. Fluid flow problems in highly heterogeneous validated the underlying

multi-level adaptative algorithms. We showed that the MHM method on such first- and second-level adapted meshes preserves the accuracy of the velocity and pressure fields on coarse global meshes. The missing scales are upscaled through base functions computed in parallel.

3. In Chapter 3 we proposed a new numerical strategy applied to the non-linear Stokes problem with mixed boundary conditions, which models the behavior of a glacier. Up to our knowledge, this is the first methodology proposed in the literature that allows applying the MHM method to non-linear problems. The method was tested in a glacier model with realistic parameters, verifying that the solutions are the physically expected ones.

## Future work

The novelty of the MHM methods gives way to multiple research branches.

1. To extend the methods to the non-stationary regime.
2. To propose a numerical analysis of the MHM method applied to the non-linear Stokes problem of the Chapter 3.
3. Based on the numerical scheme for non-linear problems showed in Chapter 3, to propose an MHM scheme for the Navier–Stokes equations, and derive a priori and a posteriori error analysis.
4. Extend the analysis to more complete glaciers models, for example, to models that consider the ice deformation due to the temperature, effect of the climate, meltwater, cracks, and channels.
5. To extend the code developed for the MHM method to the 3D case, to leverage the inherent parallelism of the method.
6. To propose and analyze a stabilized finite element scheme for elastic and viscoelastic material models. In particular, we are interested in its application in the modeling of tectonic plate subduction processes [35, 100]. Here, although it is not documented in this thesis, we already have promising numerical results.
7. To propose an MHM scheme for the viscoelasticity equations adopting as second level solver the numerical scheme developed in 6.

# Bibliography

- [1] A. Abdulle and A. Nonnenmacher. A posteriori error estimates in quantities of interest for the finite element heterogeneous multiscale method. *Numer. Methods for Partial Differential Equations*, 29(5):1629–1656, 2013.
- [2] P. Abry, R. Baraniuk, P. Flandrin, R. Riedi, and D. Veitch. Multiscale nature of network traffic. *Signal Process. Mag.*, 19(3):28–46, 2002.
- [3] S. Adamson, V. Astapenko, I. Chernysheva, V. Chorkov, M. Deminsky, G. Demchenko, A. Demura, A. Demyanov, N. Dyatko, A. Eletzkii, et al. Multiscale multiphysics nonempirical approach to calculation of light emission properties of chemically active nonequilibrium plasma: Application to Ar–GaI<sub>3</sub> system. *J. Phys. D.*, 40(13):3857, 2007.
- [4] S. Agmon. *Lectures on Elliptic Boundary Value Problems*, volume 369. AMS Chelsea Publishing, Providence, 2010.
- [5] A. Agouzal and J. M. Thomas. Une méthode d’éléments finis hybrides en décomposition de domaines. *RAIRO-Math Model Num.*, 29(6):749–765, 1995.
- [6] M. Ainsworth and J. T. Oden. *A posteriori error estimation in finite element analysis*. Pure and Applied Mathematics. Wiley-Interscience, New York, 2000.
- [7] P. R. Amestoy, I. S. Duff, J. Koster, and J.-Y. L’Excellent. A fully asynchronous multifrontal solver using distributed dynamic scheduling. *SIAM J. Matrix Anal. Appl.*, 23(1):15–41, 2001.
- [8] P. R. Amestoy, A. Guermouche, J.-Y. L’Excellent, and S. Pralet. Hybrid scheduling for the parallel solution of linear systems. *Parallel Comput.*, 32(2):136–156, 2006.
- [9] R. Araya, G. R. Barrenechea, and A. Poza. An adaptive stabilized finite element method for the generalized Stokes problem. *J. Comput. Appl. Math.*, 214(2):457–479, 2008.

- [10] R. Araya, G. R. Barrenechea, and F. Valentin. A stabilized finite-element method for the Stokes problem including element and edge residuals. *IMA J. Numer. Anal.*, 27(1):172–197, 2007.
- [11] R. Araya, C. Harder, D. Paredes, and F. Valentin. Multiscale hybrid-mixed method. *SIAM J. Numer. Anal.*, 51(6):3505–3531, 2013.
- [12] R. Araya, C. Harder, A. Poza, and F. Valentin. The multiscale hybrid-mixed method for the Stokes and Brinkman equations – The method. *Comput. Methods Appl. Mech. Engrg.*, 324:29–53, 2017.
- [13] R. Araya, A. H. Poza, and E. P. Stephan. A hierarchical a posteriori error estimate for an advection-diffusion-reaction problem. *Math. Models Methods Appl. Sci.*, 15(7):1119–1139, 2005.
- [14] R. Araya, A. H. Poza, and F. Valentin. On a hierarchical error estimator combined with a stabilized method for the Navier–Stokes equations. *Numer. Methods Partial Differential Equations*, 28(3):782–806, 2012.
- [15] R. Araya, A. H. Poza, and F. Valentin. A low-order local projection method for the incompressible Navier–Stokes equations in two- and three-dimensions. *IMA J. Numer. Anal.*, 36(1):267–295, 2016.
- [16] R. Araya and R. Rebollo. An a posteriori error estimator for a LPS method for Navier-Stokes equations. *Appl. Numer. Math.*, 127:179–195, 2018.
- [17] R. Araya, R. Rebollo, and F. Valentin. A posteriori analysis of the Multiscale Hybrid-Mixed method for Brinkman problem. *IMA J. Numer. Anal.*, (submitted).
- [18] U. Ayachit. The Paraview guide: A parallel visualization application. Clifton Park, NY: Kitware. 2015.
- [19] I. Babuska and E. Osborn. Generalized finite element methods: Their performance and their relation to mixed methods. *SIAM J. Num. Anal.*, 20(3):510–536, 1983.
- [20] S.A. Baeurle and A. Stephan. Multiscale modeling of polymer materials using field-theoretic methodologies: A survey about recent developments. *J. Math., Chem.*, 46(2):363–426, 2009.
- [21] J. Baiges and R. Codina. Variational multiscale error estimators for solid mechanics adaptive simulations: An orthogonal subgrid scale approach. *Comput. Methods Appl. Mech. Engrg.*, 325:37 – 55, 2017.

- [22] W. Bangerth and R. Rannacher. *Adaptive finite element methods for differential equations*. Birkhäuser, 2013.
- [23] R.E. Bank and K. Smith. A posteriori error estimates based on hierarchical bases. *SIAM J. Numer. Anal.*, 30(4):921–935, 1993.
- [24] R.E. Bank and A. Weiser. Some a posteriori error estimators for elliptical partial differential equations. *Math. Comp.*, 44:283–301, 1985.
- [25] G. R. Barrenechea and F. Valentin. An unusual stabilized finite element method for a generalized Stokes problem. *Numer. Math.*, 92(4):653–677, 2002.
- [26] G. R. Barrenechea and F. Valentin. A residual local projection method for the Oseen equation. *Comput. Methods Appl. Mech. Engrg.*, 199(29–32):1906–1921, 2010.
- [27] E. Bayraktar, O. Mierka, and S. Turek. Benchmark computations of 3D laminar flow around a cylinder with CFX, OpenFOAM and FeatFlow. *Int. J. Comput. Sci. Eng.*, 7(3):253–266, 2012.
- [28] M Bebendorf. A note on the Poincaré inequality for convex domains. *Z. Anal. Anwend.*, 22(4):751–756, 2003.
- [29] L. Bengtsson. Climate of the 21st century. *Agric. For. Meteorol.*, 72(1-2):3–29, 1994.
- [30] M. Braack and T. Richter. Solutions of 3D Navier–Stokes benchmark problems with adaptive finite elements. *Comput. & Fluids*, 35(4):372–392, 2006.
- [31] F. Brezzi and D. Marini. Error estimates for the three-field formulation with bubble stabilization. *Math. Comp.*, 70(235):911–934, 2000.
- [32] F. Brezzi and L. D. Marini. A three-field domain decomposition method, 1994.
- [33] A. N. Brooks and T. J. R. Hughes. Streamline Upwind/Petrov-Galerkin formulations for convection dominated flows with particular emphasis on the incompressible Navier-Stokes equations. *Comput. Methods Appl. Mech. Engrg.*, 32:199–259, 1982.
- [34] E. Burman and P. Hansbo. Edge stabilization for Galerkin approximations of convection-diffusion-reaction problems. *Comput. Methods Appl. Mech. Engrg.*, 193(15-16):1437–1453, 2004.
- [35] N. Cerpa, R. Hassani, M. Gerbault, and J. Prevost. A fictitious domain method for lithosphere/asthenosphere interaction: Application to periodic slab folding in the upper mantle. *Geochem. Geophys.*, 2014.

- [36] L. Chamoin and F. Legoll. *A posteriori* error estimation and adaptive strategy for the control of MsFEM computations. *Comput. Methods Appl. Mech. Engrg.*, 336:1–38, 2018.
- [37] Q. Chen, M. Gunzburger, and M. Perego. Well-posedness results for a nonlinear Stokes problem arising in glaciology. *SIAM J. Math. Analysis*, 45(5):2710–2733, 2013.
- [38] M. A. Christie and M. J. Blunt. Tenth SPE comparative solution project: A comparison of upscaling techniques. *PE Reservoir Eval. Eng.*, pages 308–317, 2001.
- [39] Ph. Clément. Approximation by finite element functions using local regularization. *R.A.I.R.O. Anal. Numer.*, 9:77–84, 1975.
- [40] J. Colinge and J. Rappaz. A strongly nonlinear problem arising in glaciology. *ESAIM: Mathematical Modelling and Numerical Analysis*, 33(2):395–406, 1999.
- [41] K. M. Cuffey and W. S. B. Paterson. *The physics of glaciers*. Elsevier, Oxford, 2010.
- [42] R. G. Durán. An elementary proof of the continuity from  $L_0^2(\Omega)$  to  $H_0^1(\Omega)^n$  of Bogovskii's right inverse of the divergence. *Rev. Un. Mat. Argentina*, 53(2):59–78, 2012.
- [43] Y. Efendiev, J. Galvis, and T.Y. Hou. Generalized multiscale finite element methods (GMsFEM). *J. Comput. Phys.*, 251:116–135, 2013.
- [44] Y. Efendiev and T.Y. Hou. *Multiscale finite element methods*, volume 4 of *Surveys and Tutorials in the Applied Mathematical Sciences*. Springer, New York, 2009. Theory and applications.
- [45] A. Ern and J. L. Guermond. *Theory and Practice of Finite Elements*, volume 159 of *Applied Mathematical Sciences*. Springer-Verlag, New York, 2004.
- [46] L. Franca and A. Madureira. Element diameter free stability parameters for stabilized methods applied to fluids. *Comput. Methods Appl. Mech. Engrg.*, 105(3):395–403, 1993.
- [47] L. P. Franca and S. Frey. Stabilized finite element methods. II. The incompressible Navier–Stokes equations. *Comput. Methods Appl. Mech. Engrg.*, 99(2–3):209–233, 1992.
- [48] U. Ghia, K.N. Ghia, and C.T. Shin. High-Re solutions for incompressible flow using the Navier–Stokes equations and a multigrid method. *J. Comput. Phys.*, 48(3):387–411, 1982.

- [49] V. Girault and P. A. Raviart. *Finite Element Methods for Navier–Stokes Equations: Theory and Algorithms*, volume 5 of *Springer Series in Computational Mathematics*. Springer–Verlag, Berlin, 1986.
- [50] J.M. Gregory and P. Huybrechts. Ice-sheet contributions to future sea-level change. *Philos. Trans. A.*, 364(1844):1709–1732, 2006.
- [51] P. Grisvard. *Singularities in boundary value problems*. Masson, Paris, 1992.
- [52] A.F. Gulbransen, V.L. Hauge, K. Lie, et al. A multiscale mixed finite element method for vuggy and naturally fractured reservoirs. *SPE Journal*, 15(02):395–403, 2010.
- [53] I. Harari and T. Hughes. What are C and h?: Inequalities for the analysis and design of finite element methods. *Comput. Methods Appl. Mech. Engrg.*, 97(2):157–192, 1992.
- [54] C. Harder, A .L. Madureira, and F. Valentin. A Hybrid-Mixed Method for Elasticity. *ESAIM: Math. Model. Num. Anal.*, 50(2):311–336, 2016.
- [55] C. Harder, D. Paredes, and F. Valentin. A family of multiscale hybrid-mixed finite element methods for the Darcy equation with rough coefficients. *J. Comput. Phys.*, 245:107–130, 2013.
- [56] C. Harder, D. Paredes, and F. Valentin. On a multiscale hybrid-mixed method for advective-reactive dominated problems with heterogenous coefficients. *SIAM Multiscale Model. and Simul.*, 13(2):491–518, 2015.
- [57] P. Henning and M. Ohlberger. A-posteriori error estimate for a heterogeneous multiscale approximation of advection-diffusion problems with large expected drift. *Discrete Contin. Dyn. Syst. Ser. S*, 9(5):1393–1420, 2016.
- [58] T. Y. Hou, X. Wu, and Z. Cai. Convergence of a multiscale finite element method for elliptic problems with rapidly oscillating coefficients. *Math. Comp.*, 68(227):913–943, 1999.
- [59] T. J.R. Hughes. Multiscale phenomena: Green’s functions, the Dirichlet-to-Neumann formulation, subgrid scale models, bubbles and the origins of stabilized methods. *Comput. Methods Appl. Mech. Engrg.*, 127(1-4):387–401, 1995.
- [60] T. J.R. Hughes, L. P. Franca, and M. Balestra. A new finite element formulation for computational fluid dynamics: V. Circumventing the Babuska–Brezzi condition: A stable Petrov–Galerkin formulation of the Stokes problem accommodating equal-order interpolations. *Comput. Methods Appl. Mech. Engrg.*, 59(1):85–99, 1986.

- [61] D. Irisarri and G. Hauke. A posteriori pointwise error computation for 2-D transport equations based on the variational multiscale method. *Comput. Methods Appl. Mech. Engrg.*, 311:648 – 670, 2016.
- [62] V. John. Residual a posteriori error estimates for two-level finite element methods for the Navier–Stokes equations. *Appl. Numer. Math.*, 37(4):503–518, 2001.
- [63] V. John. Higher order finite element methods and multigrid solvers in a benchmark problem for the 3D Navier–Stokes equations. *Int. J. Numer. Meth. Fluids*, 40(6):775–798, 2002.
- [64] E. Jonsson. Ice Sheet Modeling: Accuracy of First-Order Stokes Model with basal sliding. Technical report, 2018.
- [65] J. Jouvet and J. Rappaz. Analysis and finite element approximation of a nonlinear stationary Stokes problem arising in glaciology. *Adv. Numerical Analysis*, 2011:164581:1–164581:24, 2011.
- [66] R. Juanes and F. Dub. A locally conservative variational multiscale method for the simulation of porous media flow with multiscale source terms. *Comput. Geosci.*, 12(3):273–295, 2008.
- [67] A. Khaled and K Vafai. The role of porous media in modeling flow and heat transfer in biological tissues. *Philos. Trans. A.*, 46(26):4989–5003, 2003.
- [68] S. Lanteri, D. Paredes, C. Scheid, and F. Valentin. The Multiscale Hybrid-Mixed method for the Maxwell equations in heterogeneous media. *SIAM Multiscale Model. Simul.*, 16(4):1648–1683, 2018.
- [69] S.H. Lee, C. Wolfsteiner, and H.A. Tchelepi. Multiscale finite-volume formulation for multiphase flow in porous media: Black oil formulation of compressible, three-phase flow with gravity. *Comput. Geosci.*, 12(3):351–366, 2008.
- [70] W. Leng, L. Ju, M. Gunzburger, S. Price, and T. Ringler. A parallel high-order accurate finite element nonlinear Stokes ice sheet model and benchmark experiments. *J. Geophys. Res. Earth Surf.*, 117(F1), 2012.
- [71] A. Linke and C. Merdon. Pressure-robustness and discrete Helmholtz projectors in mixed finite element methods for the incompressible Navier-Stokes equations. *Comput. Methods Appl. Mech. Engrg.*, 311:304–326, 2016.

- [72] A. L Madureira, Daniele Q.M. Madureira, and P.O. Pinheiro. A multiscale numerical method for the heterogeneous cable equation. *Neurocomputing*, 77(1):48–57, 2012.
- [73] A. Målqvist and D. Peterseim. Localization of elliptic multiscale problems. *Math. Comp.*, 83(290):2583–2603, 2014.
- [74] S.J. Marshall. *The cryosphere*. Princeton University Press, 41 William Street, Princeton, New Jersey 08540, 2011.
- [75] G. Medic and B. Mohammadi. NSIKE – An incompressible Navier–Stokes solver for unstructured meshes. Technical Report 3644, INRIA, Rocquencourt, 1999.
- [76] I. Monnesland, E. Lee, M. Gunzburger, and R. Yoon. A least-squares finite element method for a nonlinear Stokes problem in glaciology. *Comput. Math. Appl.*, 71(11):2421–2431, 6 2016.
- [77] J. Nye. The distribution of stress and velocity in glaciers and ice-sheets. 239:113–133, 02 1957.
- [78] M. Ohlberger. A posteriori error estimates for the heterogeneous multiscale finite element method for elliptic homogenization problems. *Multiscale Model. Simul.*, 4(1):88–114, 2005.
- [79] F. Pattyn and T. Payne. ISMIP—HOM ice sheet model intercomparison project. Technical report, 2006.
- [80] G. Pencheva, M. Vohralík, M. Wheeler, and T. Wildey. Robust a posteriori error control and adaptivity for multiscale, multinumerics, and mortar coupling. *SIAM J. Numer. Anal.*, 51(1):526–554, 2013.
- [81] P.A. Raviart and J.M. Thomas. Primal hybrid finite element methods for 2nd order elliptic equations. *Math. Comp.*, 31(138):391–413, 1977.
- [82] R. Renka. Algorithm 660: QSHEP2D: Quadratic Shepard method for bivariate interpolation of scattered data. *ACM. Trans. Math. Softw.* 14., pages 149–150, 1988.
- [83] M. Schäfer, S. Turek, F. Durst, E. Krause, and R. Rannacher. *Flow Simulation with High-Performance Computers II: DFG Priority Research Programme Results 1993–1995*, chapter Benchmark Computations of Laminar Flow Around a Cylinder, pages 547–566. Vieweg+Teubner Verlag, Wiesbade, 1996.

- [84] O. Schenk and K. Gärtner. Solving unsymmetric sparse systems of linear equations with pardiso. *Future Gener. Comput. Syst.*, 20(3):475–487, 2004.
- [85] J.R. Shewchuk. Engineering a 2D quality mesh generator and Delaunay triangulator, applied computational geometry: Towards geometric engineering (MC Lin, D. Manocha, eds.). *Lecture Notes in Comput. Sci.*, 1148:203–222.
- [86] H. Si. Tetgen, a Delaunay-based quality tetrahedral mesh generator. *ACM Trans. Math. Softw.*, 41(2):1–36, 2015.
- [87] G.C. Sih and J.Z. Zuo. Multiscale behavior of crack initiation and growth in piezoelectric ceramics. *Theor. Appl. Fract. Mec.*, 34(2):123–141, 2000.
- [88] L. Taleb and A. Hauet. Multiscale experimental investigations about the cyclic behavior of the 304L SS. *Int. J. Plasticity*, 25(7):1359–1385, 2009.
- [89] S. Tavener and T. Wildey. Adjoint based a posteriori analysis of multiscale mortar discretizations with multinumerics. *SIAM J. Sci. Comput.*, 35(6):A2621–A2642, 2013.
- [90] R. Temam. *Navier-Stokes equations. Theory and numerical analysis*. North-Holland Publishing Co., Amsterdam-New York-Oxford, 1977. Studies in Mathematics and its Applications, Vol. 2.
- [91] R. Temam. *Navier-Stokes Equations and Nonlinear Functional Analysis*, volume 66 of *CBMS-NSF Regional Conference Series in Applied Mathematics*. SIAM, Philadelphia, 2 edition, 1995.
- [92] S. Turek. *Efficient Solvers for Incompressible Flow Problems*, volume 6 of *Lect. Notes Comput. Sci. Eng.* Springer-Verlag, Berlin, 1999.
- [93] R. Verfürth. A posteriori error estimates for nonlinear problems. Finite element discretizations of elliptic equations. *Math. Comp.*, 62(206):445–475, 1994.
- [94] R. Verfürth. *A review of a posteriori error estimation and adaptive mesh-refinement techniques*. John Wiley & Sons Inc, Chichester, 1996.
- [95] R. Verfürth. *A Posteriori Error Estimation Techniques for Finite Element Methods*. Numerical Mathematics and Scientific Computation. Oxford University Press, Oxford, 2013.
- [96] E. Weinan and B. Engquist. The heterogeneous multiscale methods. *Commun. Math. Sci.*, 1(1):87–132, 2003.

- [97] E.J. Weinberg and M. Mofrad. Transient, three-dimensional, multiscale simulations of the human aortic valve. *Cardiovasc. Eng. Technol.*, 7(4):140–155, 2007.
- [98] G. Yun and H.S. Park. A multiscale, finite deformation formulation for surface stress effects on the coupled thermomechanical behavior of nanomaterials. *Comput. Methods Appl. Mech. Engrg.*, 197(41-42):3337–3350, 2008.
- [99] G.M. Zaslavsky, P.N. Guzdar, M. Edelman, M.I. Sitnov, and A.S. Sharma. Multiscale behavior and fractional kinetics from the data of solar wind–magnetosphere coupling. *Commun. Nonlinear Sci. Numer. Simul.*, 13(2):314–330, 2008.
- [100] S. Zlotnik, P. Díez, M. Fernández, and J. Vergés. Numerical modelling of tectonic plates subduction using X-FEM. *Comput. Methods Appl. Mech. Engrg.*, 196(41-44):4283–4293, 2007.